T.R.

GEBZE TECHNICAL UNIVERSITY

INSTITUTE OF NANOTECHNOLOGY

DEVELOPMENT OF BIMETALLIC RHENIUM-RUTHENIUM NANOSYSTEMS ENCAPSULATED IN POROUS MATERIALS FOR TERTIARY AMIDE HYDROGENATION

AHMET MUSAP MERT

A THESIS SUBMITTED FOR THE DEGREE OF

MASTER OF SCIENCE

INSTITUTE OF NANOTECHNOLOGY

GEBZE

2019

T.R.
GEBZE TECHNICAL UNIVERSITY
INSTITUTE OF NANOTECHNOLOGY

DEVELOPMENT OF BIMETALLIC RHENIUM-RUTHENIUM NANOSYSTEMS ENCAPSULATED IN POROUS MATERIALS FOR TERTIARY AMIDE HYDROGENATION

AHMET MUSAP MERT
A THESIS SUBMITTED FOR THE DEGREE OF
MASTER OF SCIENCE
INSTITUTE OF NANOTECHNOLOGY

THESIS SUPERVISOR
ASSOC. PROF. ŞÖLEN KINAYYİĞİT

GEBZE
2019

T.C.
GEBZE TEKNİK ÜNİVERSİTESİ
NANOTEKNOLOJİ ENSTİTÜSÜ

TERSİYER AMİT HİDROJENASYONU İÇİN PORLU MALZEME İLE DESTEKLENMİŞ BİMETALİK RENYUM-RUTENYUM NANOKATALİZÖRLERİN GELİŞTİRİLMESİ

AHMET MUSAP MERT
YÜKSEK LİSANS TEZİ
NANOTEKNOLOJİ ENSTİTÜSÜ

DANIŞMANI
DOÇ. DR. ŞÖLEN KINAYYİĞİT

GEBZE
2019

GEBZE TEKNİK ÜNİVERSİTESİ	YÜKSEK LİSANS JÜRİ ONAY FORMU

GTÜ Nanoteknoloji Enstitüsü Yönetim Kurulu'nun 24/06/2019 tarih ve 2019/13 sayılı kararıyla oluşturulan jüri tarafından 28/06/2019 tarihinde tez savunma sınavı yapılan AHMET MUSAP MERT'in tez çalışması Nanobilim ve Nanomühendislik Anabilim Dalında YÜKSEK LİSANS tezi olarak kabul edilmiştir.

JÜRİ

ÜYE
(TEZ DANIŞMANI)   : DOÇ.DR.ŞÖLEN KINAYYİĞİT

ÜYE   : PROF.DR. AYŞE GÜL GÜREK

ÜYE   : DOÇ.DR.OZAN AKDOĞAN

ONAY

Gebze Teknik Üniversitesi Nanoteknoloji Enstitüsü Yönetim Kurulu'nun

08./07./2019 tarih ve 2019/.15... sayılı kararı.

Prof. Dr. Ahmet Yavuz ORAL
Enstitü Müdürü

SUMMARY

Amines are a versatile class of compounds finding variety of applications in the chemical industries of solvents, plastics and detergents as well as in the pharmaceutical industry. However, its production is rather difficult and expensive since the amine functionalities are often synthesized by an unsustainable multistage and low yield process where initially stoichiometric reducing agents, e.g. $LiAlH_4$, boranes, are used. Moreover, such reducing agents are hazardous and difficult to handle, particularly on large scale, and their use often involves complex and wasteful workup procedures.

The aim of this thesis is to bring a sustainable solution for industrial production of amines by designing and investigating novel nanocatalysts composed of bimetallic Ru and Re nanoclusters that have the potential to operate in a batch reactor under mild reaction conditions with high activity and selectivity by using hydrogen as a green and abundant reductant. The bottom-up organometallic approach for the catalyst synthesis will enable the achievement of bimetallic few-atoms-clusters inside silica based porous supports. Usage of porous materials as supports for these catalytically active metals (Ru and Re) will also provide stability and robustness and will prevent their sintering into metal nanoparticles.

STEM, XRD, EXAFS, XPS, TPR and NMR studies revealed highly dispersed metal on surface as atomic scale and small nanoclusters of 0.5-2.0 nm. Prepared porous ReRu nanocatalysts with SBA-15, MCM-48, Ti-SBA-15, Al-MCM-48 and for comparison, a nonporous nanocatalysts with silica support (SiO_2) were investigated in the hydrogenation of tertiary amides. Best catalytic conversion and selectivity was observed with ReRu/SBA-15 nanocatalyst.

Keywords: Amide Hydrogenation, Bimetallic nanocatalysts, Porous support materials, Rhenium, Ruthenium, Organometallic synthesis.

ÖZET

Aminler çözücülerin, plastiklerin ve deterjanların kimyasal endüstrilerinde ve ayrıca farmasötik endüstrisinde çeşitli uygulamaları bulan çok yönlü bir bileşik sınıfıdır. Bununla birlikte amin üretiminde, işlevselliklerinin çoğu zaman düşük verimde olduğu LiAlH$_4$ veya boranlar gibi stokiyometrik indirgeme ajanlarının kullanıldığı sürdürülemez bir çok kademeli işlemle sentezlendiğinden dolayı oldukça zor ve pahalıdır. Ek olarak, bu gibi indirgeyici ajanlar, özellikle büyük ölçekte tehlikeli ve kullanımı zordur ve kullanımları genellikle karmaşık ve israflı iş prosedürlerini içerir.

Bu tezin amacı, hafif reaksiyon koşullarında sentezlenen ve hafif reaksiyon koşulları altında bir reaktör içerisinde çalışma potansiyeline sahip olan yeni bir bimetalik Ru ve Re nanokümelerden oluşan yeni bir tür nanokatalizörü tasarlayıp araştırmak suretiyle sürdürülebilir bir çözüm getirmektedir. Hidrojenin yeşil ve bol miktarda bir indirgeyici olarak kullanılmasıyla seçicilik sağlanacaktır. Katalizör sentezi için aşağıdan yukarı organometalik yaklaşım, silis bazlı gözenekli desteklerin içindeki bimetalik birkaç atom kümesinin elde edilmesini sağlayacaktır. Bu katalitik olarak aktif metaller (Ru ve Re) için destek olarak gözenekli malzemelerin kullanılması ayrıca dayanıklılık, tekrardan kullanılmasını sağlayacaktır ve bunların metal nanoparçacıklara sinterlenmelerini önleyecektir.

SRTEM, XRD, EXAFS, XPS, TPR ve NMR çalışmaları yüzeyde yüksek oranda dağılmış metalin atom ölçeği ve küçük nanokümelerin boyutlarının 0.5-2.0 nm olduğunu gösterdi. Hazırlanan gözenekli (SBA-15, MCM-48, Ti-SBA-15, Al-MCM-48) ve karşılaştırma için gözeneksiz silica destekli (SiO$_2$) nanokatalizörler tersiyer amid hidrojenasyonunda kullanılmıştır. Üretilen nanokatalizörler arasında en iyi dönüşüm ve bu tepkimeye seçicilik ReRu/SBA-15 nanokatalizörü ile gözlenmiştir.

Anahtar Kelimeler: Amid hidrojenasyonu, Bimetalik nanokatalizör, Porlu destek malzemleri, Renyum, Rutenyum, Organometalik sentez.

ACKNOWLEDGEMENTS

Throughout the writing of this thesis I have received a great deal of support and assistance. I would first like to thank my supervisor, Assoc. Prof. Solen KINAYYIGIT, whose expertise was invaluable in the formulation of the research topic and methodology, in particular and for the opportunity given to study and work in an international project.

I would like to acknowledge Prof. S.C. Edman TSANG from University of Oxford and my supervisor in his laboratory in the Department of Inorganic Chemistry, Dr. Tugce AYVALI, for their valuable guidance. Dr. Ayvalı, deserves special thanks; thank you very much for your input in the completion of this thesis. You were always willing to help me. Phoebe, I would also like to thank you for your excellent cooperation.

In addition, I would like to thank to my parents and my wife for their wise counsel and sympathetic ear. You are always there for me. Finally, there are my friends, who were of great support in deliberating over our problems and findings, as well as providing happy distraction to rest my mind outside of my research.

TABLE of CONTENTS

LIST of ABBREVIATIONS and ACRONYMS

Symbols and Abbreviations	Descriptions
Å	: Angstrom
eV	: Electron Volt
MHz	: Mega Hertz
nm	: Nanometer
ADF	: Annular Dark Field
CN	: Coordination Number
EXAFS	: Extended X-Ray Absorption Fine Structure
iwi	: Incipient Wetness Impregnation
MCM-48	: Mobil Composition of Matter No. 48
MNPs	: Metal Nanoparticles
NMR	: Nuclear Magnetic Resonance
NPs	: Nanoparticles
POSS	: Polyhedral Oligomeric Silsesquioxanes
PVP	: Polyvinylpyrrolidone
r.t.	: Room Temperature
SBA-15	: Santa Barbara Amorphous-15
STEM	: Scanning Transmission Electron Microscopy
TCD	: Thermal Conductivity Detector
TPR	: Temperature Programmed Reduction
XANES	: X-Ray Absorption Near Edge Spectrum
XAS	: X-Ray Absorption Spectroscopy
XPS	: X-Ray Photoelectron Spectroscopy
XRD	: X-Ray Diffraction

LIST of FIGURES

LIST of TABLES

1. INTRODUCTION

Amines are used in various fields such as dyes, plastics, detergents and the pharmaceutical industry as high value-added organic materials [1]. Methods such as alkylation of ammonia with alcohols or haloalkanes and reduction of compounds containing a nitrogen atom in the event of a higher oxidation are some of the methods used to produce amines at small-scale. (for example: nitro, nitrile, amide, imine, oxime compounds) [1]. However, in the case of large-scale production, most of these methods are not commercially viable for reasons such as cost of starting materials, several reaction steps, regioselectivity, formation of a considerable amount of waste material and lack of complete control over crushing purification procedures [2]. For instance, it has been reported that a common method to reduce amides into amines by using stoichiometric amounts of metal hydride reagents such as $LiAlH_4$, $NaBH_4$ or borane (B_2H_6) is applicable for only 0.6% of chemical transformations [2]. For example, a common method of reducing amides to amines has been reported to be applicable to only 0.6% of chemical conversions using stoichiometric amounts of metal hydride reagents such as $LiAlH_4$, $NaBH_4$ or borane (B_2H_6). In general, industries that produce amines in such high-cost, multi-step processes deal with a large number of by-products as waste which in return gives separation and disposal problems. In addition, most processes result in the synthesis of the equilibrium distribution of primary, secondary and tertiary amines, which exhibit low selectivity to the desired one [3].

For environmental and practical issues, hydrogen gas is the ideal reductant for C=O functional groups due to high atom efficiency with no waste production and water as being the only by-product. However, amides are known to be thermodynamically highly stable carboxylic acid derivatives due to the least electrophilic amide functional groups [4]. Therefore, hydrogenation of amides by molecular hydrogen is a challenging reaction which requires an active and effective catalyst. Nevertheless, the simplistic picture of amide hydrogenation is frequently not realized in practice due to competing side reactions having lower activation energies. Catalytic reduction of amides can follow two pathways: C-O or C-N bond cleavage [5,6]. The first route leads to the preferred amine while the latter results in less desirable alcohol and primary/secondary amines. The alteration in geometric and electronic effects on a new class of encapsulated bimetallic catalysts may offer exciting way to tune the adsorption

mode and strength of substrates that would be selective for the hydrogenation of amides to desired amines. Developing a long-live, selective, robust and reusable catalyst working under mild reaction conditions can reduce the reaction steps, increase the yield, minimize the waste and decrease the energy consumption used during the synthesis and workup.

In this study, we used the organometallic synthesis method for the production of well-defined bimetallic Rhenium-Ruthenium (ReRu) nanoclusters in terms of size, composition and atom ordering. During the synthesis, we benefited from the use of porous materials as hosts for bimetallic nanoparticles (NPs) rather than using traditional non-porous structures. The morphology of the porous materials used (SBA-15, MCM-48, Ti-SBA-15, Al-MCM-48) can provide stability and robustness due to their rigid structure, which prevents the sintering of particles and limits their growth according to their pore size. Moreover, the presence of extra framework cations (Na^+ or K^+) or Bronsted acidic sites (H^+) and Lewis acidity of metal cation introduced might act as electronic promoters for the adsorption and activation of C=O functional groups. After the synthesis of novel solid-state materials, their catalytic performance in amide hydrogenation were investigated first under batch conditions and compared with the nanocatalysts produced with the nonporous support materials such as TiO_2 and SiO_2.

Low abundancy and high cost of the chosen metals, Re and Ru, might be contradictory to the ideas of this study. However, aim of this study is to develop highly atom-efficient, stable and reusable class of heterogeneous catalysts having low metal content by synthesizing small nanoclusters (<2 nm) with more than 70% of atoms exposed to surface. The encapsulated metal clusters are well-controlled in size and surface composition within the pores of micro/meso-porous materials. Moreover, additional functionalities such as Bronsted acid or Lewis acid sites could be simultaneously introduced to enhance adsorption of amide substrates. Such a new class of porous composite catalysts can provide high efficiency and low operational costs which will compensate the cost of the precious metal used.

1.1. Chemical Synthesis Techniques of Metal Nanoparticles

Over the last few years, importance of nanoscience and nanotechnology increases such that many scientific and engineering communities are interested in this

field as well as funding agencies that invest the money in their research [7]. When the number of publications is searched between 1999 and 2018, an exponential increase is observed where number of publications exceeds over 14,000 in 2018 (Figure 1.1). One of the most important forces for the evaluation of this field is the high potential of NPs, predominantly the metallic one, finding their place in the wide spread scientific areas such as chemistry [8], physics [9], biology [10], medicine [10], electronics [11], and material science [12].
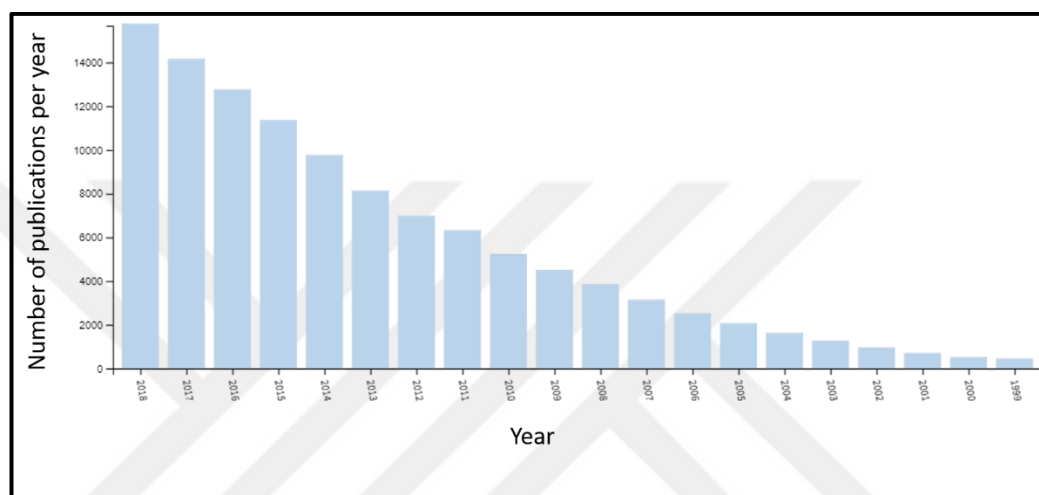
Figure 1.1: Number of publications about metal nanoparticles (1999-2018). Web of Science, Keyword: Metal nanoparticles.

Metal nanoparticles (MNPs) are called as "nanoclusters" because they are between molecular and bulk counterparts with respect to their state of matter [13]. Their size is larger than individual atoms and molecules, but they are still small enough not to be considered as bulk solid. Therefore, they obey neither absolute quantum chemistry nor laws of classical physics and thus have properties that differ markedly from those expected. Electronic properties of MNPs such as conductivity, magnetism etc. are differ from bulk metal; the electronic states in the valence band and the conductivity band reduces respectively with the reduction of size to such an extent that the electronic properties change dramatically [14]. Quantum size effect shows that electronic state of matter will decrease incessantly from bulk system (three-dimensional system) to quantum dots (zero-dimensional system). NP is thought as a package that has thousands of atoms. It is of great properties that electrons trapped in

such a particle must have discrete energy levels [15]. The electronic configuration of matters is presented in Figure 1.2.
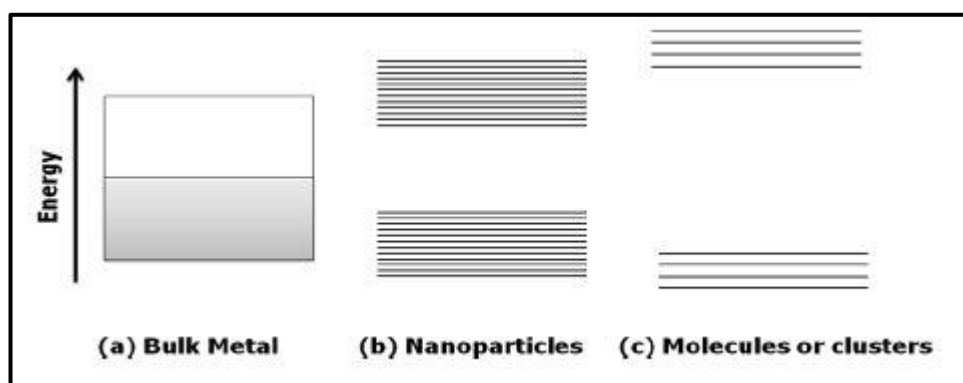
Figure 1.2: The electronic state of matters.

In literature, there are a lot of different types of synthesis methods for MNPs. In these methods, main parameter for effectivity of the techniques can be listed as control of size, shape, crystal structure and stable chemical and physical properties. Moreover, the control of the aggregation rate, the lowest possible impurities present and possibility of scaling up and reproducibility with the lowest costs are important for production of MNPs. All of these techniques can be collected in two main approaches. The first, top-down method is a technique that applies external forces to bulk material in order to break into smaller particles. It is also called "breakdown" method. The second is bottom-up method that produces NPs starting from atoms. It is called "build-up" method [16]. These two approaches are summarized in Figure 1.3.
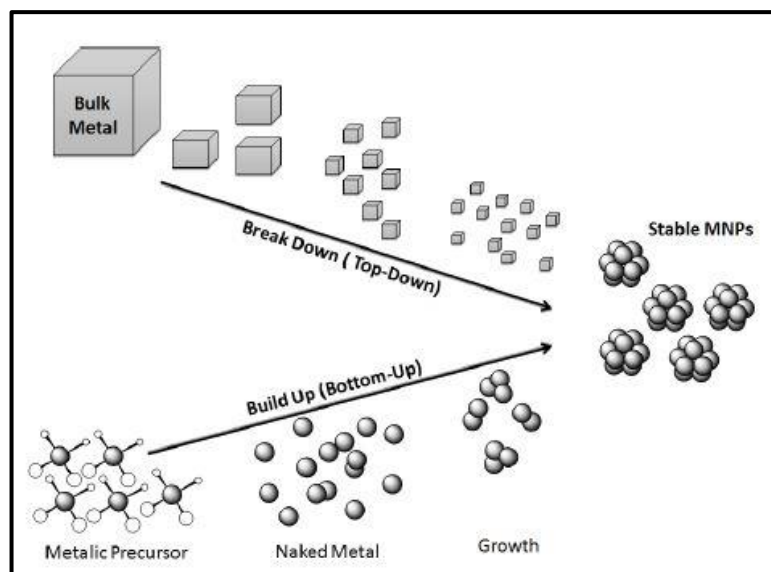
Figure 1.3: The general approaches for production of nanoparticles.

In the top-down approach, physical forces like shock, compression, friction etc. are used for breaking down a bulk material into intended size particles. This application occurs in the wet or dry media. But, it is so hard to obtain dispersed particles especially in dry media for the condensation of the small particles. The wet medium solves this problem but decreasing particle size of matter causes agglomeration problems [17]. On the other hand, bottom-up approach is a widely used technique to eliminate the condensation of particles. This method is divided into two main groups; gaseous phase and liquid phase techniques. Liquid phase methods are major preparation routes to produce NPs. Chemical reduction method is a branch of liquid phase and commonly used one to obtain fine NPs. The chemical reduction method has many advantages for production of NPs. Various sizes and shapes of NPs such as nanowires, nanorods, nanoplates and hollows can be synthesised by using this method with basic chemistry equipments. Also, by this method, tune of the morphology and size of the NPs by changing different reaction parameters such as metal source, reducing agent, stabilizer, solvent, reaction time, temperature and pressure are possible [18,19].

1.1.1. Nucleation and Growth Nanoparticles Mechanism

Many scientists try to explain the mechanism for stepwise formation of nanoclusters. Most known and provided theory was developed by LaMer, Turkevich

and Finke [20,21]. LaMer described the formation of sulphur sols from the decomposition of sodium thiosulfate in hydrochloric acid in 1950. This widely cited mechanism assumes that homogeneous nucleation occurs until a nucleus of critical size is obtained. After LaMer's work, Turkevich and co-workers tried to explain for the stepwise formation of gold NPs based on nucleation, growth, and agglomeration by electron microscopy. In 1997, Finke and Watzky reported a two-step mechanism for metal salt reduction and then, a more general mechanism for transition metal nanocluster formation was reported [22]. The general mechanistic formation of MNPs can be simplified on three steps; nucleation, growth and agglomeration. Difference between the redox potentials of the metal salt, the reducing agent, the reaction conditions including the rate of addition and the reaction temperature are factors that they affect the particle size, the shape and the morphology [20,21]. The nucleation mechanism is shown in Figure 1.4.
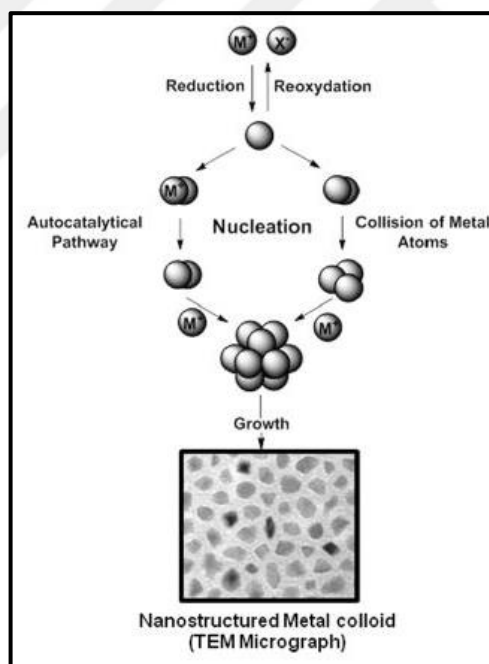
Figure 1.4: The metal nanoparticle growing mechanism.

Nucleation is the most important step for MNP production. It is very hard to control the formation of nuclei directly in real space and time. The particle is visible only using an electron microscopy, but it has grown beyond the nucleation stage. In the first step of the nucleation process, the metal salt is reduced to give zero-valent metal atoms, which crash into with other atoms, or small clusters, to form the first

permanent "seeds" of stable metal nuclei [23]. The diameter of the ''seeds'' can be well below 1 nm depending on the strength of the metal-metal bonds and the difference between the redox potentials of the metal salt and the reducing agent applied.

1.1.2. Chemical Reduction Methods

In 1857, first chemical reduction of transition metal salts was published by Faraday. The aim of this study was to synthesize zero-valent metals in aqueous media through stabilizing agents [24]. This method has been accepted as most suitable and powerful approach for synthesis of NPs in the bottom-up approach. Controlling size and shape of transition MNPs are the most important parameters of the chemical reduction method. Also, the characteristic properties of NPs are very important with respect to their targeted applications. Many scientists modified this method according to their applications. Some of these NPs were used as catalysts and some important routes for the synthesis of catalysts are summarized below.

- The transition metal salts in solution can be reacted with using different type of reducing agents like alcohols, dihydrogen, silanes, sodium borohydride etc. Under high H_2 atmosphere, metal salts can be reduced by using mild temperature [25].
- Another reduction method was developed by using thermal, photochemical, sonochemical decomposition etc. [26].
- Using organometallic precursors and stabilizing ligands is a technique for reduction [27].
- Metal vapor synthesis and electrochemical reductions can give as example of reduction of transition metal salts [28].

Most important parameter of reducing MNPs is the stabilization in order to restrain agglomeration or aggregation. Especially in catalysis applications, the stabilizer has an important role on the catalyst performance. Therefore, the choice of the stabilizer is vital for MNP reactivities.

1.1.3. Organometallic Synthesis Approach

The size, shape and surface of MNPs have an effect on physical and chemical properties of the materials. Therefore, scientists need efficient synthetic methods for

controlling these characteristic properties of MNPs by using modern nanoscience techniques. The organometallic chemistry techniques are very suitable for the achievement of well-controlled nanostructures. The organometallic synthesis approach is based on the use of the metal complexes as the source of metal and their reduction or decomposition in the presence of appropriate stabilizing agents which may be several functional molecules like surfactants, polymers, dendrimers etc. [29,30].

The type of stabilizer has an important role in the synthesis as well as the performance of MNPs. The MNPs have Van der Waals forces among them. Thus, normally these NPs tend to come together and aggregate. This will affect the size and the surface area of the MNPs, so the active surface area of MNPs will decrease [31].

Organometallic precursors are chosen according to their ability of decompose under the mild reaction conditions. The decomposition prosses are conducted by using reactive gases like H_2 or CO to obtain naked zerovalent metal atoms. These naked atoms will tend to join together to form the permanent seeds. The control of size and blocking of agglomeration is important until the growing reaction, so stabilizers make a steric barrier around MNPs through chemical or physical interactions between the NP surface and the stabilizer (Figure 1.5). The polymers or dendrimers limit the excess growing of particles according to electrostatic forces which comes from coordinating ligands or sterical hindrance [32,33].
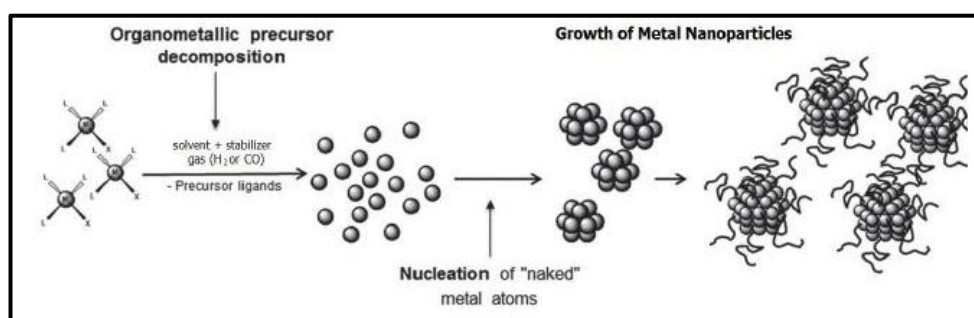
Figure 1.5: Organometallic approach representation for production of metal nanostructures.

The main advantage of the organometallic synthesis method is the control of the reaction conditions and the size, the shape and the morphology of the MNPs. The absence of oxidation and surface species gives clean and good quality chemical and physical properties of NPs.

Olefinic and allylic complexes are widely used metal precursors because they are reduced under mild reaction conditions by using dihydrogen pressure and ligands transform to alkanes which are lack of surface of the NPs. Tris-Allyl Rhodium ($Rh(C_3H_5)_3$), Bis- 1,5-Cylooctadiene Nickel (Ni (COD)$_2$), 1,5-Cylooctadiene 1,3,5-Cylooctatrien Ruthenium (Ru (COD)(COT)), Tetra-allyl di-Rhenium ($Re_2(C_3H_5)_4$) are some examples of easily decomposable metal precursors. They are good metal sources for NP synthesis where in some cases, they also release potential stabilizing molecules for the NPs. For example, complexes such as [Rh(acac)(C_8H_{12})] (acac = (CH_3CO)$_2$CH) or CpCuBuNC (Cp = C_5H_5), that release acacH and CpH/ BuNC respectively [34–36]. In addition to these precursors, some carbonyl complexes such as $Co_2(CO)_8$, $Rh_6(CO)_{16}$ and $Ir_4(CO)_{12}$ are used for the synthesis of well stabilized NP, but reaction conditions for reduction is so high with respect to temperature. Moreover, CO molecules coordinate to surface of MNPs, blocking the active cites.

1.1.4. Metal Nanoparticles (MNPs) for Catalytic Activities

A catalyst is a chemical compound that accelerates a chemical reaction but moves out from the reaction without any changes. They are generally used for catalytic reactions in industry or laboratory studies [37]. The catalysts make alternative reaction pathways available through different transition states or lowering the activation energy. The activation energy is an important parameter for a chemical reaction because it is defined as the minimum energy to overcome in order to have a reaction, so lower activation energy increases the probability of collisions of molecules which in return aid in reaching the transition state of molecules. Moreover, the catalysts enhance reaction rate, selectivity and reaction conditions such as low temperature. The energy profile diagram of a reaction is shown in Figure 1.6. In this figure, all thermodynamic properties of reaction remain stable because the catalysts spring from reaction as unchangeable. Briefly, they do not have an effect to the chemical equilibrium of reaction by affecting forward and reverse reactions at the same rate [38].
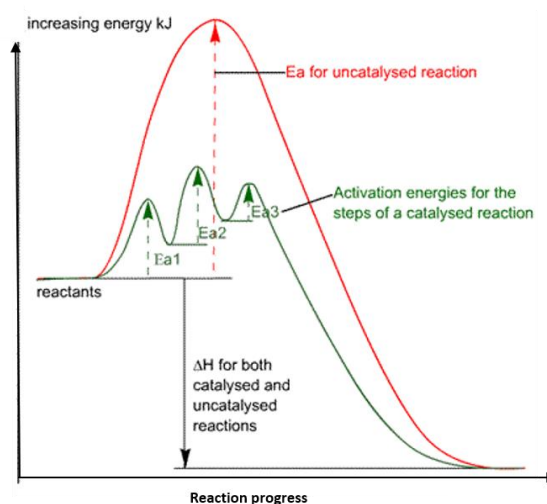
Figure 1.6: The energy diagrams for a chemical reaction according to catalysed or uncatalyzed.

The environmentally friendly catalysts should have some characteristics such as rapid and selective chemical transformations, easily removal from the reaction media and reusability with respect to green catalysis aspects [2,39]. This perspective brings new idea for catalysis scientific area. It is called as "nanocatalysis" [40,41]. The nano-catalysts performance is better than the bulk catalyst types because the nanocatalysts have smaller particle size. The nano-sized particles enhance the surface area of the catalysts so the active contact surfaces between reactants and catalysts increase. Also, mostly heterogeneous nanocatalysts are insoluble in solvents, so they can easily isolate from reaction mixture at the end of the reaction. The selectivity of nanocatalysts can be adjusted by changing chemical and physical features such as size, shape, composition and morphology [42,43]. In addition to these advantages, NPs reusability. The transition metal (Pt, Pd, Ni, Re, Ru, Co, Fe etc.) NPs have more activity than their bulk-counterparts in different types of the chemical reactions such as Heck-type couplings, Suzuki couplings, McMurry couplings, aromatization processes, hydrocracking and catalytic reforming reactions etc. [13,43,44].

NPs are used in many different areas such as optical, medicine, food safety, energy etc. without understanding precisely their features and behaviours. But, in the last century, the development in the areas of both nanoscience and nanotechnology gave rise to better understand of NP properties and behaviours. NPs have vital properties such as large surface area to volume ratio and special confinement of

electrons [45,46]. The recent studies about the properties of NPs make them easier to use for industrial developments. Some of applications are summarized below.

In biology area, NPs such as gold, silver, platinum etc. have been used for cancer treatments, non-toxic drug delivery and gene delivery applications. Other MNPs such as cerium oxide have been used as antioxidants in patient's bloodstream and for the cure of traumatic injuries. Also, silver and titanium MNPs have been used as antimicrobial agents. Titanium dioxide are used as additives, and in personal care products etc. [47,48].

In energy and electronics areas, MNPs have been used for the fabrication of the electrically conductive nanopatterns such as photovoltaic cells, light-emitting diodes, organic thin film transistors, smart clothing, sensors and fuel cell applications. MNPs have unique electrical features and this feature can be modified according to the targeted application areas. Also, MNPs have been used in fuel cell technologies in order to have large surface area and good oxidation-reduction features as electrocatalysts [49,50].

In environmental areas, MNPs have been used for solving big environmental problems, which come from using excess and uncontrolled chemical compounds, such as pesticides, dyes, polychlorinated hydrocarbons etc. Iron MNPs (Fe NPs), a good example for this application, are used for groundwater, hazardous waste treatment and for Fischer-Tropsch reactions etc. MNPs appear as a great solution for fuel problems with respect to biofuel evolution and syngas technologies [51,52].

1.2. Catalytic Hydrogenation of Amides

Amines are very valuable organic compounds used for different purposes in industries including dyes, pharmaceutical industry, solvents, additives, anti-foam agents, corrosion inhibitors, plastics [53]. The production capacity of amines reaches to 100.000 tonnes per year. Amines should not be seen as bulk chemicals but as high value intermediates for chemical compounds in organic synthesis [5]. Especially in laboratory scale, amine productions are conducted by using several methods such as alkylation of ammonia with alcohols and reduction of compounds at a higher oxidation state [54]. The reaction steps, waste materials formations, cost of materials and

difficult purification processes are reasons in restraining for large scale productions [2]. The reduction of amides to amines process is explained in Figure 1.7.
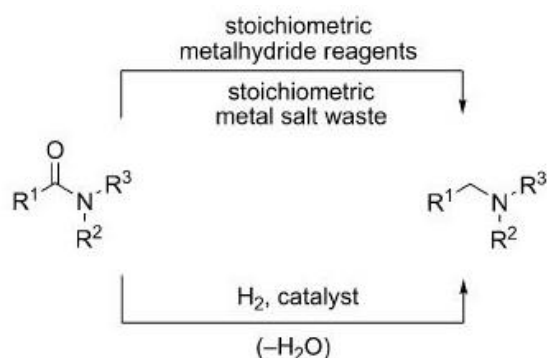
Figure 1.7: The amides hydrogenation process.

Commonly, stoichiometric amounts of metal hydride reagents such as $LiAlH_4$, $NaBH_4$, borane (B_2H_6), DIBAL, RedAl, triethyl silane or polymethylhydroxysilane are used for reduction of amides to amines products. These reagents are listed in Table1. The chemical transformation of these reagents is very low which is around 0.6% [2,55]. In addition, these reagents have poor atom efficiency, the removal of stoichiometric metal waste and safety is always a problem. Thus, hydrogen gas is the ideal reductant for amide hydrogenation in order to obtain only water at the end of reaction. Against to this advantage, amides are a carboxylic acid derivates which are highly stable thermodynamically. The ACS Green Chemistry and pharmaceutical companies published a list about future chemical reactions for production of chemicals with more economical, safe and environmental issues in 2005. Amine reduction is a top member of this list [56]. In 2007, the ACS Green Chemistry Institute announced a desire for amide reduction according to selective and environmentally aspects [2].

Table 1.1: The summary of stochiometric metal hydrate reagents for amide hydrogenation.

Reducing Agent	Reaction Conditions	Functional Groups Reduced	Advantages	Disadvantages	Refs.
LiAlH$_4$	Ambient	Carboxamides, acids, esters, acyl halides, aldehydes, ketones, nitriles, no reduction of alkenes	mild conditions, efficient	stoichiometric reaction, limited selectivity, hazardous, difficult to handle, workup/waste disposal	[57–59]
NaBH$_4$	Ambient	Aldehydes, ketones, acyl halides	mild conditions, less hazardous than LiAlH$_4$	stoichiometric reaction, dehydration to nitrile (for primary amides), workup/waste disposal	[60–63]
NaBH$_4$	>100 °C	All acyl groups, nitriles		stoichiometric reaction, higher reaction temperatures, workup/waste disposal	[64–66]
B$_2$H$_6$/THF	Ambient	Preferred for carboxamides, carboxylic acids, and nitriles	efficient, selective, quantitative yields of amine	stoichiometric reaction, hazardous/pyrophoric, workup/waste disposal	[67,68]
Electrolytic reduction	Ambient, H$_2$, e$^-$	All groups	mild conditions	stoichiometric reaction, limitation to substrates generating aryl radicals, product selectivity, energy intensive	[69,70]
Reaction of amides with halogens and hypohalites, and subsequent reduction using above reagents	Ambient	General	less energy intensive than hydrogenation using H$_2$ (until recent developments)	indirect, multistage, stoichiometric, waste disposal costs	[71]

For this purpose, effective and selective catalysts are necessary for amide hydrogenation with the elimination of the undesired product such as alcohol or other organic compounds [6]. Many different types of catalysts were developed by scientists

13

in order to obtain desired amine products. In addition to catalyst type, the scientists focused on the process conditions for hydrogenation of amides. Some of the reduction mechanisms of amides are shown in Figure 1.8.
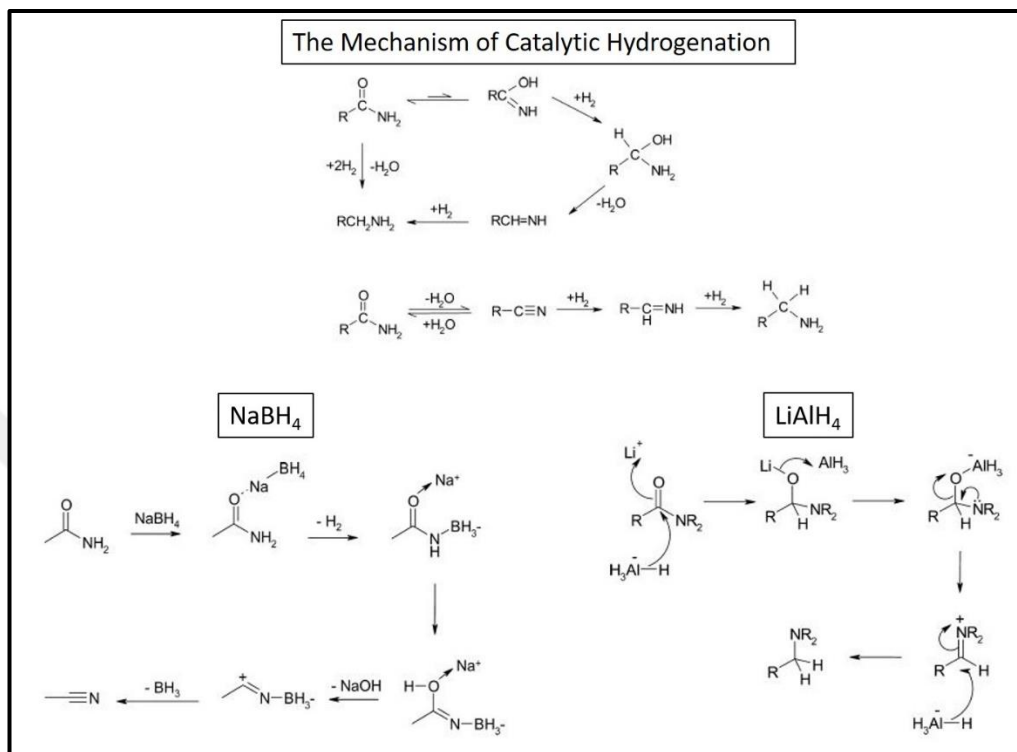
Figure 1.8: Schematic of the Different methods for hydrogenation of amides.

In this section, catalysts types which were used for hydrogenation of amides are summarized in Table 1.2 and some of them are explained detailly [72].

Table 1.2: Summary of the MNPs used for the amide hydrogenation reactions.

	Amide substrates	Catalyst component	Press. (bar H_2)	Temp. (°C)	Time (h)	Products	% yield	% Conv..	Ref.
1	$C_{11}H_{23}C(O)NH_2$	Co, Ni	200	230	8	$(C_{12}H_{25})_2NH$			[73]
2	$C_{11}H_{23}C(O)NH_2$	Cu/Cr	200-300	250	0.8	$C_{12}H_{25}NH_2$	48		[73, 74]
						$(C_{12}H_{25})_2NH$	49		
3	$C_7H_{15}C(O)NH_2$	Cu/Cr/NH_3	250-330	275-350		$C_8H_{17}NH_2$	90	>99	[75]
						$(C_8H_{17})_2NH$	10		
4	$C_7H_{15}C(O)NH_2$	Ni/NH_3	370	280		$C_8H_{17}NH_2$	55		[75]
						$(C_8H_{17})_2NH$	21		
5	$CH_3C(O)NH_2$	ReO_3	205	200	18	$C_2H_5NH_2$	88		[76]
6	$H_2NC(O)(CH_2)_4C(O)NH_2$	Ru/alumina /NH_3	100	240-290	12	$H_2N(CH_2)_6NH_2$	poor		[77]
7	$CyC(O)NH_2$	Ru/Re	50–100	160	16	$CyCH_2NH_2$	90	100	[78]
						$(CyCH_2)_2NH$	poor		
						$CyCH_2OH$	poor		
8	$CyC(O)NH_2$	Rh/Mo	50–100	130–160	16	$CyCH_2NH_2$	85	100	[79]
						$(CyCH_2)_2NH$	poor		
						$CyCH_2OH$	poor		
9	$CyC(O)NH_2$	Rh/Re	50–100	150-160	16	$CyCH_2NH_2$	90	98	[78]
						$(CyCH_2)_2NH$	poor		
						$CyCH_2OH$	poor		
10	$PhC(O)NH_2$	Ru/Mo	100	160	16	$CyCH_2NH_2$	83	100	[80]
						$CyCH_2OH$	16		
11	$CH_3C(O)N(H)Ph$	Re_2O_7	280	170	52	$C_2H_5N(H)Ph$	66		[76]
						$PhNH_2$	34		
12	$CH_3(CH_2)_2N(H)C(O)CH_3$	Pd/Re/C	30	160	20	$CH_3(CH_2)_2N(H)C_2H_5$	100	>99	[81]
13	*N*-acetylpyrrolidine	PtV/TiO_2	10	130	16	*N*-ethylpyrrolidine	20		[82]
14	*N*-methylpyrrolidin-2-one	PtRe/TiO_2	20	120	24	*N*-methylpyrrolidine	99	>90	[83]
15	$(C_2H_5)_2NC(O)CH_3$	Pd/Re/graphite	30	160	20	$N(C_2H_5)_3$	100	>99	[81]

The catalysts are mainly divided into two groups; homogenous and heterogeneous types. The pathway of reaction affects the final product, so the catalysts must be selective for the desired amine product. Possible catalytic pathways are shown in Figure 1.9.
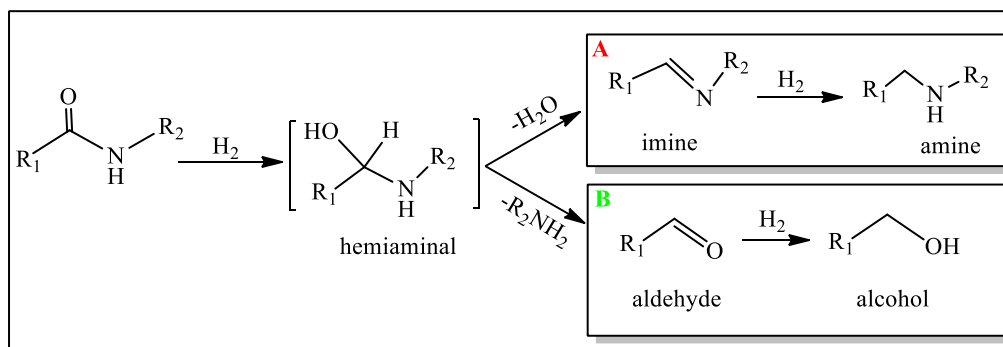
Figure 1.9: The catalytic pathway for amide hydrogenation.

The homogenous catalysts are in the same phase with the reactants in the reaction which is generally in the gas or solid phase. In the amide hydrogenation process, the catalysts that include ruthenium (**Ru**) as metal, can follow both pathways, such as C-N or C-O bond cleavage [6]. The bond cleavage is shown in Figure 1.10. [6].
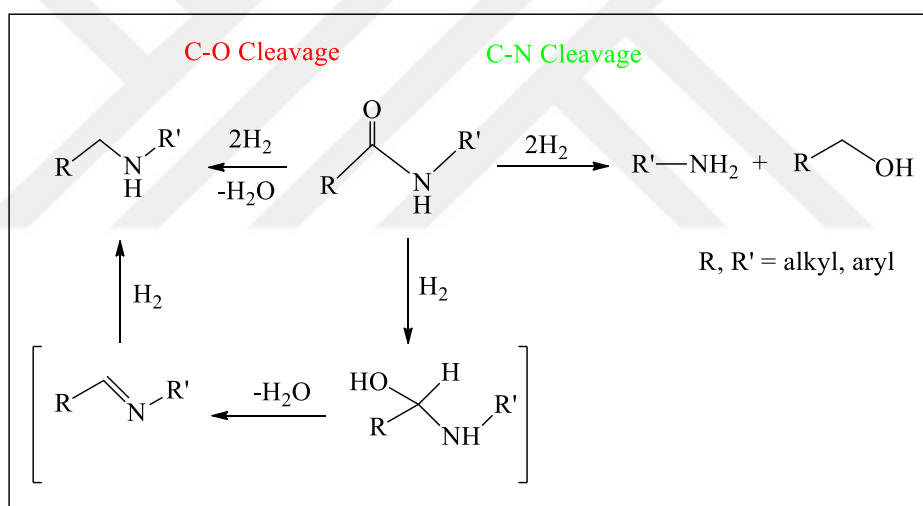
Figure 1.10: The pathway of bond cleavage for C-N and C-O.

There are many examples of catalysts used for hydrogenation of amides in the literature. The examples of C-N bond cleavage are summarized below:

Crabtree and co-workers published the first example of homogenous catalyst for amide hydrogenation in 2003. Using Ru(acac)$_3$ with several phosphines, the propenamide was hydrogenated at 164°C and 69 bar H$_2$ pressure. The activity and selectivity were recorded 76.4% and 93.7%, respectively [17].
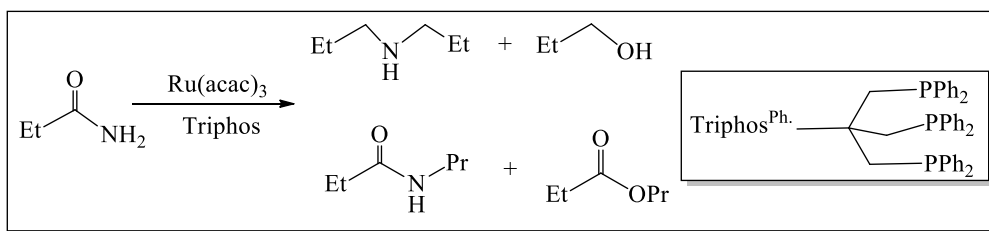
Figure 1.11: The hydrogenation of amides was conducted by Crabtree and co-workers in 2003.

In 2010, Milstein and co-workers enhanced a Ru pincer complex which was used for the hydrogenation of various types of amides. It had no selectivity; both alcohols and amines were obtained at the end of the reaction which occurred under mild reaction conditions ($110^{\circ}C$ and 10 bar H_2) without the use of any additives. These are good advantages for this type of reaction mechanism [84].
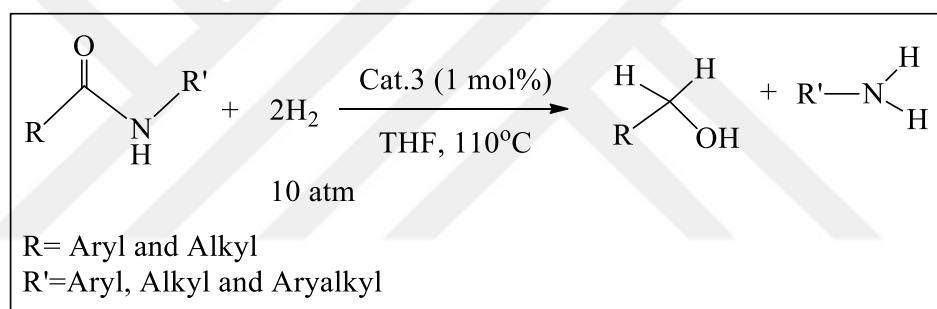
Figure 1.12: The hydrogenation of amides was conducted by Milstein and co-workers in 2010.

In 2011, Ikariya and co-workers developed highly selective catalysts for hydrogenation of carboxamides and esters to primary alcohols at $100^{\circ}C$ and 50 bar H_2 by using $Cp*RuCl(2-C_5H_4NCH_2NH_2)$ as a catalyst [85].
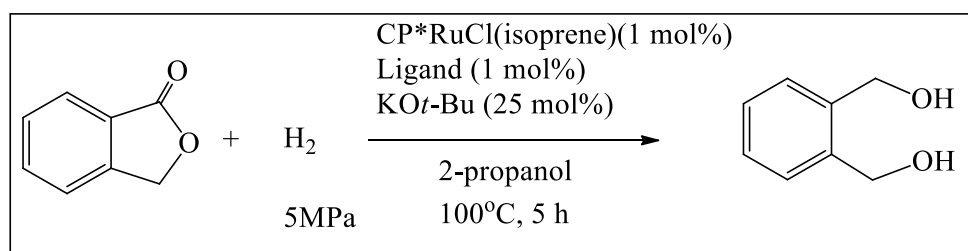
Figure 1.13: The hydrogenation of amides was conducted by Ikariya and co-workers in 2011.

In 2011, Bergens and co-workers advanced the catalysts, which was in principle the same as the Milstein's catalyst; a π-allyl ruthenium complex and a base (KN [Si (CH$_3$)$_3$]$_2$), for using especially secondary and tertiary amides reduction at 100°C and 50 bar H$_2$. Final products of reaction were same as Milstein's reaction [86].
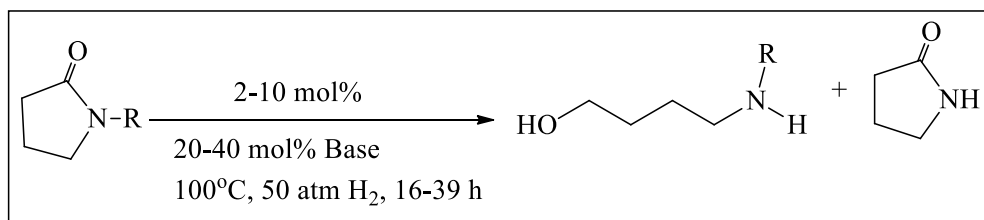
Figure 1.14: The hydrogenation of amides was conducted by Bergens and co-workers in 2011.

In 2017, Saito and co-workers developed a more selective method for the amide hydrogenation by using Ru complexes in a bulk base at 110°C and 10 bar H$_2$ pressure. The catalyst was selective for C-N or C=O bonds [87].
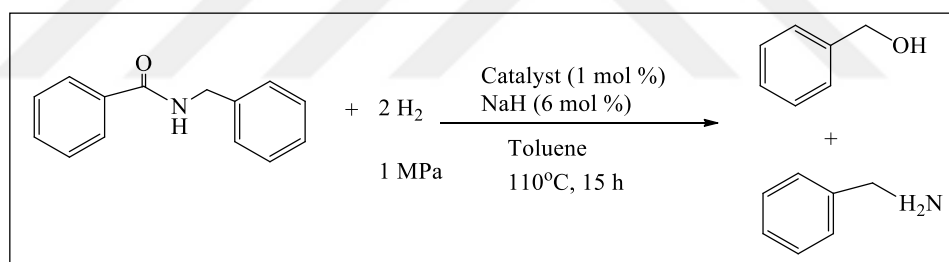
Figure 1.15: The hydrogenation of amides was conducted by Saito and co-workers in 2017.

Other than the catalysts mentioned above that enabled the C-N bond-cleavage, the C-O bond cleavage process was investigated by Cole-Hamilton and co-workers in 2007 [88]. They changed the reaction conditions of the traditional technique developed by Crabtree. They prepared a catalyst using Ru(acac)$_3$ and triphos mixture. The mixture worked well under 164°C and 40 bar H$_2$ pressure. Full conversion of N-phenylnonamide and 99% selectivity was observed at the end of reaction. But, the catalyst could not stay stable under these reaction conditions. Moreover, they realized that when the reaction temperature was decreased, the selectivity of catalyst was also decreasing, and alcohol production was increasing. The final product was only alcohol

at 100°C. In 2013, a new procedure of hydrogenation of aliphatic and aromatic amides was published by Cole-Hamiltan and co-workers. The mechanism was developed by using methane sulfonic acid (MSA) with $Ru(acac)_3$ and triphos at high temperature (200-220°C) and low pressure H_2 gase (10 bar). The aromatic amides were hydrogenated to amines without any C-N bond cleavage in this method [89].
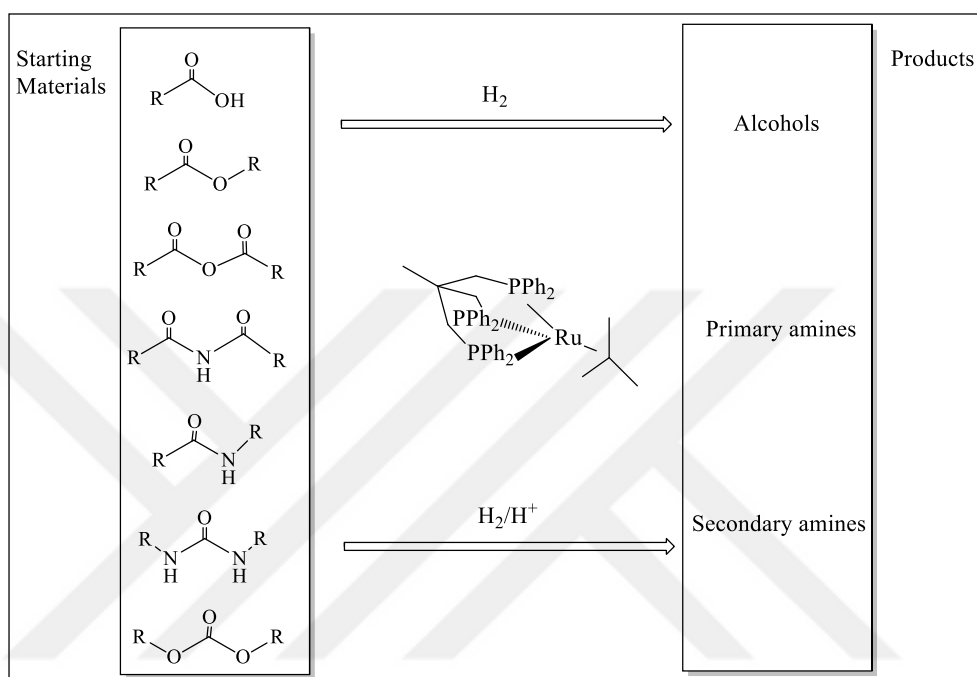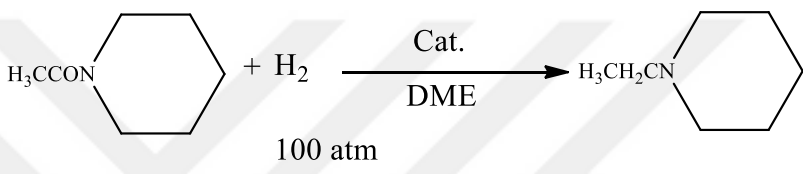
Figure 1.16: The new method for hydrogenation of amides was conducted by Cole-Hamilton and co-workers in 2013.

The heterogenous catalysis differ from homogenous catalysis according to phase of the catalyst and reactants. The catalyst and reactant phases are in different phases in the heterogeneous catalysis. This type of catalysts is useful in order to increase the rate of reaction. Different type of heterogenous catalysts have been used in the hydrogenation of amides. The significant achievements are shown below.

The first example of heterogenous catalysts for hydrogenation of amides is copper chromite [90] or rhenium oxide [91] under harsh reaction conditions (170-260°C and 100-352 bar H_2 pressure). The improvement of catalyst by using copper chromite with zeolite for hydrogenation of tertiary amides was achieved under 200-400°C and 140-350 bar H_2 pressure without any change in the final products. This reaction was conducted by Richard M.King in 1984 [92].

In 1990, Dobson and co-workers developed the first bimetallic catalyst of palladium (Pd) and Re on the graphite/zeolite surface. The catalyst was used for the hydrogenation of the propionamide at 200ºC and 260 bar H_2 pressure. The conversion rate was obtained as 99%, but the selectivity was low because di and tri-propylamines were acquired instead of mono-propylamine [93].

In 1996, Fuchikami and Whyman [94] used rhodium based catalysts such as Rh/Re, Rh/W or Rh/Mo etc. for amide hydrogenation under mild reaction conditions (130-170ºC and 20-100 bar H_2 pressure). The catalysts and the corresponding reaction conditions are shown in Figure 1.17. [95].

Entry	Cat. 1	Cat. 2	Temp. (ºC)	Conv. (%)	Yield (%)
1	$Rh_6(CO)_{16}$		160	24	19
2	$Ru_3(CO)_{12}$		160	1	1
3	$Re_2(CO)_{10}$		160	14	7
4	$Mo(CO)_6$		160	2	2
5	$W(CO)_6$		160	1	1
6	$Rh_6(CO)_{16}$	$Re_2(CO)_{10}$	160	100	96
7	$Rh_6(CO)_{16}$	$W(CO)_6$	160	51	50
8	$Rh_6(CO)_{16}$	$Mo(CO)_6$	160	100	98
9	$Ru_3(CO)_{12}$	$Re_2(CO)_{10}$	160	100	96
10	$Ru_3(CO)_{12}$	$Mo(CO)_6$	170	55	54
11	$Ru_3(CO)_{12}$	Re/ C	170	83	82
12	Rh/ C	Re/ C	170	100	98
13	$Ru_3(CO)_{12}$	Re/ Al_2O_3	170	100	94
14	Ru/ Al_2O_3	Re/ Al_2O_3	170	100	92

Figure 1.17: The hydrogenation of N-acetylpiperidine by using different types of catalysts.

In 2005, Smith et al. developed bi and tri-metallic catalysts for hydrogenation of amide under the below 200ºC and 50 bar H_2 pressure. Many catalysts combinations

were tried with different support materials. PtReIn/silica trimetallic catalyst gave best activity for 1-acetylpiperidine at 130°C and 10 bar H_2, but corrosive acetic acid was used in this reaction [96].

In 2011, Thompson's group explained the role of metals in the catalyst by using DFT calculations. It was found out that rhenium activates the C=O cleavage and platinum metal acts as a good hydrogenation catalyst. The increase in velocity observed on the TiO_2 support was attributed to the presence of an oxygen gap allowing the adsorption and attenuation of the C = O bond [97].
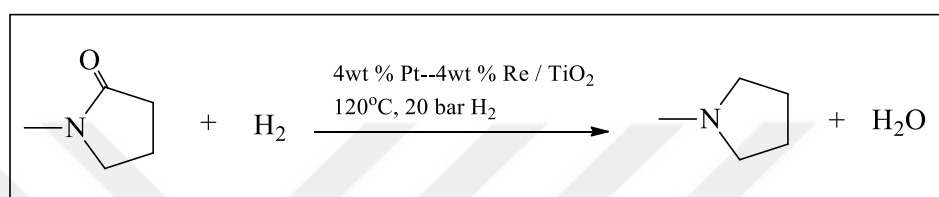
Figure 1.18: The hydrogenation of amides for DFT analysis was conducted by Thompson and co-workers in 2011.

In 2013, Breit and co-workers enhanced the Re based bimetallic catalysts for hydrogenation of various types amides under mild reaction conditions. Pd/Re/graphite catalyst was used for the hydrogenation of N-acetylpyridine at 120°C and 10 bar H_2 pressure with 85% conversion [55].
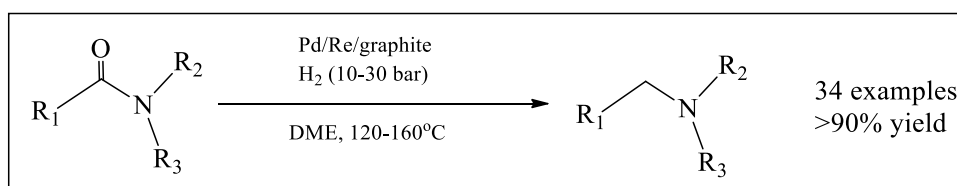
Figure 1.19: The hydrogenation of N-acetylpyridine was conducted by Breit and co-workers in 2013.

In 2017, Mitsudome and co-workers used Pt-based bimetallic nanocatalysts for amide hydrogenation under the mild reaction conditions where many different support materials were tested. PtV/HAP bimetallic catalyst gave best performance for different type of amide groups at 70°C temperature and 30 bar H_2 pressure [98].
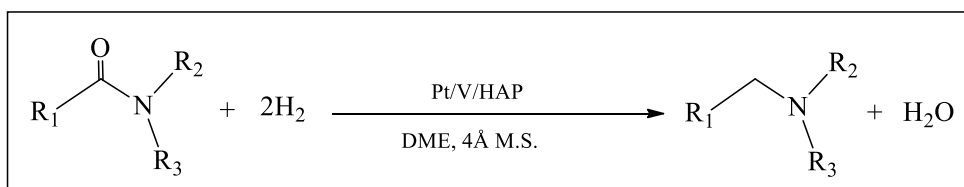
Figure 1.20: The hydrogenation of amides was conducted by Mitsudome and co-workers in 2017.

The formation of NPs affects the activity and selectivity of catalysts in the reactions. All these catalysts are prepared under harsh conditions such as wet-impregnation of metals on a support, high temperature calcination process etc. [55,93,97,99]. For these reasons, highly active, selective and high conversion rate ReRu bimetallic nanocatalyst was synthesised by using incipient wetness impregnation technique and organometallic approach in this MS study.

There are some differences between heterogenous and homogenous catalyst types of catalysts. The heterogenous catalysts are preferred in the amide hydrogenation in order to have reusability features. Main advantages and disadvantages are summarized in Figure 1.21. [100].
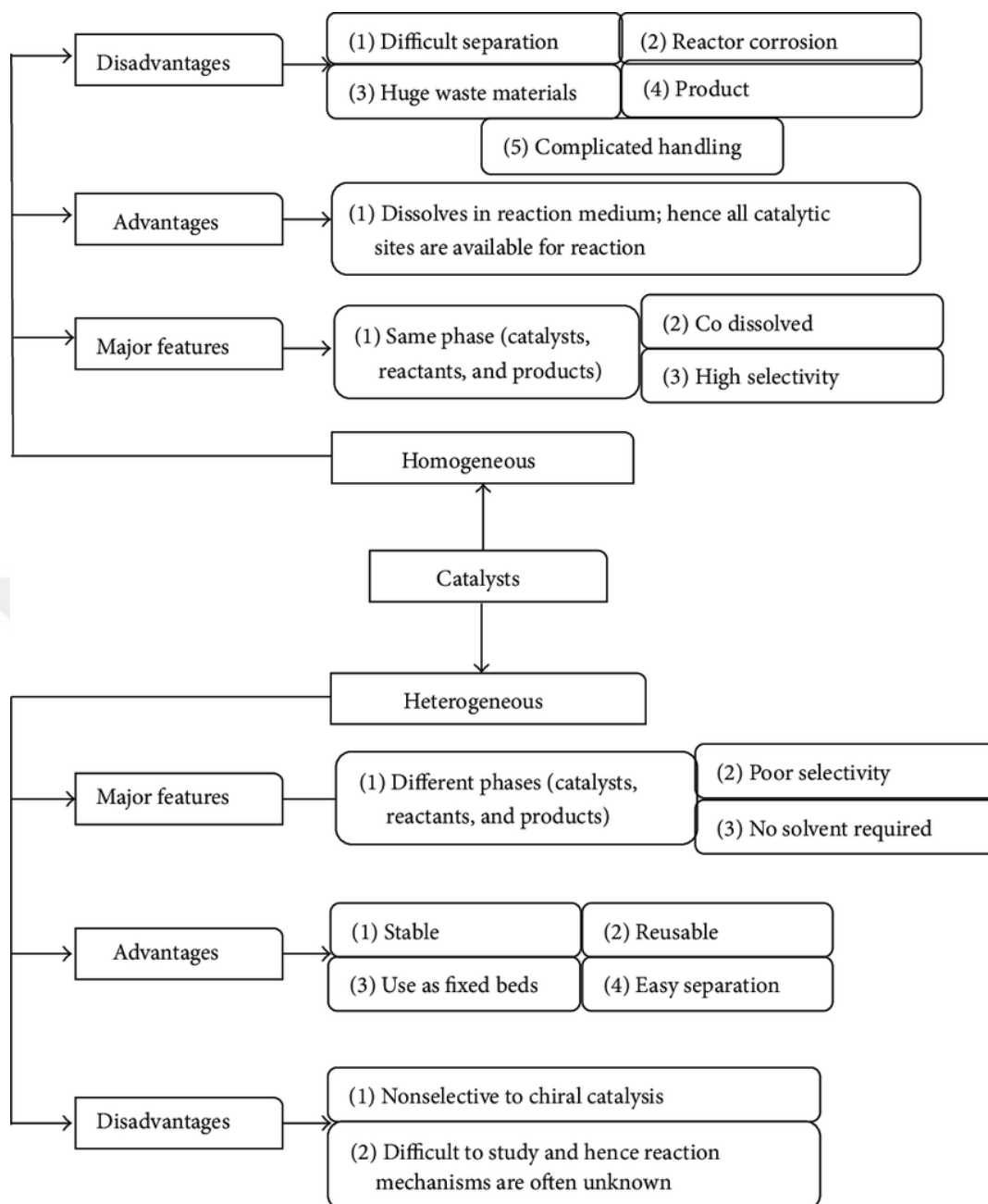
Figure 1.21: The advantages and disadvantages between homogenous and heterogeneous catalysts.

2. EXPERIMENTAL METHODS AND INSTRUMENTATION

2.1. Materials

All operations were carried out using Standard Schlenk tube and Fischer-Porter bottle (AG glass) techniques or in a Glove-box (Braun) under argon atmosphere. All solvents were purified and degassed by freeze-pumping before using. Pentane, toluene, and anisole were dehydrated through filtration on a column in a purification apparatus (Braun). Polyvinylpyrrolidone 40000 (PVP40, Sigma-Aldrich) was dried over P_2O_5 (Sigma-Aldrich) and TiO_2 (P25, Degussa), SBA-15 and MCM-48 (Glantreo Ltd) were calcined at $500^{\circ}C$ prior to usage. The other chemicals listed below were used as received unless otherwise specified.

- Bis(2-methylallyl) (1,5-cyclooctadiene) ruthenium (II) [Ru (Me-Allyl)$_2$COD] (Sigma-Aldrich)
- Tetraallyldirhenium(II) [Re$_2$(C$_3$H$_5$)$_4$] (>97 %, Prepared according to the literature procedure [101].)
- Rhenium(V) chloride (ReCl$_5$) (Sigma-Aldrich)
- Tetramethylethylenediamine (99%, Sigma-Aldrich)
- Allylchloride (98%, Sigma-Aldrich)
- Magnesium tunings (99.9%, Sigma-Aldrich)
- Iodine (99.8%, Sigma-Aldrich)
- 1,2-Dibromoethane (98%, Sigma-Aldrich)
- N-Methylpyrrolidone (99.5 % anhydrous, Sigma-Aldrich)
- 1-Acetylpiperidine (Santa Cruz Chemicals)
- N-Methylacetanilide (Sigma-Aldrich)
- N-Methyl-2-Pyrrolidone (Fluka)
- Dimethyl carboxyl chloride (98%, Sigma-Aldrich)
- Methyl-2-(2-oxopyrrolidin-1-yl) acetate (Fluorochem)
- Octane (99.9 % anhydrous, Sigma-Aldrich)
- n-Dodecane (>99% anhydrous, Sigma-Aldrich)
- 1,2 Dimethoxyethane (DME) (>99.5% anhydrous, inhibitor free Sigma-Aldrich)

- 1,4 Dioxane (99.8% anhydrous, inhibitor free Sigma-Aldrich)
- Argon (BOC)
- Dihydrogen (BOC)

2.1.1. Synthesis of C_3H_5MgCl Grignard in Diethylether

In a typical experiment, 7.44 g (0.31 mol) of Mg turnings were placed in a 1000 ml two-neck flask using a glove box. 300 ml of diethyl ether, previously degassed by three freeze-vacuum cycles, were transferred to canola at room temperature over Mg turnings under argon gas. The condenser was attached to a neck of the flask to recover the evaporated diethyl ether. Then, 2 small spatulas of iodine and 1.5 ml of dibromoethane were added to activate the Mg surface, and the reaction mixture was vigorously stirred with the magnetic stirrer. During this time, the colour of the solution changed from reddish orange to colourless transparency and the temperature increased. After the temperature had reached room temperature, 20 ml (0.31 mol) C_3H_5Cl diluted in 100 ml diethyl ether was added dropwise to the reaction mixture using a dropping funnel for 5 hours and the temperature of the mixture was controlled using a water bath. The slow addition of allylchloride and the fact that the reaction temperature is controlled is very important in the synthesis of Grignard. Rapid addition leads to a sudden increase in reaction temperature, which leads to polymerization of the Grignard reagent and formation of a thick white cloud. During the addition of C_3H_5Cl on Mg turnings in diethyl ether, a white solid ($MgCl_2$ and Mg $(OH)_2$) precipitate and a yellowish transparent supernatant formation were observed (Figure 2.1). After the addition of C_3H_5Cl was complete, the reaction mixture was stirred at room temperature for a further 1 hour. The transparent top sheet was then transferred to another flask with canola and the concentration of C_3H_5MgCl was determined by acid-base titration in the presence of phenolphthalein indicator.
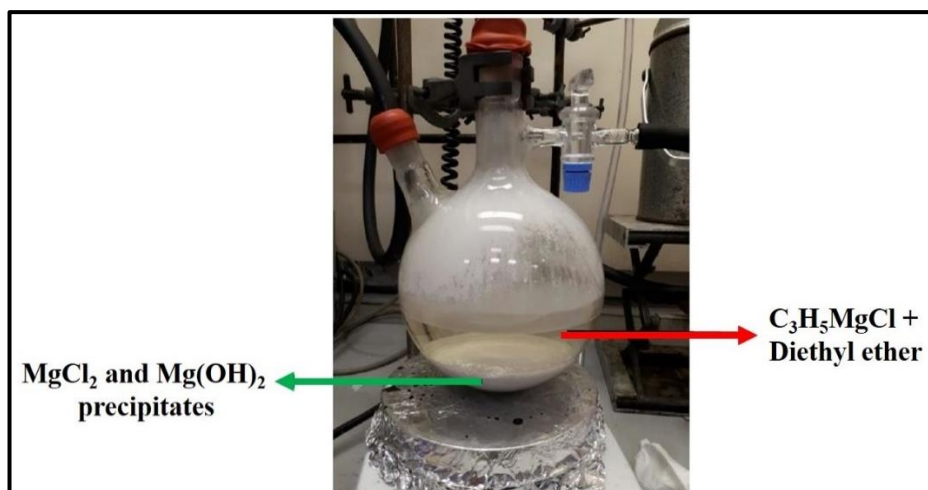
Figure 2.1: Image of the mixture formed as a result of the Grignard reaction.

2.1.2. Synthesis of Re$_2$(C$_3$H$_5$)$_4$

In a typical experiment, 3 g (8.2 mmol) of ReCl$_5$ was placed into a 500 ml flask in a glove box. The flask was removed from the glove box with the mouth closed and cooled to -78°C (dry ice-acetone mixture) under argon (Ar) gas using the Schlenk system. Approximately ~100 ml of cold diethyl ether (dehydrated and deoxygenated by cooling and vacuuming before use) were added into the 500 ml flask. The dropping funnel was installed on the flask and 75 ml (0.55 M, 0.041 mol) of C$_3$H$_5$MgCl Grignard complex previously prepared was transferred to the funnel under argon with the help of canola. Subsequently, with vigorous stirring, ReCl$_5$ was added dropwise over 2 hours on diethyl ether solution under Ar atmosphere. During this time, the colour of the solution turned dark brown and a precipitate formation was observed. After the addition of C$_3$H$_5$MgCl was finished, the cooling bath was removed, and the reaction mixture was slowly brought to room temperature. Meanwhile, the colour of the solution changed from brown to yellow and ultimately orange. The reaction mixture was stirred for a further 1 hour. After stirring at room temperature, tetramethyl ethylenediamine (TMEDA) (3-5 ml) was added under Ar to precipitate impurities. Using a canola, this orange solution was filtered through a column of celite and the filtrate collected in another 500 ml flask. The diethyl ether of the collected red-orange solution was removed in vacuum and the resulting solid was extracted by adding

pentane (4 * 50 ml). The pentane was then evaporated in vacuum and the remaining solid was collected and stored at -50°C in the glove box (Figure 2.2).
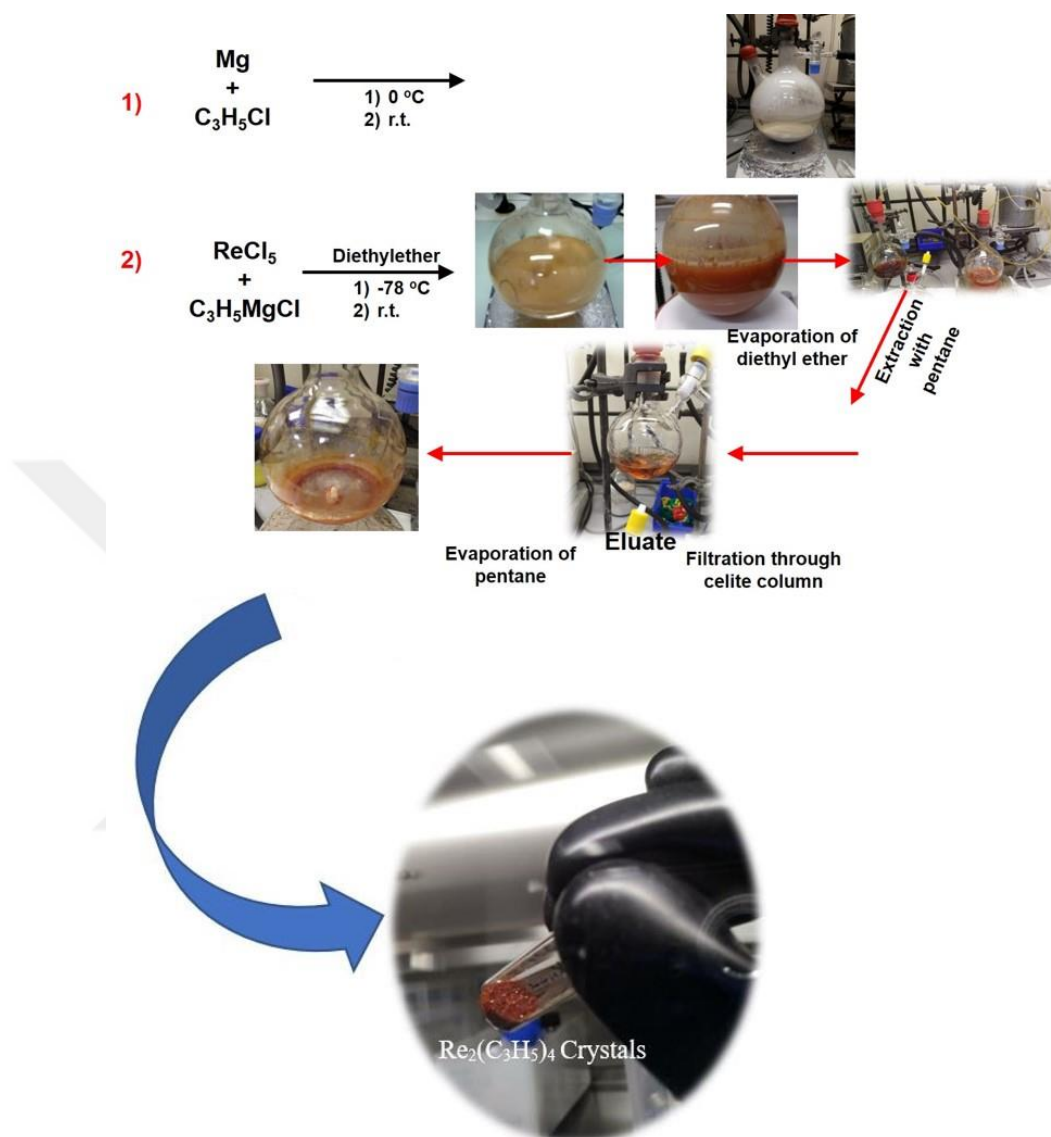
Figure 2.2: The process of $Re_2(C_3H_5)_4$ synthesis.

2.2. Catalyst Preparation

2.2.1. Calcination of Support Materials

SBA-15 and MCM-48 were calcined in a tube furnace for 4 hours at 500°C with a heating rate of 10°C/min under a constant flow of air (50 ml/min) then stored inside

the glovebox after evacuation of air trapped inside the pores. The physical properties of support materials were summarized in Appendix A.

2.2.2. Impregnation of Ru and Re Organometallic Complexes on Supports

2.2.2.1. Impregnation

Impregnation is defined as the adsorption of a material on the support material with minimum solvent usage. In the catalyst preparation, a metal precursor salt in solution was impregnated onto the support materials used in this study [101]. This process is sometimes referred to as wet impregnation because the pores of the support are filled with solvent before contact with the precursor salt. One of the problems with impregnation is the number of variables affecting precursor salt adsorption and the final metal charge and position of the metals in the support particle. Important variables include the concentration of the precursor salt, the type of the salt, the solvent, the temperature, the nature of the support, the duration of contact with the support, and the presence of other materials. While absorbing a porous material from the solution with a metal salt, four different conditions can be provided for a system consisting of an external solution and a single pore [102]. There are numerous scenarios for the distribution of the metal precursor in the system where the solution reaches the end of the pore. The assumption is that the penetration of the solute into the pore and the rate of diffusion are slow compared to the adsorption rate. All the metal precursor material of the penetrating liquid adsorbs in the walls of the first part of the pore through which it passes. It contains liquid active material that passes more into the pore. If the solvent is removed by drying, the metal precursor will only be present in the pore closest to the external solution. Instead of drying at this time, the pore is removed from contact with a simple solution, but is left filled with liquid, redistribution of metal precursors occurs due to premise desorption and diffusion through the pore wall. The result is a uniform precursor dispersion in the pore. This process can be used in catalyst synthesis if the desorption rate is fast enough [102,103]. In the case where the pore is left in contact with the outer solution, the external solution provides a uniform distribution of the metal salt in the pore by diffusion to the

adsorption zones until the equilibrium is reached with the additional activating material and the external impregnation solution. Otherwise, it is observed that the external metal delivery prior to dispensing the external solution is depleted.

The advantage of impregnation is the synthetic simplicity; no complicated equipment is required to prepare the catalyst by impregnation. It works with any combination of porous material and metal salt as long as a compatible solvent is present. The simplicity of the preparation method allows large catalysts. The primary disadvantage of the technique is the poor control of the distribution of MNPs in the pores, and activation steps, such as evaporation of the solvent, require special attention, since these procedures often cause agglomeration of metal precursors and the formation of large particles after reduction. Another natural disadvantage is that high-density catalysts do not produce highly dispersed catalysts [101,102].

2.2.2.2. Incipient Wetness Impregnation

Also known as dry impregnation, it comprises contacting a dry support with only an impregnating solution to fill the pores of the support. The volume of fluid needed to reach this stage of the initial wetness is generally determined by slowly adding a small amount of solvents to a well-mixed, weighed amount of support until the mixture is slightly liquid [102]. This weight and volume ratio is then used to prepare a solution of the precursor salt having the appropriate concentration to give the desired metal loading. Since the entire impregnating solution is adsorbed into the pores of the support, this procedure can only be used to prepare predetermined metal loads for specific catalysts.

Incipient wetness impregnation has the same advantages and disadvantages as the impregnation method. Similar to impregnated catalysts, the reduction of the precursor to MNPs should be carried out at low temperatures due to poor interaction between the metal precursor and the support.

2.2.3. Reduction of Catalysts

After the integration of the metal compounds into the support (Section 2.2.2.), the reduction reaction conditions (120ºC, 3 bar H_2, 2 days) were kept the same based

on our previous observations. According to a typical synthesis (1: 1 molar ratio), 13.4 mg of $Re_2(C_3H_5)_4$ and 16 mg of Ru (Me-Allyl)$_2$COD organometallic compounds were dissolved in 1 ml of toluene. This mixture was added to 486 mg of porous support in 250 µL portions and mixed until a homogeneous mixture was obtained. After drying the toluene, the solid was taken up in the Fischer-Porter glass reactor, allowed to be reduced for 2 days at 120°C in solid phase under 3 bar H_2 pressure. At the end of 2 days, the solid was washed with pentane and dried under vacuum.

Hydrogen gas was used as reducing agent for ReRu NPs. Any chemical reducing agents were not used in this experiment in order to establish green synthesis. The reducing temperature and pressure were set as mild conditions to obtain metal cluster in porous and on surface of supports. The experimental reducing procedure is shown at Figure 2.3.
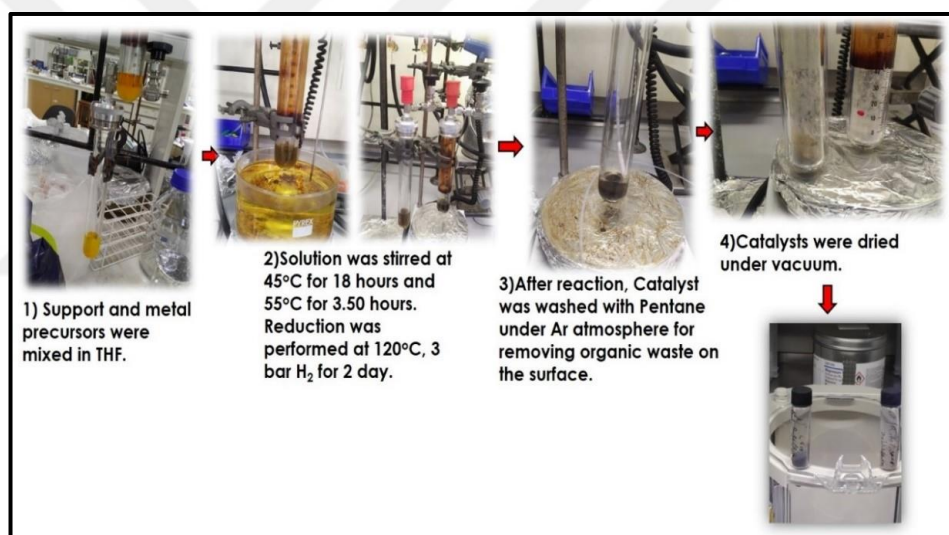
Figure 2.3: The process diagram of catalyst reduction in Fischer-Porter reactor.

2.3. Catalysis

The catalytic performance of as-prepared samples was performed under batch conditions (Figure 2.4). In a typical experiment, 100 mg catalyst (2 mol % total metal in respect to amide amount) and 50 mg molecular sieves, 4Å were placed in 15 mL HEL stainless-steel autoclave with a Teflon magnetic stir bar, followed by addition of was 3 ml octane (solvent), 0.3 mmol n-dodecane (internal standard) and 1 mmol amide substrate inside the Glove-box. At the end of the reaction, the reactors were quickly

cooled to room temperature in an ice bath. Then, the pressure was released inside a fume hood. The catalyst was removed by filtration of liquid mixture through a microfilter (0.2µL) and the reaction solution was analysed by GC-MS to determine the conversion and selectivity.
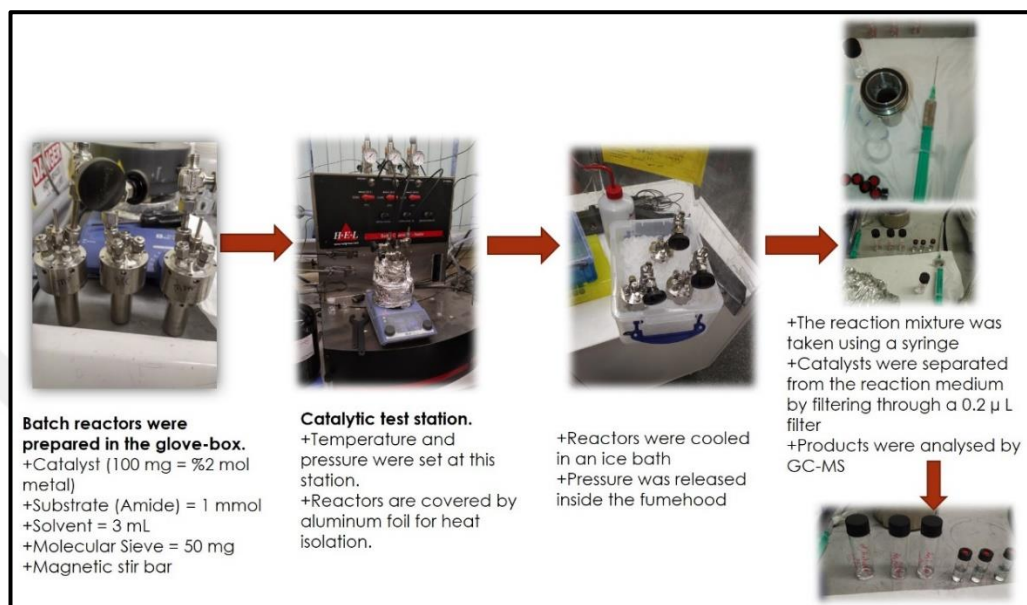
Figure 2.4: The pathway of catalytic test preparation.

2.4. Analytical Methods

A range of techniques were employed to characterise the as-prepared catalysts, namely: Temperature Programmed Reduction (TPR), X-Ray Diffraction (XRD), Nuclear Magnetic Resonance (NMR), Scanning Transmission Electron Microscopy with High-Angle Annular Dark-Field Detector (STEM-HAADF), X-Ray Photoelectron Spectroscopy (XPS), X-Ray Absorption Spectroscopy (XAS) were used for characterization of catalyst and metal precursors.

Where appropriate, experiments which were performed by other group members or external facilities due to equipment and experience constraints will be noted.

2.4.1. Temperature Programmed Reduction (TPR)

Temperature-programmed reduction (TPR) is a commonly used instrument to characterize metal oxides, combined metal oxides, and distributed metal oxides on a

support. The TPR technique provides precise data about the oxide layer reducibility as well as the reducible surface heterogeneity. A detector of thermal conductivity (TCD) is used to evaluate modifications in the gas stream's thermal conductivity. Using a rank calibration, the TCD signal is then transformed to active gas concentration. Integrating the area below concentration vs. time (or temperature) results in full fuel consumption. Figure 2.5 demonstrates a response TPR profile where MxOy is a metal oxide.
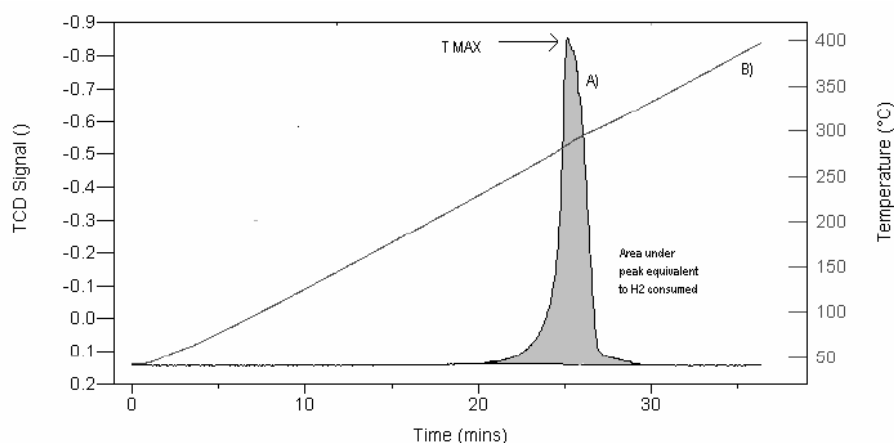
Figure 2.5: Temperature-programmed reduction profile for a metal oxide. Trace A displays the TCD signal output as a function of time. Trace B displays the temperature as a function of time during a 10°C heating rate from ambient to 400°C.

This graph shows a TPR range in which the maximum value shows the temperature corresponding to the maximum decrease frequency. The TPR technique offers a qualitative, and sometimes quantitative, image of the reproducibility of the catalyst surface and its elevated sensitivity to chemical changes arising from promoters or metal / support relationships. The TPR technique is therefore also appropriate for quality control of various catalyst fees as variations in production techniques often result in distinct decrease models.

Reduction affinities of metal precursors and the as-prepared samples were determined by temperature programmed reduction (TPR), using a Quantachrome ChemBET Pulsar TPR/TPD automated chemisorption analyzer. Samples were heated to 800°C at a rate of 10°C.min^{-1}, under a 20 mL.min^{-1} of 5% H_2 in N_2. The resulting spectra were drawn in Origin 2017 and details were discussed in Section 3 Results and Discussion.

2.4.2. X-Ray Diffraction (XRD)

X-ray powder diffraction analysis (XRD) is perhaps the most widely used X-ray based analytical techniques for characterizing materials. As the name suggests, the sample is usually in a powdery form, consisting of fine grains of crystalline material to be studied. The term 'powder' really means that the crystalline domains are randomly oriented in the sample. Therefore, when the 2-D diffraction pattern is recorded, it shows concentric rings of scattering peaks corresponding to the various d spacings in the crystal lattice. The positions and the intensities of the peaks are used for identifying the underlying structure (or phase) of the material. For example, the diffraction lines of graphite would be different from diamond even though they both are made of carbon atoms. This phase identification is important because the material properties are highly dependent on structure.

The three-dimensional structure of crystalline materials, such as minerals, is defined by regular, repeating planes of atoms that form a crystal lattice. When a focused X-ray beam interacts with these planes of atoms, part of the beam is transmitted, part is absorbed by the sample, part is refracted and scattered, and part is diffracted. Diffraction of an X-ray beam by a crystalline solid is analogous to diffraction of light by droplets of water, producing the familiar rainbow. X-rays are diffracted by each mineral differently, depending on what atoms make up the crystal lattice and how these atoms are arranged. When an X-ray beam hits a sample and is diffracted, we can measure the distances between the planes of the atoms that constitute the sample by applying Bragg's Law, named after William Lawrence Bragg, who first proposed it in 1921. Bragg's Law is: $n\lambda = 2d\sin\theta$, where the integer n is the order of the diffracted beam, is the wavelength of the incident X-ray beam, d is the distance between adjacent planes of atoms (the d-spacings) and is the angle of incidence of the X-ray beam. Since we know, and we can measure, we can calculate the d-spacings. The geometry of an XRD unit is designed to accommodate this measurement. The characteristic set of d-spacings generated in a typical X-ray scan provides a unique "fingerprint" of the mineral or minerals present in the sample. When properly interpreted, by comparison with standard reference patterns and measurements, this "fingerprint" allows for identification of the material.

In X-ray powder diffractometry, X-rays are generated within a sealed tube that is under vacuum. A current is applied that heats a filament within the tube; the higher the current the greater the number of electrons emitted from the filament. This generation of electrons is analogous to the production of electrons in a television picture tube. A high voltage, typically 15-60 kilovolts, is applied within the tube. This high voltage accelerates the electrons, which then hit a target, commonly made of copper. When these electrons hit the target, X-rays are produced. The wavelength of these X-rays is characteristic of that target. These X-rays are collimated and directed onto the sample, which has been ground to a fine powder (typically to produce particle sizes of less than 10 microns). A detector detects the X-ray signal; the signal is then processed either by a microprocessor or electronically, converting the signal to a count rate. Changing the angle between the X-ray source, the sample, and the detector at a controlled rate between preset limits is an X-ray scan. Applications XRD analysis has a wide range of applications in material science, chemistry, geology, environmental science, forensic science, and the pharmaceutical industry for characterizing materials. Amorphous materials are readily recognized by the absence of peaks in an XRD chart. The technique is also used for studying particles in liquid suspensions or polycrystalline solids (bulk or thin film materials). Other applications of XRD analysis include determination of phase transitions in a given substance, semi-quantitative determination of phases present in a sample, measurement of crystallite size particularly in nano materials, analysis of stress and crystal structure analysis by Reitveld refinement.

Figure 2.6: Air tight sample holder for XRD analysis.

The sample powders were packed onto at glass stages for analysis in an X'Pert PRO PANalytic X-ray diffractometer and scanned over a range of $2\Theta = 5\text{-}80^{\circ}$ with a

step-size of 0.0167º and scanning at 212 s per step. The system used Cu Kα radiation and was powered with 40 kV and 40 mA. Diffraction patterns were then compared against a database of known compounds using X'pert HighScore to identify the present phases.

2.4.3. Nuclear Magnetic Resonance (NMR)

Nuclear magnetic resonance (NMR) spectroscopy is a strong method to solve the divide created by various characterization methods of strong inorganic metals and molecular stage solution species. It promotes regular, immediate, molecular scale assessment in solution and solid phase of the formation of NPs and morphology [102].

Application of NMR in NPs surface chemistry research is especially important, as organic molecules often contain MNPs prepared by wet chemical methods. By connecting the distinctive effect of metal conduction electrons on ligand atoms with traditional NMR spectroscopy methods, NMR analysis of these capping ligands can provide thorough insight into particle key characteristics (e.g., electronic structure, nuclear composition, or compositional architecture). In addition to significant ligand shell elements including ligand identification, structure and dynamics [32].

Nuclear Magnetic Resonance (NMR) experiments were performed on a Bruker 500 MHz spectrometer at the Chemistry Department of University of Oxford, UK.

2.4.4. Scanning Transmission Electron Microscopy with Annular Dark Field Detector (STEM-ADF)

STEM samples were prepared by deposition of a drop of colloidal solution of as-prepared catalysts in ethanol, over a covered holey copper grid inside the Glove-box. STEM Analyses were then performed at Materials Department of University of Oxford by using JEOL ARM200F electron microscope operating at 200 kV.

2.4.5. X-Ray Photoelectron Spectroscopy (XPS)

The XPS sample preparation for as-prepared and spent catalysts were performed inside the Glove-box filled with argon to prevent air exposure. The sample holder was

carefully evacuated under vacuum for 20 minutes prior to experiment. The measurement was conducted using a Thermo Fisher Scientific NEXSA spectrometer in Harwell Research Complex in Diamond with the help of Dr Shaoliang Guan. The samples were analysed using a micro-focused monochromatic Al X-ray source (72 W) over an area of approximately 400 microns. Data were recorded at pass energies of 200 eV for survey scans and 50 eV for high resolution scans with 1 eV and 0.1 eV step sizes respectively. Charge neutralisation of the sample was achieved using a combination of both low energy electrons and argon ions. C 1s electron at 284.8 eV was used as standard reference to calibrate the photoelectron energy shift. The measured spectra were fitted using a least-squares procedure to a product of Gaussian–Lorentzian functions after removing the background noise using the CasaXPS software. The concentration of each element was calculated from the area of the corresponding peak and calibrated with the sensitivity factor of Wagner.

2.4.6. X-Ray Absorption Spectroscopy (XAS)

Re L3-edge and Ru K-edge X-ray absorption spectra (XAS) was conducted in transmission mode with a 13-Channel Ge detector at the B18 XAS beamline at the Diamond Light Source, UK. To examine the electronic state and local chemical environment around Ru and Re atoms, X-ray Absorption Near Edge Structure (XANES) and Extended X-Ray Absorption Fine Structure (EXAFS) data were extracted respectively from XAS spectra. The Demeter ATHENA program was used for XAFS data analysis, where the data were background subtracted, normalised and Fourier transformed. The Demeter ARTEMIS program was used to perform the least-squares curve fitting analysis of the EXAFS $\chi(k)$ data. The EXAFS Wavelet analysis was performed following the protocol and calculations developed by Marina Chukalina and Harald Funke, where the backscatter atoms are distinguished within the same atomic shell. To confirm the reproducibility of the experimental data, at least 2 scan sets were collected and compared for each sample. The spectra were calibrated with a Ru or Re foil as reference.

3. RESULTS AND DISCUSSION

3.1. Preparation of Catalysts

As mentioned in the introduction of this dissertation, our strategy in the preparation of catalysts is the use of organometallic synthesis approach for the synthesis of well-defined ReRu bimetallic nanosystems and the use of porous materials as supports. In this way, it is aimed to control the particle size, composition and atomic order. The morphology and solid structures of porous materials can prevent the formation of NPs and limit the size of the growing particles according to their pore size and provide robustness and stability. It should be noted that our target is to form alloy type of nanoclusters in which two metal atoms are homogeneously distributed in the particles as previous studies [83,103] indicate that Re and co-metal (Ru, Pt) need to be in close contact for efficient and selective amide hydrogenation. The precise control of chemical order in a small NP was previously shown to be possible by organometallic approach [104,105]. In this case, our plan was to use Re and Ru organometallic precursors having similar decomposition temperature and rate in order to decompose them at the same time, control the nucleation and growth, then form uniform atom distribution within the NPs. Previously, it was shown that $Re_2(C_3H_8)_4$ and $Ru(C_4H_8)_2(C_8H_{12})$ are ideal precursors for the formation of alloy type NPs, leading to the formation of 1 nm particle size in the presence of PVP as stabilizing agent when reduced under 3 bar H_2 at $120^\circ C$ for 2 days [104]. Their olefinic ligands can easily be hydrogenated and the resultant alkane molecules do not interact with the growing NPs, providing a clean surface (Figure 3.1). This is why these organometallic complexes were chosen as the metal sources.
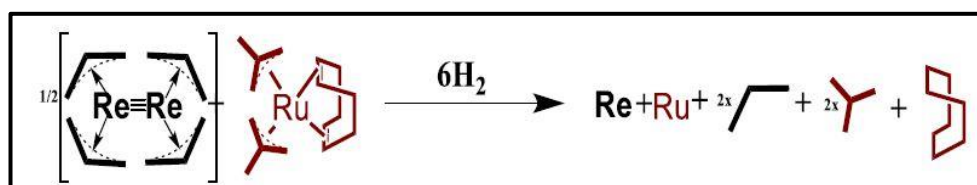
Figure 3.1: Decomposition of $Re_2(C_3H_8)_4$ and $Ru(C_4H_8)_2(C_8H_{12})$ organometallic complexes under H_2 gas.

In order to avoid the adsorption of metal precursors on the external surface of porous supports, the synthesized porous materials were calcined/desolvated prior to impregnation of metal precursors. Then, incipient wetness impregnation method, which involves dissolution of metal precursors in a solvent having a volume less than the pore volume of the support and addition of this solution in small portions to the support, was chosen as catalyst preparation method in order to create capillary effect to force the metal precursors get into the channels [106]. In addition, the external surface of porous structures is quite small when compared with the internal one. Therefore, it is thought that the adsorption is more likely to happen within the channels.

In the light of these informations, the synthesis of ReRu/mesoporous support materials was prepared using an *"incipient wetness impregnation method"* (see Section 2, Experimental) with a total weight of the two metals in the catalyst as 2.87%. After the impregnation of the metal complexes to the support materials, the catalysts were taken into a Fischer-Porter reactor and reduced under 3 bar H_2 at 120°C for 2 days. At the end of the reaction, the solid was washed with pentane and dried under vacuum (Figure 3.2)
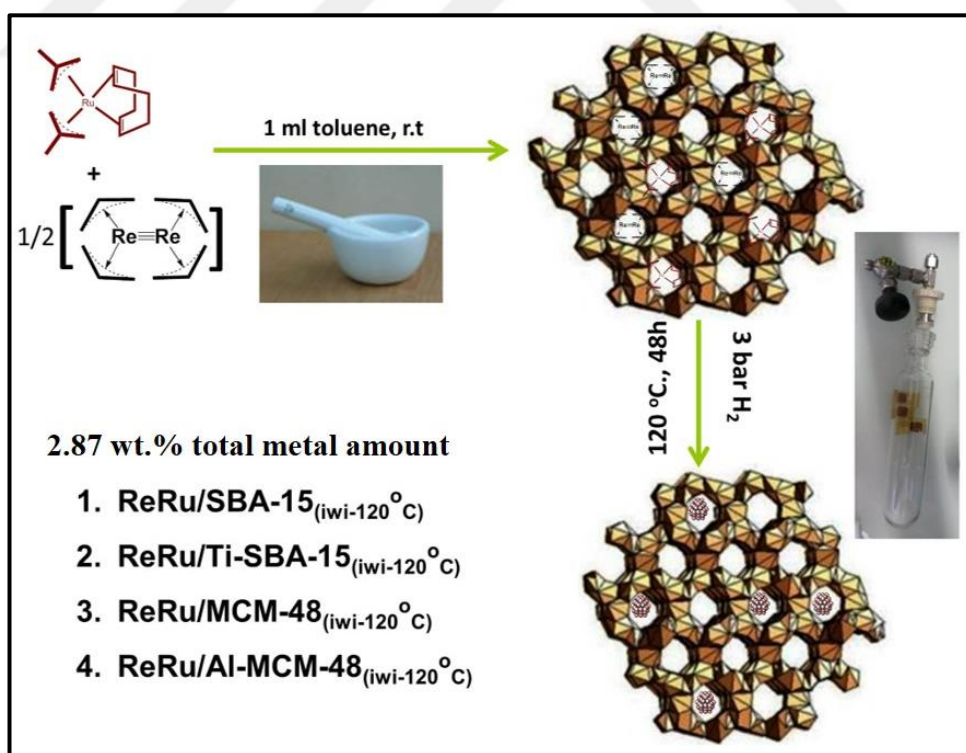
Figure 3.2: Schematic representation of the catalyst preparation steps using mesoporous materials as supports. iwi= incipient wetness impregnation and 120°C = catalyst reduction temperature.

Table 3.1: The list of catalysts, which are used for amide hydrogenation. iwi: incipient wetness impregnation. -sol: Solution synthesis. -PSN: Pre-synthesis of NPs.

	Catalyst	Stabilizing Agent/ Support	Synthesis Method	Reduction Temperature	Pressure	Time (h)
1	ReRu	SBA-15	-iwi	120ºC	3 bar H_2	48
2	Re	SBA-15	-iwi	120ºC	3 bar H_2	48
3	Ru	SBA-15	-iwi	120ºC	3 bar H_2	48
4	$ReRu_2$	SBA-15	-iwi	120ºC	3 bar H_2	48
5	$ReRu_3$	SBA-15	-iwi	120ºC	3 bar H_2	48
6	Re_2Ru	SBA-15	-iwi	120ºC	3 bar H_2	48
7	Re_3Ru	SBA-15	-iwi	120ºC	3 bar H_2	48
8	ReRu	SBA-15	-iwi	550ºC	Flow of 5%H_2 in N_2	2
9	ReRu	SiO_2	-iwi	120ºC	3 bar H_2	48

The choice of different reduction temperatures for the catalysts were determined based on Temperature Programmed Reduction (TPR) analysis which will be discussed in Section 3.3 Characterization in detail.

3.2. Catalyst Screening in 1-Acetylpiperidine Hydrogenation and Optimization of Reaction Conditions

The preliminary catalytic activity of synthesized materials were investigated in 1-Acetylpiperidine, a tertiary amide. The catalysts were put in high pressure autoclaves together with octane (solvent), n-dodecane (internal standard) and acetylpiperidine (amide substrate) under N_2 atmosphere. After purging the autoclaves with 10 bar N_2 and 30 bar H_2 3 times, the autoclaves were pressurized with 40 bar H_2 and initially heated to 70ºC, following the latest literature conditions. Under these conditions, no catalytic activity was observed after 2 hours of reaction period. However, increasing the temperature to 150ºC led to catalytic transformation of acetylpiperidine to ethylpiperidine (Figure 3.3).
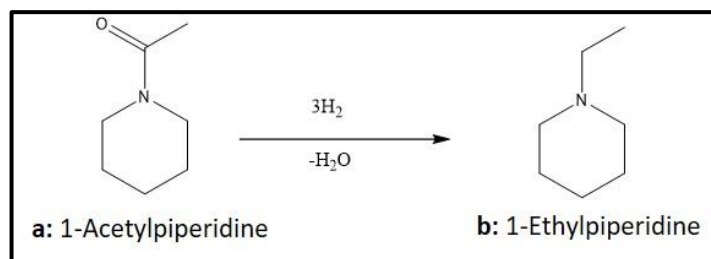
Figure 3.3: Hydrogenation of 1-Acetylpiperidine.

The catalytic performances of the prepared catalysts are summarized in Table 3.2.

Table 3.2: The catalytic test result for 1-Acetylpiperidine.

	Amide	Catalyst	Time-Conditions	Product	Conversion (%)	Selectivity
1		ReRu/SBA-15	2 hours		65.1	>99
2		ReRu/SBA-15	24 hours		100	>99
3		Re/SBA-15	2 hours		4.8	>99
4	a	Ru/SBA-15	2 hours	b	2.8	0
5		ReRu/MCM-48	2 hours		64.0	98
6		ReRu/SiO$_2$	2 hours		25.6	98

Catalytic conditions: 3 mL octane (solvent), 66 μL of n-dodecane (internal standard), 120 μL (1 mmol) amide, 2 mol% metal (100 mg) catalyst, 150 ºC, 40 bar H$_2$, 2 h, 1000 rpm. Sub-indices: representation of the synthesis methods of the catalyst and reduction temperatures. *iwi* = incipient wetness impregnation method, *sol* = solution synthesis and the reduction temperature of the catalysts. For the catalysts that do not have sub-indices (entries 1-5, 9 and 13) were always prepared by iwi method and reduced under 120 ºC for 2 days under 3 bar H$_2$ in a F-P bottle. a: 1-acetylpiperidine; b: 1-ethylpiperidine.

According to the results given in Table 3.2, it was observed that Ru or Re metals alone could not provide a good catalytic conversion (entries 3 and 4). This result clearly indicates that two metals should be in close proximity and work synergistically in order to hydrogenate amides to amines. Similarly, no activity was observed with polymer stabilized catalysts due to the bulk structure of the stabilizing agent surface and prevents the amide substrate approaching to the active metal surface. It is known in the literature that olefinic Ru(II) organometallic compounds can be reduced under hydrogen gas and form new intermediates in the presence of an aromatic ring [107,108]. General type π-complexes [(arene)(diene)Ru (0)] are known as stable under

moderate conditions but can be decomposed at more forcing conditions. Therefore, the decomposition of [Ru (anisole, toluene) (COD)] is expected to be more difficult and slower than $Ru(C_4H_8)_2(C_8H_{12})$ at the selected temperature.

Nonporous and low-surface area SiO_2 did not provide enough stabilisation and dispersion for Ru and Re atoms, resulting in low catalytic conversion (25.6%, entry 6). However, when high surface area porous silica was used as a support (entries 1 and 5), the catalytic conversion boosted to 64.7 and 73% for ReRu/MCM-48 and ReRu/SBA-15 catalysts respectively. The observation of slightly low activity in MCM-48 supported catalysts compared to SBA-15 might be due to small pore size of MCM-48 (3.0 nm) which limits the diffusion of molecules thus decreases the reaction kinetics.

In summary, ReRu/SBA-15 catalyst presented the best catalytic activity among the prepared samples presented 73% conversion in 2h and 100% within 24h with >99% selectivity towards ethylpiperidine. These results are very promising and better than many Re-based catalysts in the literature which are generally been reported after 18 to 24 hours of reaction at high temperature and pressure. The reason for not observing any activity at 70°C might be because there is an induction period at which the catalytically active species did not form within 2h time period or 70°C is thermodynamically not sufficient for chemical transformations on the catalyst surface. These results were found to be very promising and led to further studies to optimize the reaction conditions for maximum efficiency and gain in understanding of the true nature of active catalyst via advanced characterization techniques which will be discussed in the following sections of the thesis.

3.2.1. Effect of Solvent in Catalytic Activity

In the literature, octane, dioxane and dimethoxyethane (DME) were reported as efficient solvents for amide hydrogenation reactions. The solubility of amides and the corresponding amines in the chosen solvent is important for effective catalysis and product analysis. Therefore, we investigated the effect of these solvents in catalytic performance of ReRu/SBA-15 in 1-acetylpiperidine hydrogenation. The results are shown in Table 3.3. Although DME seems to be superior among selected solvents the GC-MS analysis was not constant. In the second analysis, the conversion was

measured to be 66%. The reduction value might be due to low solubility/miscibility of ethylpiperidine in polar solvents such as DME. The phase separation and/or inhomogeneity in reaction solution is expected to result in inconsistency in product analysis. Therefore, octane was used as the solvent for further optimizations. However, it should be noted that in some cases, the hydrogenation of tertiary amides with functional groups were performed in DME due to low solubility of reactants and/or products. The changes in reaction conditions will be specified wherever necessary in this dissertation. These results indicate that amide hydrogenation is quite sensitive to establishing the right reaction conditions and one should assess the conditions carefully.

Table 3.3: Catalytic activity of ReRu/SBA-15 in hydrogenation of 1-acetylpiperidine to ethylpiperidine using different solvents. *GC-MS analysis showed lower activity (66%) in the second and third run.

	Octane	Dioxane	Dimethoxyethane (DME)
Conversion %	65,1	58,3	70,4*

Reaction conditions: 3 mL solvent, 66 µL (0.3 mmol) of n-dodecane (internal standard), 120 µL (1 mmol) amide, 2 mol% metal (100 mg) catalyst, 150°C, 40 bar H_2, 2 h.

3.2.2. Effect of Ru: Re Molar Ratio

Figure 3.4 shows the performance relationship of the catalysts according to their molar ratios. As depicted in the graph there is a critical line for the amount of Ru. When the molar ratio of Ru:Re is below 0.5, the catalytic activity drops sharply. Increasing the amount of Ru in the catalysts increases the reaction rate constantly, which is presumably due to faster H_2 activation and hydrogen transfer to the amide substrates. Ruthenium is very well known for activating molecular hydrogen at low pressures and temperatures. Thus, despite the observation of high activity with increase in the amount of Ru, a careful balance should be established not to over hydrogenate amide substrates consisting functional groups such as olefins or aromatics.
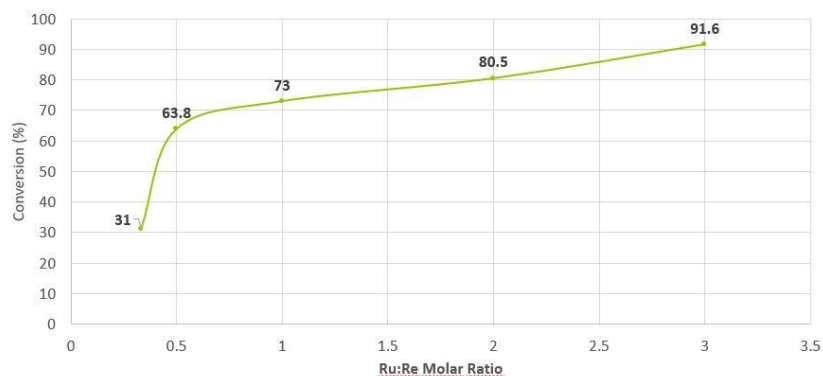
Figure 3.4: The relationship of molar ratio and catalytic performance for 1-Acetylpiperidine hydrogenation.

3.2.3. Effect of Mass and Heat Transfer

Heterogeneous catalysis involves, by definition, at least two phases. Exchange of heat and mass between the phases is required for the reaction to take place. Therefore, optimization of mass and heat transfer is important for efficient catalytic transformations on heterogeneous catalysts, especially for porous systems. As seen in Table 3.4 (entries 1 and 2), the hydrogenation of 1-acetylpiperidine proceeded faster when reaction was performed directly inside the stainless-steel reactor without using glass inlet vial. This result indicates that more efficient heat transfer occurs in the reaction medium when reaction mixture is heated directly. In addition, various types of magnetic stir bars and stirring rates were used in order to overcome the internal mass transfer limitations and to find the most optimum reaction conditions. Entries 3-6 clearly indicate that vigorous stirring is necessary to overcome the internal mass transfer limitations through the pores. The conversion values almost doubled when medium sized magnetic stir bar was used at a high spinning rate.

Table 3.4: Stirring and vial effects of catalytic tests.

	Catalyst	Time-Conditions	Stirring Rate (rpm)	Conversion (%)
1	ReRu/SBA-15	2h-vial	1000	65.1
2	ReRu/SBA-15	2h-w/o vial	1000	73
3	Re$_2$Ru/SBA-15	2h-w/o vial[a]	500	26.9
4	Re$_2$Ru/SBA-15	2h-w/o vial[b]	1000	63.8
5	Re$_3$Ru/SBA-15	2h-w/o vial[a]	500	17.1
6	Re$_3$Ru/SBA-15	2h-w/o vial[b]	1000	31

w/o: without, [a]: Big size magnetic stirrer bar, [b]: medium size magnetic stirrer bar

3.3. Characterizations

Among the as-prepared catalysts, given *vide supra*, Re$_x$Ru$_y$/SBA-15 catalysts were found to be superior. In order to understand the reason of higher catalytic activity and correlate reactivity with structure, a series of characterization techniques were applied such as XRD, STEM-ADF, NMR, XPS, EXAFS *etc.*, results of which are discussed in detail in the following sections.

3.3.1. Structural Characterization

The XRD pattern of ReRu/SBA-15 in comparison with SBA-15 is shown in Figure 3.5. As seen in the figure, no appreciable differences are found in the XRD pattern of ReRu/SBA-15 with respect to the diffractograms observed for the amorphous SBA-15 support and sample holder. This indicates that Ru and Re would appear in a highly dispersed state. Normally, the most intense peaks corresponding to Ru and Re expected to appear at 51.54° and 50.29°, respectively but it must be considered that the Ruthenium and the Rhenium content, and its diffraction cross section with respect to SBA-15, is relatively low as to produce relatively intense peaks [109].
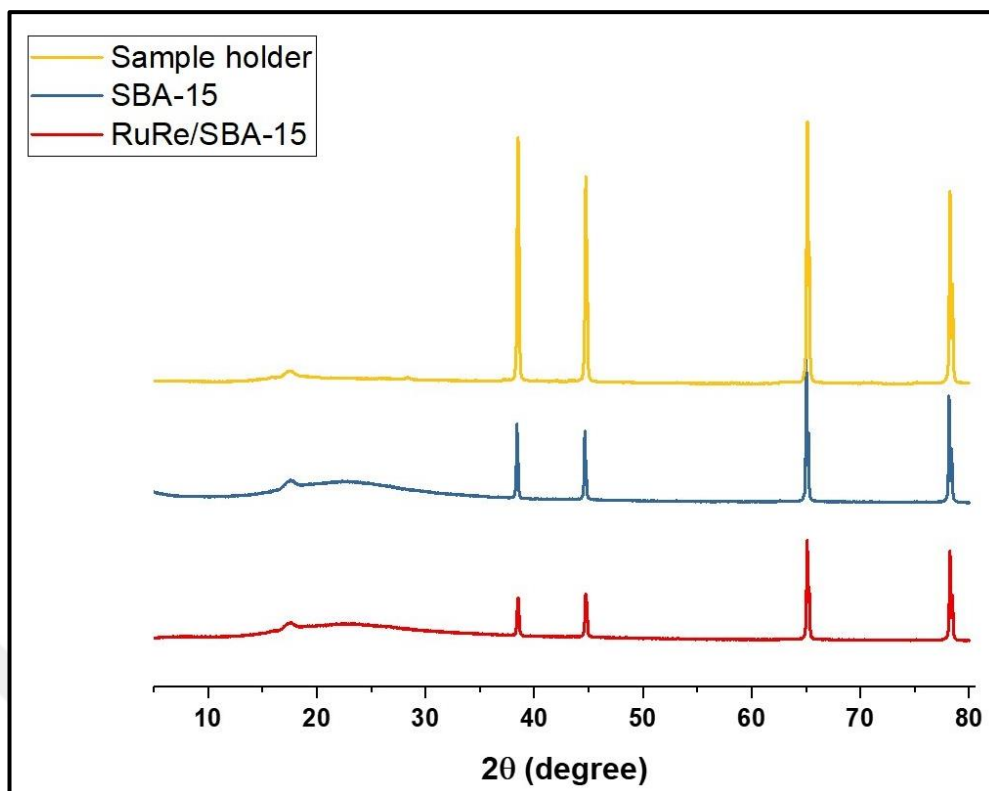
Figure 3.5: XRD diffractograms of sample holder, SBA-15 and ReRu/SBA-15.

In order to gain information about the general structure and textural properties of the catalysts, ReRu catalysts supported on porous and non-porous supports with best catalytic performance were selected and analysed under electron microscopy.

STEM image (Figure 3.6) of ReRu/Ti-SBA-15$_{(iwi-120^oC)}$ revealed that amorphous Ti-SBA-15 support accommodates mainly single atoms (The STEM images taken from ReRu/SBA-15 catalysts showed similar results but were blurred due to the limitations of the instrument, so they were not included in the thesis). These atoms were found to be very labile under electron beam. A few parts of catalyst also showed the presence of few-atoms nanoclusters (Figure 3.6d).

These results clearly show that high surface template can disperse Ru and Re atomically which can account for higher catalytic activity. It is observed that the organometallic precursors are grafted to high surface area Ti-doped silica support to ensure a high dispersion; however, treatment under H$_2$ at chosen 120°C did not lead to the cleavage of the M-O bond and to aggregation which would yield large supported metal particles. Controlling or even avoiding the aggregation process on oxide supports by surface organometallic chemistry tools would lead to smaller NPs of a few atoms (<1 nm) or analogues of the early transition-metal surface hydrides which could

be of great interest for catalytic applications. It is important to understand metal-support interaction to correlate the activity with the structure. Therefore, we decided to perform molecular level characterisation.
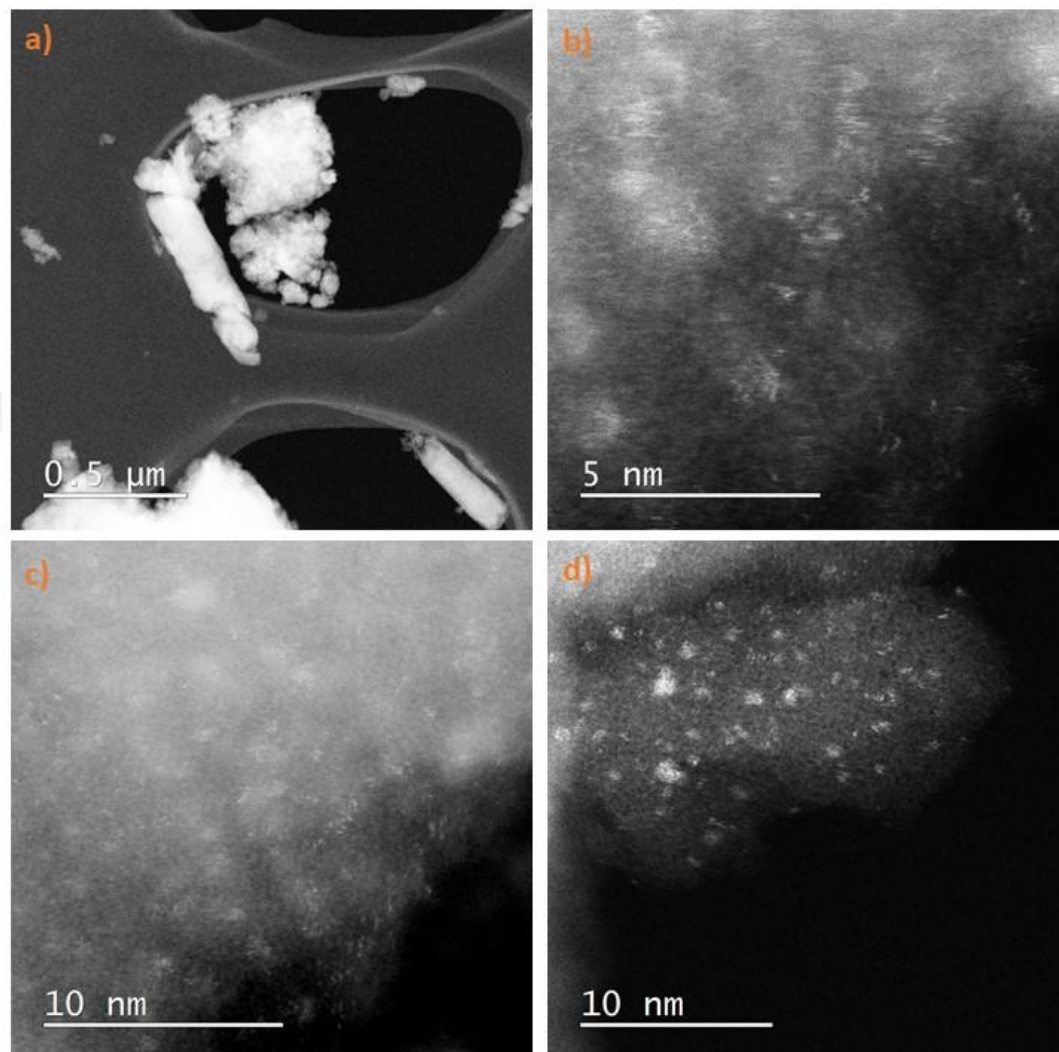
Figure 3.6: STEM Images of as-prepared ReRu/Ti-SBA-15$_{(iwi-120^oC)}$ at different magnifications.

3.3.2. Study of Support Surface-Organometallic Complex Interaction

The achievement of a structure–activity relationship for heterogeneous catalysts is a desirable step for improving existing catalysts or for predicting new catalytic reactions. Solid state field still suffers from a lack of tools to characterize the so-called single sites, even if a variety of techniques coming from surface science and molecular chemistry have emerged: in situ IR, in situ 1H, 13C NMR, 2D NMR, EXAFS *etc*. The

use of molecular models to mimic the surfaces of inorganic oxide supports might lead to better understanding for surface-grafted organometallic fragments [110]. Such molecular models can help gain insight in the molecular understanding of the whole catalytic act occurring on heterogeneous catalysts. One should not forget that heterogeneous catalysis is a molecular phenomenon occurring on a surface and surface organometallic fragments are real reaction intermediates in most cases. For silica, molecular models of surface-grafted organometallic derivatives have been obtained with model ligands such as the polyhedral oligomeric silsequioxanes (POSS), characterized by a self-organized cage-like structure and reactive silanol moieties (Figure 3.7). In the polyhedral oligomeric silsesquioxanes, the cubic framework of the molecular cage is made of Si–R moieties in the corner positions and oxygen atoms between them R being cyclohexyl in this study.
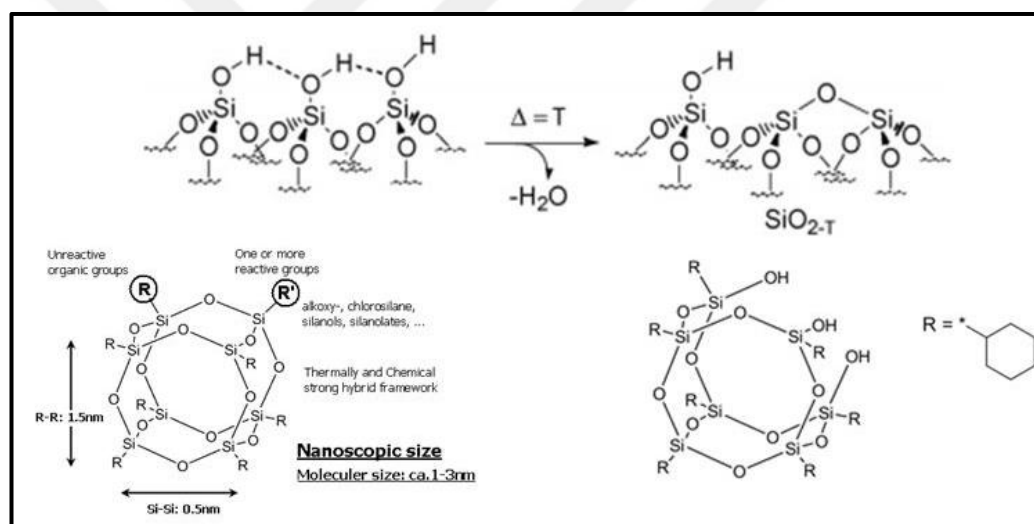
Figure 3.7: Top: Silica surface at solid state before and after calcination; Bottom left: Structure of Fully condensed polyhedral oligomeric silsesquioxanes (PSS), Bottom right: Structure of partially condensed polyhedral oligomeric silsesquioxanes (POSS).

Figure 3.8 shows the ^{1}H-NMR Study of $Re_2(C_3H_5)_4$ with POSS at room temperature. $Re_2(C_3H_5)_4$ in C_6D_6 shows 3 proton peaks at δ 5.6(sep), 3.9(t) and -1.1 (dd). For POSS molecule, peaks at δ 0.7-2.3 ppm are assigned for cyclohexyl protons and singlet appears at δ 7.5 ppm is attributed to hydroxyl groups (-OH) on silanols. As seen from the figure, a mixture of $Re_2(C_3H_5)_4$ with POSS (1:1 molar ratio) does not make a drastic change in ^{1}H-NMR spectra despite the observation of slight colour

change. -OH, peak position at δ 7.5 ppm slightly shifts to high field while the remaining peak positions stay the same. The observation of high field shift of -OH groups indicates that hydroxyl protons are under influence of a high electron density environment which might be due to the interaction with allyl group of $Re_2(C_3H_5)_4$. In addition, the loss of coupling of POSS peaks (broadening) might be due to low solubility of POSS in C_6D_6 or due to the restricted mobility of POSS molecules in the presence of $Re_2(C_3H_5)_4$. ^{29}Si NMR (Figure 3.9) taken before and after mixing of POSS with $Re_2(C_3H_5)_4$ also did not show a change in the position of the peaks.
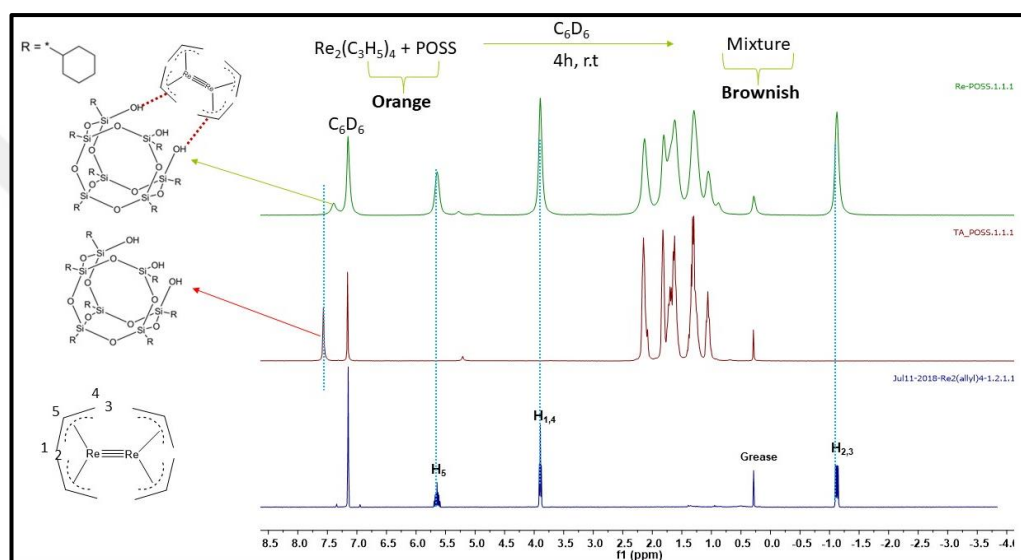
Figure 3.8: ^{1}H-NMR of bottom: $Re_2(C_3H_5)_4$, middle: POSS and top: mixture of $Re_2(C_3H_5)_4$ with POSS in C_6D_6 at room temperature.
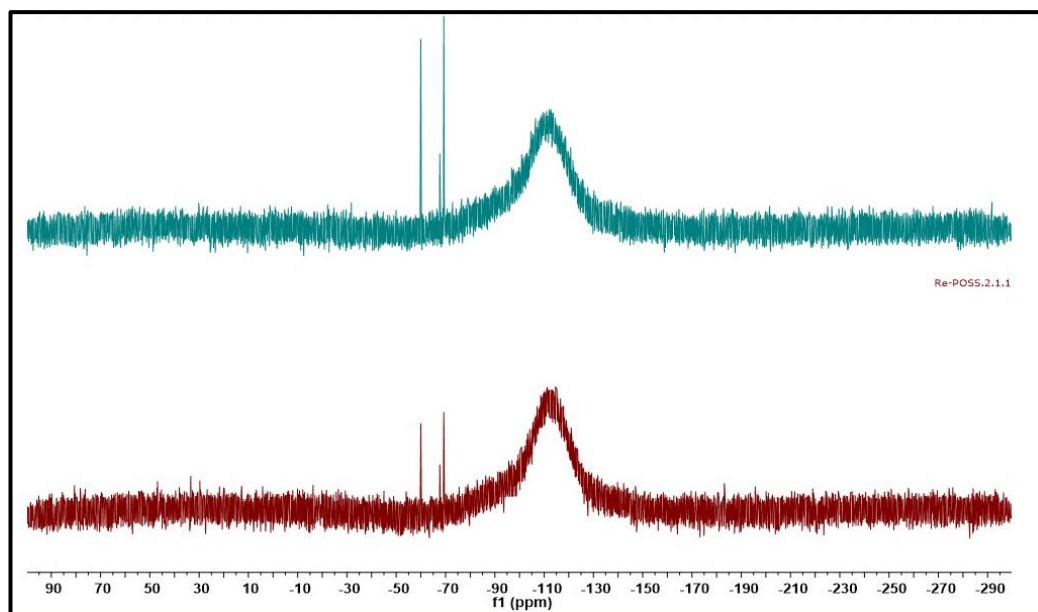
Figure 3.9: ^{29}Si-NMR of bottom: POSS and top: mixture of $Re_2(C_3H_5)_4$ with POSS in C_6D_6 at room temperature.

When $Re_2(C_3H_5)_4$, and POSS mixture was heated to 78°C in C_6D_6, the proton peaks derived from $Re_2(C_3H_5)_4$ disappeared while small quantity of -OH groups remained (Figure 3.10). In addition, new peaks at δ 5.7(m), 5.0(dp), 4.9(dq) and 1.5(dt) appeared which are assigned to propylene peaks evolved from the protonation of allyl groups of $Re_2(C_3H_5)_4$ after abstracting acidic protons of -OH moieties of silanol groups. ^{29}Si-NMR spectrum (Figure 3.11) after heating shows several Si peaks which evidences the symmetry of POSS molecules are disturbed. This might be due to different coordination environment of Re atoms on POSS surface some of which are illustrated below.
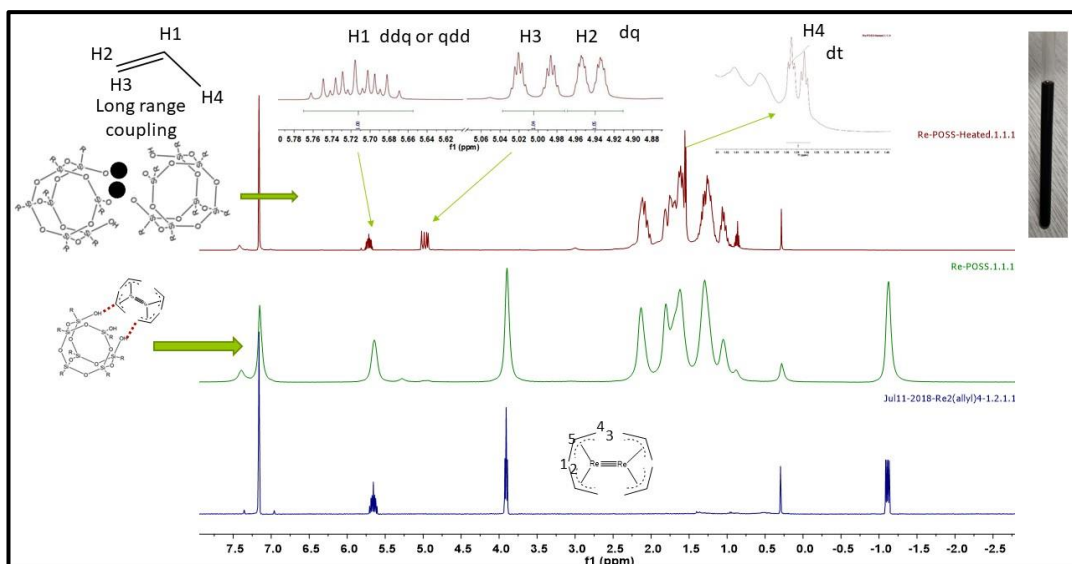
Figure 3.10: ^{1}H-NMR of bottom: $Re_2(C_3H_5)_4$, middle: POSS and $Re_2(C_3H_5)_4$ mixture at r.t. and top: mixture of $Re_2(C_3H_5)_4$ with POSS in C_6D_6 at 78°C.
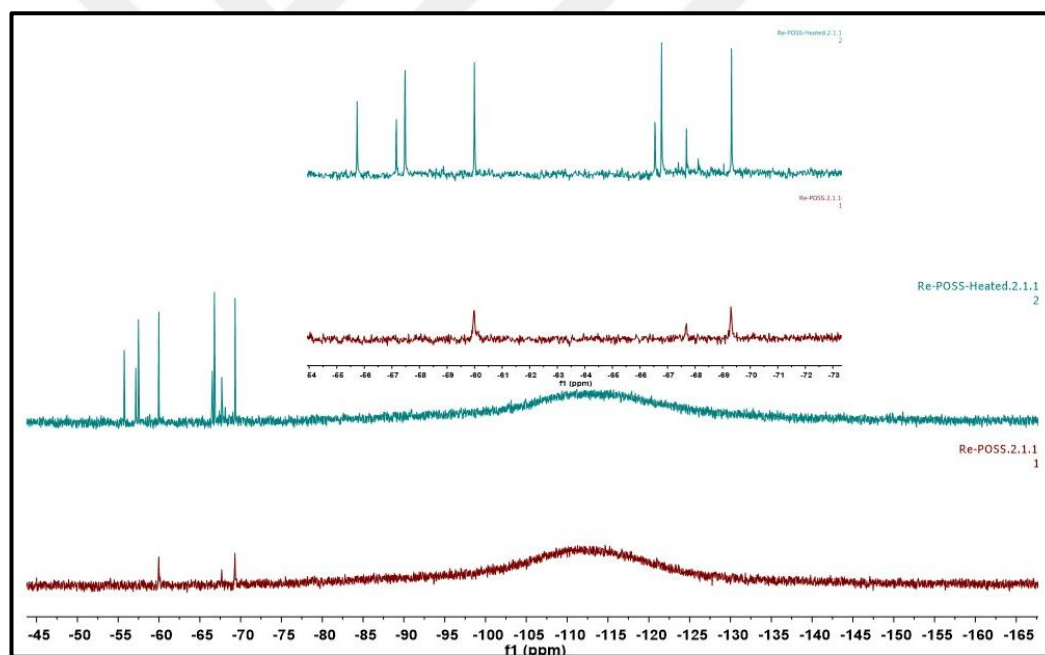
Figure 3.11: ^{29}Si-NMR of bottom: POSS and top: mixture of $Re_2(C_3H_5)_4$ with POSS in C_6D_6 after heating to 78°C. Inset is the zoom of Si peaks areas.

Control experiments were also performed in order to get information about the stability of POSS under high temperature. As seen in Figures 3.12 and Figure 3.13, POSS structure remains intact when heated. No drastic change was observed in ^{1}H and ^{29}Si NMR spectra before and after heating the solutions. The increase in the intensity of peaks result from better solubility of POSS in C_6D_6 upon heating.
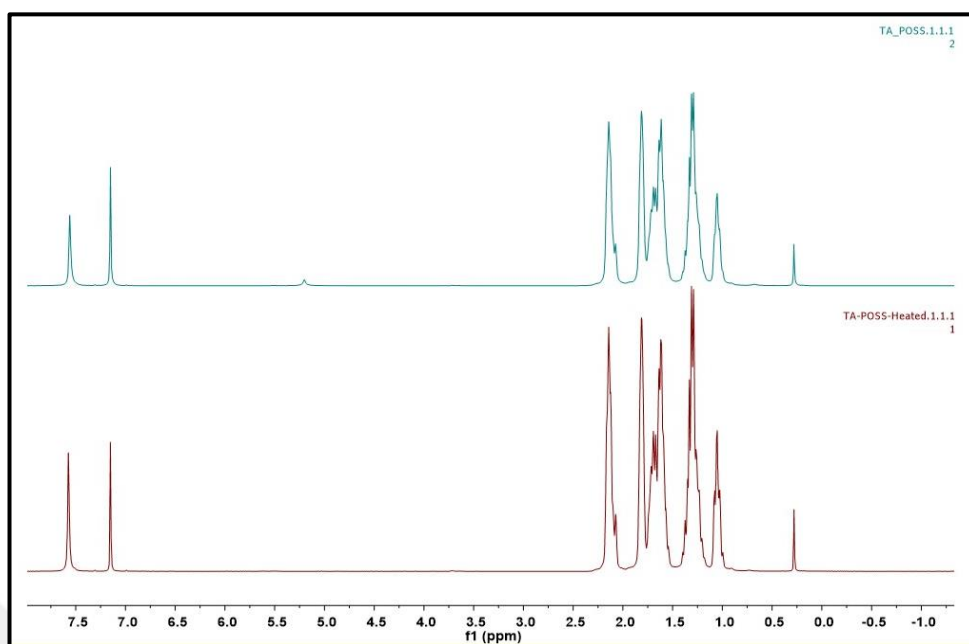
Figure 3.12: ^{1}H-NMR of POSS top: at r.t. and bottom: after heating to 78°C.
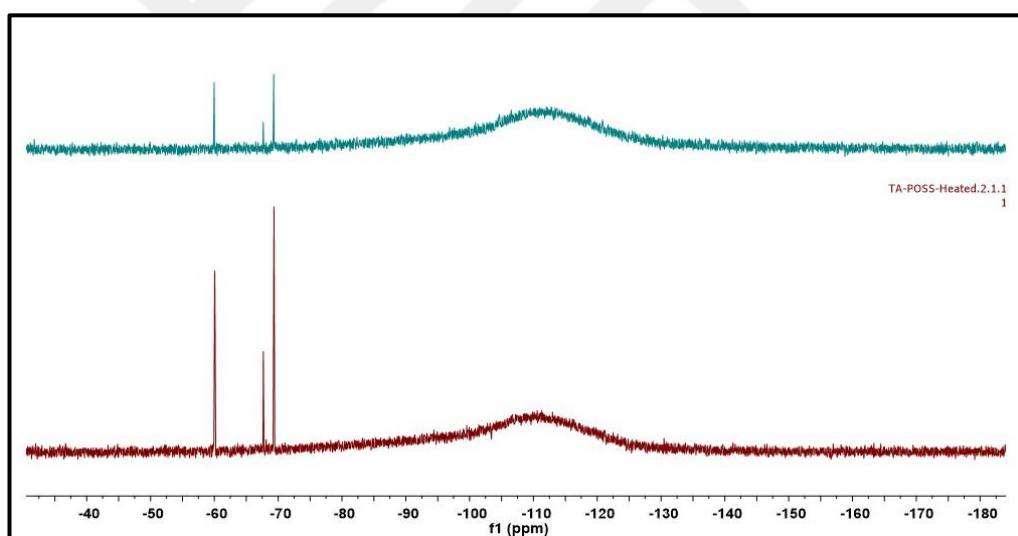
Figure 3.13: ^{29}Si-NMR of POSS top: at r.t. and bottom: after heating to 78°C.

Similarly, the reactivity of Ru(C$_4$H$_8$)$_2$(C$_8$H$_{12}$) with silanol groups of POSS was investigated under the same conditions of Re$_2$(C$_3$H$_5$)$_4$. Figure 3.14 shows the ^{1}H-NMR Study of Ru(C$_4$H$_8$)$_2$(C$_8$H$_{12}$) with POSS at room temperature. ^{1}H-NMR spectrum of Ru(C$_4$H$_8$)$_2$(C$_8$H$_{12}$) in C$_6$D$_6$ gives peaks at δ 0.20 (2H, s, *anti* H of Me-allyl), 1.08-1.26 (2H, m, CH of COD), 1.45-1.70 (4H, m, CH2 of COD), 1.56 (2H, s, *syn* H of Me-allyl), 1.70 (6H, s, CH3 of Me-allyl), 2.64-3.00 (4H, CH2 of COD), 2.88 (2H, s, *anti* H of Me-allyl), 3.52 (2H, d, J = 2 Hz, *syn* H of Me-allyl), 3.98 (2H, dd, J = 5, 9 Hz,

CH- of COD) ppm. Similar to the case of $Re_2(C_3H_5)_4$ - POSS mixture, ^{1}H-NMR spectrum of a mixture of $Ru(C_4H_8)_2(C_8H_{12})$ with POSS (1:1 molar ratio) in C_6D_6 at r.t. (Figure 3.14c) mainly does not change the peak positions of Ru complex and POSS except slight high field shift of -OH peak position at δ 7.5 ppm. As mentioned before, this observation is attributed to interaction of acidic –OH protons with organometallic ligands, presumably Me-Allyl. The broadening of peaks and loss of splitting are thought to be due to the lack of molecular mobility, resulting from Van der Waals interactions. Upon heating (Figure 3.14d), the colour of the solution turned into brown and new peaks at δ 1.7 and 4.7 ppm, attributed to isobutene, appeared. Formation of isobutene clearly shows that Methyl-allyl ligands of $Ru(C_4H_8)_2(C_8H_{12})$ abstracts proton from surface silanol groups of POSS upon heating. Interestingly, hydroxyl peaks of POSS disappeared while majority of the proton peaks derived from $Ru(C_4H_8)_2(C_8H_{12})$ remained. It should be noted that 1:1 molar ratio of POSS (3 –OH groups are present in each POSS molecule) and $Ru(C_4H_8)_2(C_8H_{12})$ were used which means there was enough hydroxyl groups that could interact with all Me-Allyl ligands. The total consumption of –OH groups is thought to be catalytic dihydroxylation of POSS in the presence of Ru.
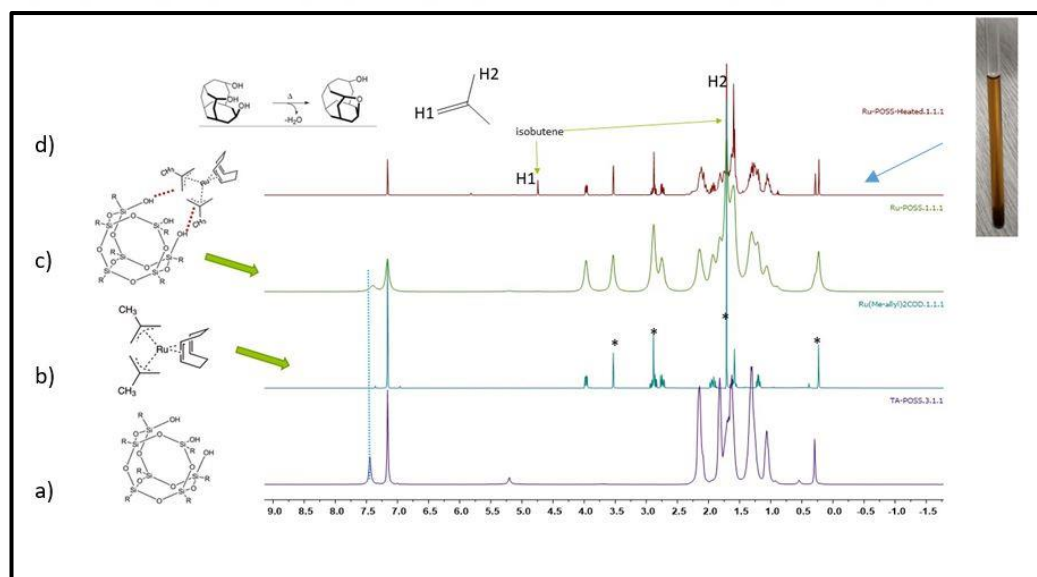
Figure 3.14: ^{1}H-NMR of a) POSS, b) $Ru(C_4H_8)_2(C_8H_{12})$, c) the mixture of $Ru(C_4H_8)_2(C_8H_{12})$ with POSS at r.t and d) the mixture of $Ru(C_4H_8)_2(C_8H_{12})$ with POSS after heating to 78°C. * Protons from Me-Allyl group of $Ru(C_4H_8)_2(C_8H_{12})$.

^{29}Si-NMR spectrum (Figure 3.15) after heating shows several Si peaks which evidences the symmetry of POSS molecules are disturbed due to different coordination environments of POSS with Ru complex.
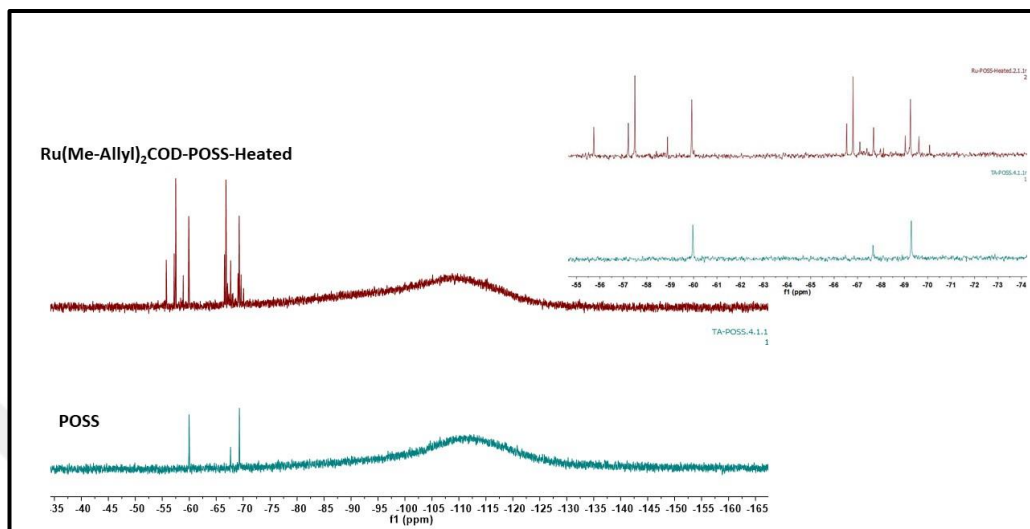
Figure 3.15: ^{29}Si-NMR of bottom: POSS and top: mixture of $Ru(C_4H_8)_2(C_8H_{12})$ with POSS in C_6D_6 after heating to 78°C. Inset is the zoom of Si peaks areas.

3.3.3. Chemical State and Local Environment of Active Species

The chemical state and local structures surrounding the Ru and Re species were probed by X-ray absorption spectroscopy (XAS). Ru K-edge X-ray Absorption Near Edge Spectrum (XANES) of as-prepared catalyst mainly indicates the metallic character of Ru in the sample. However, the increase in white line intensity and the slight shift at the pre-edge to the higher binding energy compared to Ru foil evidences mildly charged state of Ru ($\delta+$) atoms which is expected due to the electronic effect of framework oxygens surrounding Ru atoms. Mildly oxidized state of Ru ($\delta+$) was evident by X-ray absorption near edge spectra (XANES) on as-prepared ReRu/SBA-15 catalyst while Re edge revealed a high oxidation state, presumably +5 based on comparison with reference rhenium salts (Figures 3.16 and 3.17).
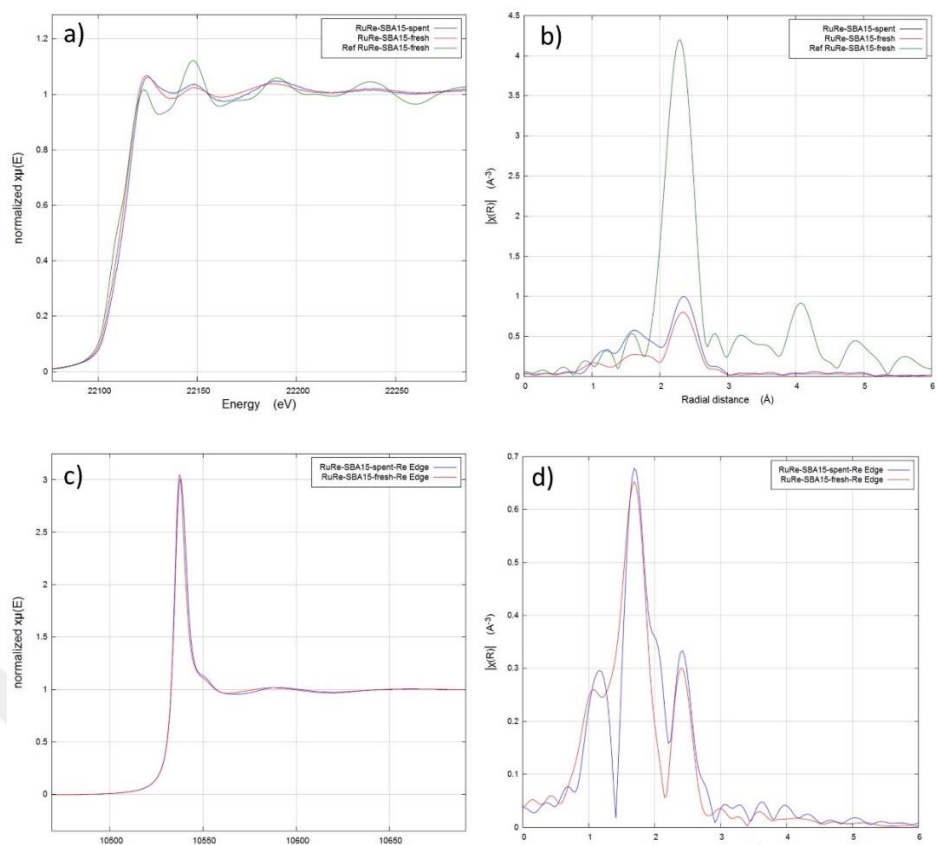
Figure 3.16: a and c) XANES spectra of as- prepared and spent ReRu/SBA-15 catalysts at Ru and Re edges respectively, b and d) EXAFS functions of as- prepared and spent ReRu/SBA-15 catalysts at Ru and Re edges respectively.
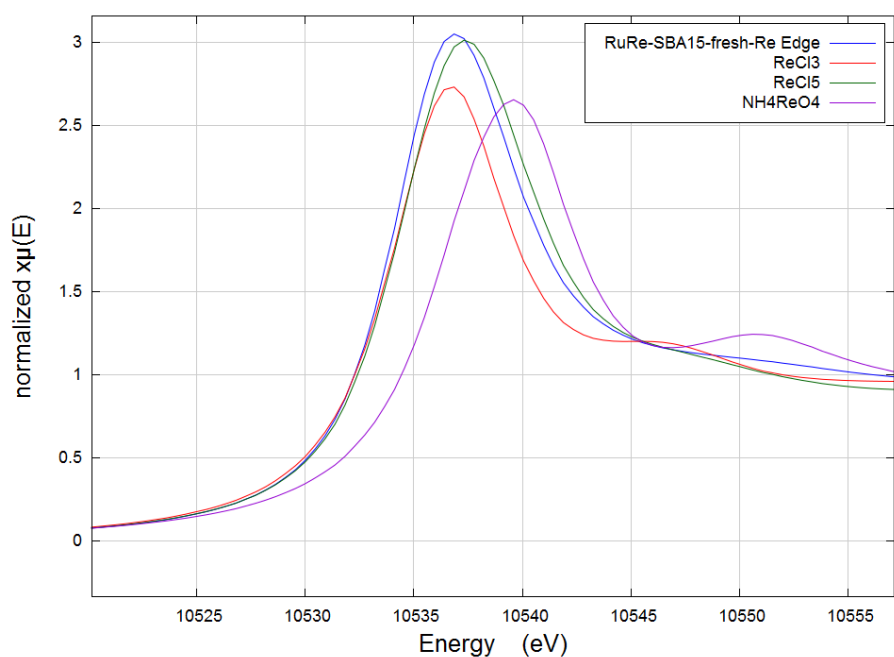
Figure 3.17: XANES spectra for Re L3 edge of as-prepared ReRu/SBA-15 catalyst together with $ReCl_3$, $ReCl_5$ and NH_4ReO_4 as references.

The extended X-ray absorption fine structure (EXAFS) functions of as-prepared and spent catalysts after Fourier Transform along with Morlet wavelet analysis, used to determine back-scatters, presented detailed information about the local environment of Ru and Re (Figure 3.18). As shown in Table 3.5, the short-range distances (R < 3 Å) and coordination numbers (CN) of Ru were determined in the as-prepared samples (two Ru-O shells at R = 1.81 Å, CN = 0.7; R = 2.1 Å, CN = 2.5; and one Ru-Ru/Ru-Re shell at R = 2.66 Å, total CN = 4.0). Although EXAFS could not distinguish Ru-Re and Ru-Ru distance, our best fitting suggests some heavy atom contribution in the Ru edge which is attributed to nearby Re atoms.
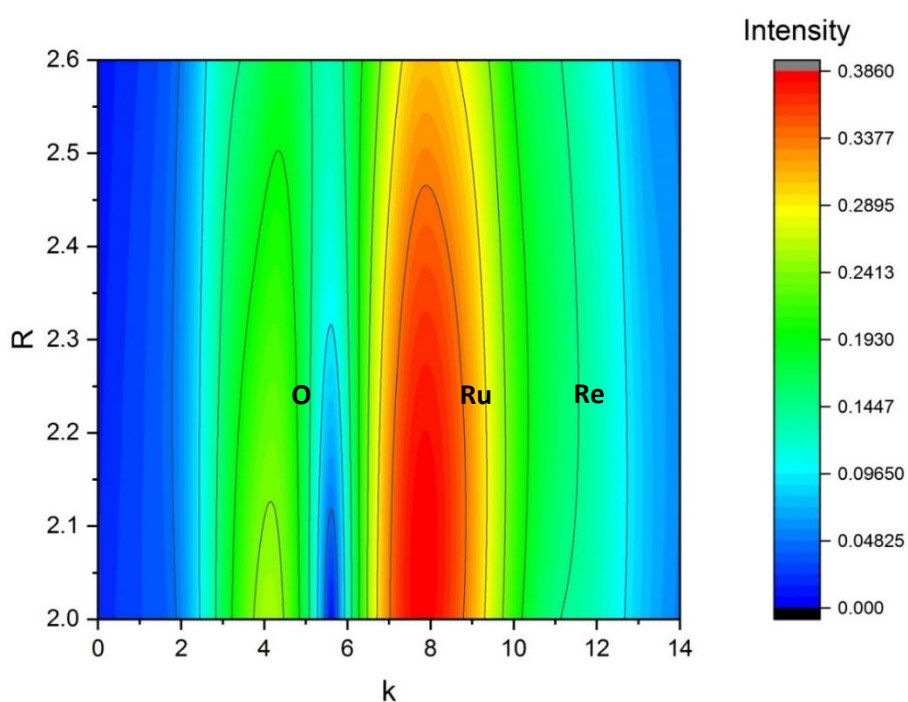
Figure 3.18: Morlet wavelet transform analysis of ReRu/SBA-15 spent catalyst.

Table 3.5: Fitting parameters of the curve fitted k3-weighted EXAFS analyses of as-prepared and spent ReRu/SBA-15 catalysts at Ru K-Edge.

Sample	Shell	Distance, R (Å)	Coordination Number (CN)	Debye-Weller factor
RuRe/SBA-15-as-prepared catalyst	Ru-O1	1.81 (1)	0.7 (3)	0.013
	Ru-O2	2.10 (1)	2.5 (3)	0.015
	Ru-Re	2.66 (2)	0.3 (1)	0.003
	Ru-Ru	2.66 (1)	2.7 (1)	0.007
RuRe/SBA-15-spent catalyst	Ru-O1	1.81 (1)	3.1 (3)	0.008
	Ru-O2	2.02 (2)	0.6 (2)	0.003
	Ru-Re	2.66 (1)	1.0 (2)	0.003
	Ru-Ru	2.66 (1)	3.0 (2)	0.005

As-prepared catalyst: R = 0.2%; k range 3–13.3; R range 1.15–3.0; spent catalyst: R = 0.5%; k range 3–13.3; R range 1.0–3.0.

Interestingly, after catalysis, the XANES of spent catalyst follows a very similar pattern to that of as-prepared catalyst, suggesting the preservation of oxidation state and evidencing that the active form of Ru is the metallic state. EXAFS pattern after catalysis shows 2 oxygen bindings to Ru at short (R=1.81Å, CN=3.1) and longer distances (R=2.02 Å, CN=0.6) as observed in as-prepared catalyst. Unlike to as-prepared sample, the contribution of heavier atoms in spent catalyst is more evident (R=2.66 Å, CN=1.0). The Morlet wavelet (Figure 3.18) analysis of spent catalyst also confirms the presence of a heavier element in longer distances.

Re L3-edge XANES patterns of as-prepared and spent catalysts are presented in Table 3.6. It is interesting to note the increase in oxidation state of Re from +2 to +5, estimated based on comparison with reference rhenium salts presented in Figure 3.20, under reductive conditions. This may be attributed to the strong interaction of Re atoms, released after hydrogenation of allyl ligands to propylene, with support surface oxygens inside the pore channels due to its extremely oxyphilic nature. Similar to Ru, Re oxidation state before and after catalysis did not change, suggesting Re+5 is active in amide hydrogenation. Our best EXAFS fitting of as-prepared catalyst at Re L3-edge evidences the presence of only Ru-Re bond at R=2.66 °A with a CN of 1.1. Such a small CN evidences the atomic distribution of Re near Ru atoms.

Table 3.6: Fitting parameters of the curve fitted k_3-weighted EXAFS analyses of as-prepared and spent ReRu/SBA-15 catalysts at Re L3-Edge.

Sample	Shell	Distance, R (Å)	Coordination Number (CN)	Debye-Weller factor
RuRe/SBA-15-as-prepared catalyst	Re-O1	1.85 (4)	1.1 (3)	0.013
	Re-O2	2.02 (1)	1.6 (2)	0.003
	Re-Ru	2.66 (1)	1.1 (2)	0.008
RuRe/SBA-15-spent catalyst	Re-O1	1.71 (1)	1.4 (2)	0.006
	Re-O2	1.98 (1)	1.8 (3)	0.004
	Re-Ru	2.64 (2)	1.4 (3)	0.008
	Re-Re	2.67(3)	1.4(4)	0.010

As-prepared catalyst: R = 2.5%; k range 3–14.1; R range 1.0–3.0; spent catalyst: R = 2.1%; k range 3–13.9; R range 1.0–3.0.

These results are consistent with STEM-HAADF analysis which revealed 2 populations: individual atoms and few-atoms-clusters region. Presumably, the oxyphilic nature of Re prevents its aggregation to clusters and remain as individual atoms in the SBA-15 channels. Ru is known as easily reducible and mobile on support materials. The few-atom-clusters region observed in STEM might be Ru atoms clustering. Likely, the excessive coalescence of Ru atoms is prevented by well dispersed Re atoms. However, further EDS analysis is necessary to confirm this hypothesis which was not available at the time when we performed STEM-HAADF experiments.

To investigate the chemical state of the Re and the Ru on the surface of the ReRu/SBA-15 (Initial) and ReRu/SBA-15 (Spent) catalysts. The XPS characterization was carried out, as shown in the Figure 3.19.
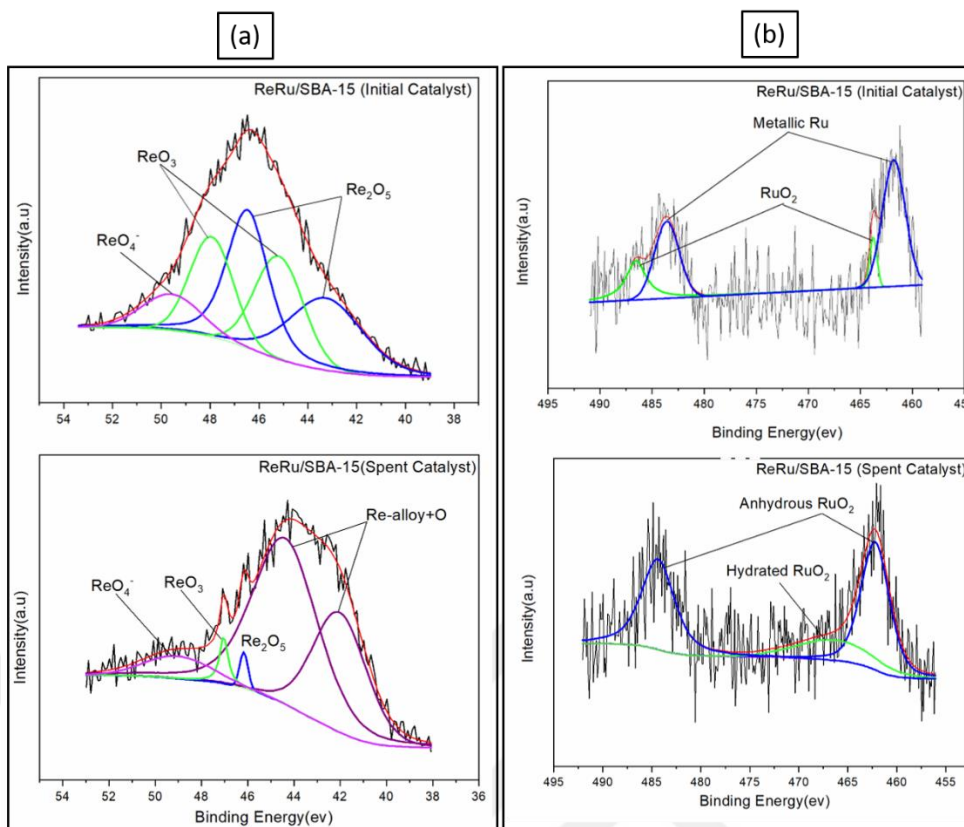
Figure 3.19: (a) The XPS spectra for the indicated catalyst in Re 4f region and (b) The XPS spectra for indicate catalyst in Ru 3p region.

Figure 3.19 (a) display the XPS spectra in the Re 4f of the initial ReRu/SBA-15 and spent ReRu/SBA-15. For the initial catalyst ReRu/SBA-15, we observed 5 main peaks at ca. 43.6 eV, 45.0 eV, 46.1 eV, 47.4 eV and 49.2 eV. According to the literature, the most intense peak at 46.1 associate with the larger peak 43.6 eV can be attributed to Re +5 (Re_2O_5). This result would quantitively agree with the results of XANES described above (Figure 3.16 and 3.17). The peaks at about 45.0 eV - 47.4 eV and 49.2 eV can be assigned to Re +6 (ReO_3) and Re+7 (ReO_4^-), respectively. Similar to the initial catalyst the spectra of spent catalyst ReRu/SBA-15 reveal 5 main peaks, the most two intense peaks at 41.0 eV and 44.2 eV can be attributed to Re-alloy+O. The most important difference between the two catalysts are the decrease intensity of the peaks characteristic Re+5 and Re+6 at 46.1 eV and 47.4 eV, respectively [94,111].

Concerning Ru 3p zone (Figure 3.19 (b)) for initial and spent ReRu/SBA-15 catalysts. It shows two main peaks for $3p_{1/2}$ and $3p_{3/2}$. According to the literature, the peaks at 461.2 eV and 485.0 eV can be attributed to metallic Ru. We can show that the most quantity of Ru is Ru (0) because these peaks are larger and more intense than

58

other peaks. These results confirmed the results obtained by XANES, where we are shown that the active form of Ru is the metallic state. The other peaks at 462.5 eV and 486.2 eV are attributed to Ru+4 (RuO_2). On the other hand, compared to the initial ReRu/SBA-15 catalyst, for the spent ReRu/SBA-15 catalyst two peaks in $3p_{3/2}$ zone are observed at 462.5 eV and 465.2 eV, but only one peak for the $3p_{1/2}$ zone. According to literature, the peaks at 462.5 eV and 465.2 eV attributed to anhydrous ReO_2 and hydrated ReO_2, respectively [94,112].

3.3.4. Investigation of Reduction Behaviour of the Catalysts

Observation of no significant color change in the prepared catalysts after the reduction and purification and similar catalytic activities of ReRu/SBA-15$_{(iwi-120^oC)}$ and unreduced ReRu/SBA-15$_{(crude)}$ catalysts, led us to investigate the reduction profiles of the prepared catalysts. Figure 3.20 shows the temperature-programmed reduction profiles of Ru and/or Re organometallic compounds placed on MCM-48, SBA-15 or SiO_2 using the incipient wetness impregnation method, together with TPR profiles of $Re_2(C_3H_5)_4$ and $Ru(C_4H_8)_2(C_8H_{12})$ organometallic compounds as referenced. According to the graph, the reduction of the organometallic compounds $Re_2(C_3H_5)_4$ and $Ru(C_4H_8)_2(C_8H_{12})$ in the absence of a support starts at 107°C and ends at 280°C. The observed peaks are compatible with the decomposition temperatures of $Re_2(C_3H_5)_4$ and $Ru(C_4H_8)_2(C_8H_{12})$ compounds in solution under hydrogen gas. The subsequent observation of a negative curve results from the effect of the released gases (propane and isobutane) on the TCD detector as a result of the breakdown of the compounds. The broad signal observed after 460°C is thought to be an artificial peak formed while the TCD signal was returning to zero after the release of propane and isobutane gases. However, in order to be sure of this assumption, the amount of hydrogen consumed will be calculated by integrating the observed peak areas and these results will be compared with the amount of catalyst used during the analysis.

When the organometallic compounds are impregnated on a support, the reduction curves differ from each other. In the reduction profile of Ru/SBA-15, a peak summiting at 166°C was observed initially. Then, a sharp second peak was observed at 416°C, followed by a broad shoulder at 504°C. In the reduction profile of Re/SBA-15, 2 significant peaks were observed, but the reduction temperatures were shifted to

high temperatures compared to pure Re precursor. Although the locations of the peaks in the reduction profile of ReRu/SBA-15 were found to be identical to those observed in Re/SBA-15, the relative height between the two peaks was different. Unlike ReRu/SBA-15, the reduction curve of ReRu/MCM-48 catalyst was found to be similar to the TPR profile of Ru/SBA-15. Although the reason of different reduction curves of Ru and Re organometallic compounds on a support substance has not been fully understood yet, it is known in the literature that organometallic complexes might interact with the oxide support either by physisorption or chemisorption. The strength of interaction might affect the reduction temperature of the complexes.
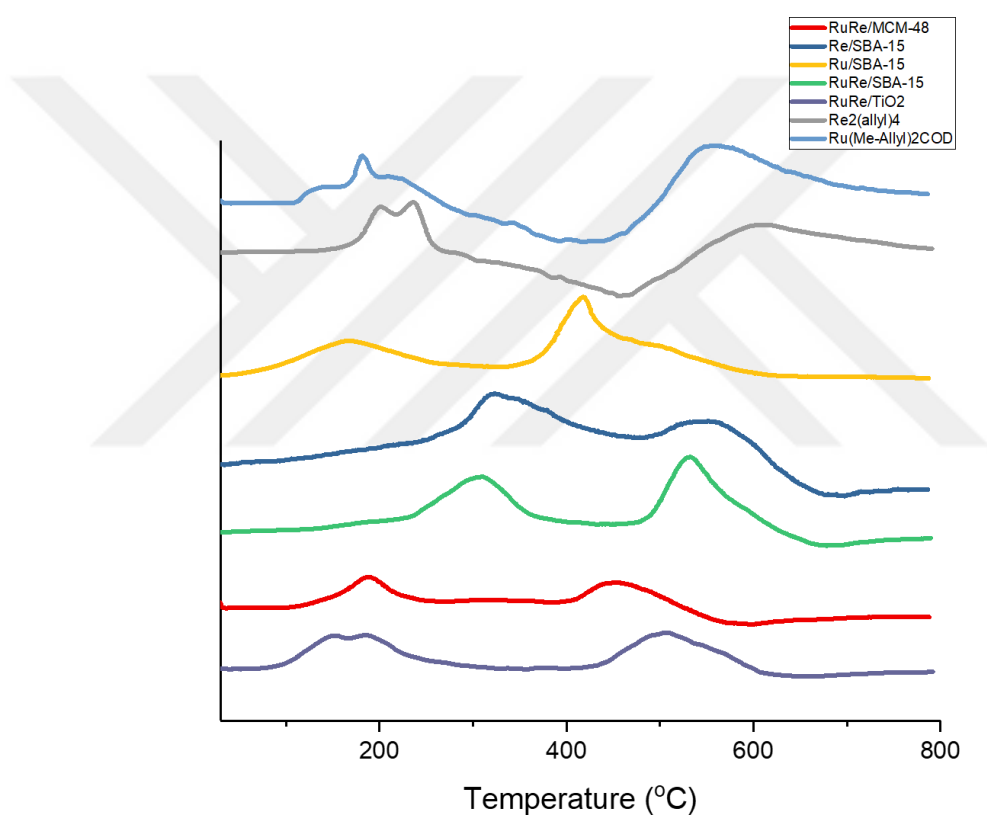
Figure 3.20: TPR profiles of organometallic precursors and ReRu catalyst.

3.4. Catalytic Performance of ReRu/SBA-15 in Tertiary Amides with Functional Groups

Being motivated from the promising fast and selective hydrogenation of 1-acetylpiperidine, we decided to expand the scope of amide substrates to have some insights to the catalytic performance and tolerance of ReRu/SBA-15 catalysts towards

functional groups. In this section of the thesis, the catalytic performance of ReRu/SBA-15 catalyst towards tertiary amides having arene, halogen and ester will be presented and discussed.

3.4.1. Catalytic Test for N-Methylacetanilide

N-Methylacetanilide is a tertiary amide product that was purchased from Fluorochem company (FCM02-FMMH). Molecular weight is 149,193 g/mol. The catalytic reaction was shown in Figure 3.21 and reaction conditions were listed below.
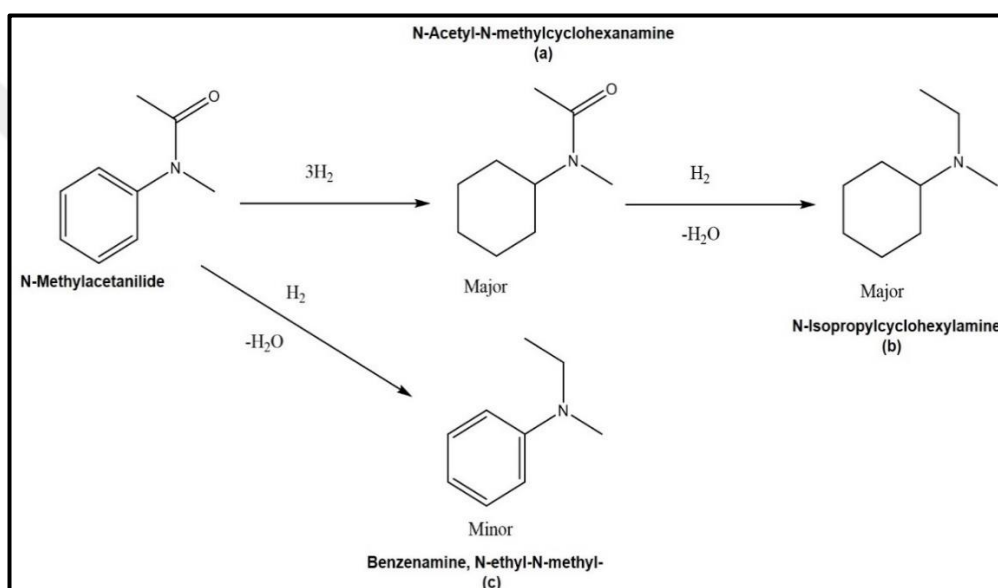
Figure 3.21: The mechanism of N-Methyl acetanilide hydrogenation.

DME was used as solvent in this reaction because N-Methyl acetanilide is not soluble in Octane at room temperature. First reactions were performed with Octane, then same reactions were repeated with DME solvent. On the other hand, the products which were observed at the end of the reaction, are soluble in Octane at room temperature. The catalytic test results were listed in Table 3.7.

Table 3.7: The catalytic test result for N-Methyl acetanilide.

	Amide	Catalyst	Time-Conditions	Product	Conv. (%)	Selectivity
1		ReRu/SBA-15	2 h-Octane	(a)	100	73.1
				(b)		26.9
2		ReRu/SBA-15	24 h-DME	(a)	100	47.3
				(b)		52.6
3	N-Methylacetanilide	Re$_3$Ru/SBA-15	2 h-Octane	(a)	100	69
				(b)		30
				(c)		1
4		ReRu$_3$/SBA-15	2 h-Octane	(a)	100	41.6
				(b)		58.4
5		ReRu$_3$/SBA-15	2 h-DME	(a)	100	62.9
				(b)		37.1

Catalytic conditions: 3 mL octane or DME (solvent), 66 µL of n-dodecane (internal standard), 120 µL (1 mmol) amide, 2 mol% metal (100 mg) catalyst, 150ºC, 40 bar H$_2$, 2 h, 1000 rpm. Sub-indices: representation of the synthesis methods of the catalyst and reduction temperatures. (a) N-Acetyl-N-methylcyclohexanamine, (b) N-methyl,N-cyclohexane ethanamine, (c) N-ethyl-N-methyl-Benzenamine.

Table 3.7 shows that the catalysts were hydrogenated for all the double bonds in the reactant, so some different amides can be observed at the end of the reactions as product (b). Small amount of desired product (c) was observed for Re$_3$Ru/SBA-15 catalyst as 1% indicated that the diluting the of extended surface of Ru with Re can enhance the selectivity towards the desired product. In experiments 1 and 2 show that amine product (b) amount is higher for DME solvent (experiment 2) because the solubility of reactant in DME is better than Octane.

3.4.2. Catalytic Test for N-Methyl-2-Pyrrolidone

N-Methyl-2-Pyrrolidone is a tertiary amide product that was purchased from Fluorochem company (Lot:1162143). Molecular weight and density are 99.13 g/mol, 1028 g/L, respectively. The catalytic reaction was shown in Figure 3.22 ((a) N-Methyl-2-Pyrrolidine) and reaction conditions were listed below;

Figure 3.22: The mechanism of N-Methyl-2-Pyrrolidone hydrogenation.

The catalytic test results were shown in Table 3.8.

Table 3.8: The catalytic test result for N-Methyl-2-Pyrrolidone.

	Amide	Catalyst	Time-Solvent	Conversion (%)	Products	Selectivity (%)
1	N-Methyl-2-Pyrrolidone	ReRu/SBA-15	24h-Octane	70.5	(a)	>95

Catalytic conditions: 3 mL octane (solvent), 66 µL of n-dodecane (internal standard), 120 µL (1 mmol) amide, 2 mol% metal (100 mg) catalyst, 150ºC, 40 bar H_2, 2 h, 1000 rpm. Sub-indices: representation of the synthesis methods of the catalyst and reduction temperatures. (a) N-Methyl-2-Pyrrolidine.

3.4.3. Catalytic Test for Dimethyl carboxyl chloride

Dimethyl carboxyl chloride is a tertiary amide product that was purchased from Sigma-Aldrich company (Lot: D152803). Molecular weight and density are 107.54 g/mol, 1168 g/L, respectively. The catalytic reaction was shown in Figure 3.23 ((a)

tetramethylurea, (b) dimethylamine, 1) and 2) hydrogenation reaction mechanism) and reaction conditions were listed below.
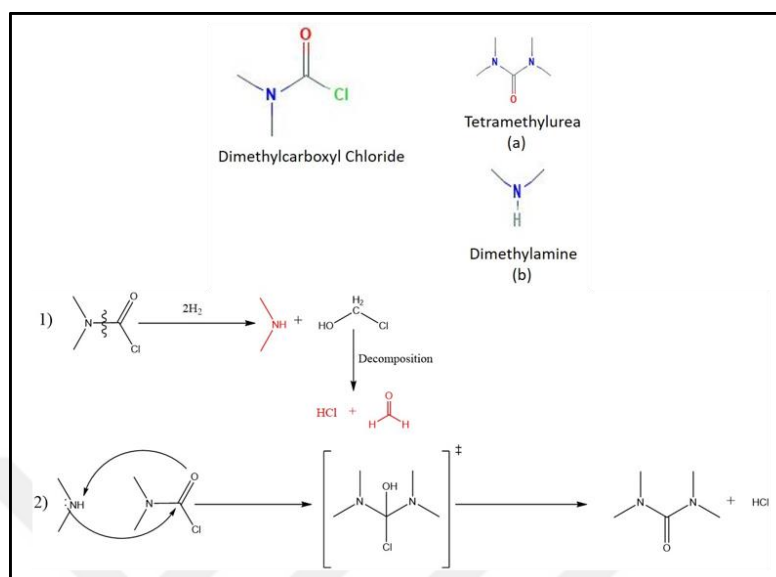
Figure 3.23: The mechanism of Dimethyl carboxyl chloride hydrogenation.

The catalytic test results were shown in Table 3.9.

Table 3.9: The catalytic test result for dimethylcarboxyl chloride.

	Amide	Catalyst	Time-Solvent	Conversion (%)	Products	Selectivity (%)
1	Dimethylcarboxyl Chloride	ReRu/SBA-15	24h-Octane	96.4	(a)	>99
					(b)	trace
2		ReRu₃/SBA-15	24h-Octane	97.2	(a)	>99
					(b)	trace

Catalytic conditions: 3 mL octane (solvent), 66 µL of n-dodecane (internal standard), 120 µL (1 mmol) amide, 2 mol% metal (100 mg) catalyst, 150°C, 40 bar H_2, 2 h, 1000 rpm. Sub-indices: representation of the synthesis methods of the catalyst and reduction temperatures. (a) Tetramethylurea, (b) Dimethylamine, 1) and 2) hydrogenation reaction mechanism.

At the end of the reaction, desired amine product was not observed, but new formation product was observed, and the mechanism was explained above.

3.4.4. Catalytic Test for Methyl-2-(2-oxopyrrolidin-1-yl) acetate

Methyl-2-(2-oxopyrrolidin-1-yl) acetate is a tertiary amide product that was purchased from Fluorochem company (Lot: 329559). Molecular weight and density are 157.169 g/mol, 1170 g/L, respectively. The catalytic reaction was shown in Figure 3.26 ((a) Methyl 2-(2-oxopyrrolidin-1-yl) acetate, (b) 1-(2-hydroxyethyl) pyrrolidin-2-one and (c) 2-(pyrrolidin-1-yl) ethanol) and reaction conditions were listed below;
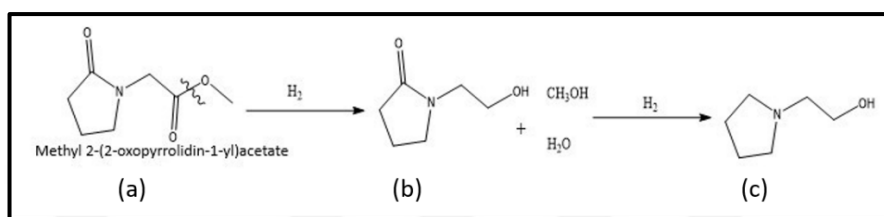
Figure 3.24: The mechanism of Methyl-2-(2-oxopyrrolidin-1-yl) acetate hydrogenation.

The catalytic test results were shown in Table 3.10.

Table 3.10: The catalytic test result for Methyl-2-(2-oxopyrrolidin-1-yl) acetate.

	Amide	Catalyst	Time-Solvent	Products
1	(a)	ReRu/SBA-15	24h-Octane	(b) Major
				(c) Minor

Catalytic conditions: 3 mL octane (solvent), 66 µL of n-dodecane (internal standard), 120 µL (1 mmol) amide, 2 mol% metal (100 mg) catalyst, 150°C, 40 bar H_2, 2 h, 1000 rpm. Sub-indices: representation of the synthesis methods of the catalyst and reduction temperatures. (a) Methyl 2-(2-oxopyrrolidin-1-yl) acetate, (b) 1-(2-hydroxyethyl) pyrrolidin-2-one and (c) 2-(pyrrolidin-1-yl) ethanol.

Quantitative analysis could not be performed in order to lacking solubility of product (b) in Octane. Melting point of product (b) was determined as 19-21°C. Desired amine product was not observed at the end of reaction, but alcohol product was observed. Different amides groups were detected in GC-MS analysis.

4. CONCLUSION

In this manuscript, the synthesis, characterization and preliminary catalytic application of supported ruthenium and rhenium bi-metallic nanocatalysts are reported.

The reason to choose Re-derived from the observation of high catalytic activities with good selectivity values for Re-based catalysts reported in the literature. Rhenium is known to give high adsorption and high activity for hydrogenation of stable adsorbates in terms of intrinsic high catalytic activity and selectivity in the hydrogenation of difficult functional groups such as carboxylic acids and amides. Particularly the oxophilic nature of Re facilitates the binding of C=O under mild reaction conditions. The role of co-metal is thought to activate H_2 and contribute desirable geometric and electronic promotions for the selective hydrogenation of carboxylate group. In this regard, Ru was thought to be a convenient partner as it is well known to activate H_2, even at low temperatures and the hcp crystal structure of Ru is 100% miscible inside the hcp structure of Re.

The main objective was to design and to prepare in a controlled manner, high surface area rhenium and ruthenium nanostructures in order to evaluate them as catalysts in the hydrogenation of amides.

Ruthenium and rhenium containing catalysts were prepared by decomposition of organometallic complexes, namely $[Ru(C_4H_8)_2(C_8H_{12})]$ and $[Re_2(C_3H_5)_4]$. The synthesis was carried out at solid state, after impregnating the metal precursors in various ways (incipient wetness impregnation, solution impregnation etc.) on a porous (SBA-15, MCM-48) or a non-porous support for comparison (SiO_2), under mild pressure of dihydrogen (3 bar) and at 120°C. The characterization of the so-obtained catalysts was performed by using a combination of the state-of-the art techniques (XRD, EXAFS, XPS and STEM-HAADF). In addition, support-organometallic complex interaction, reducibility of the precursors and the surface state of active metal atoms were studied by NMR spectroscopy in order to apprehend their properties better in catalysis.

Scanning transmission electron microscopy and x-ray diffraction techniques revealed that Re and Ru metals are mainly atomically dispersed on high surface area on mesoporous support materials. It is concluded that the large amount of aromatic

solvents used during solution synthesis of catalysts are not a good choice for the synthesis of ReRu bimetallic catalysts. Because the arene groups in the solvent can interact with $Ru(C_4H_8)_2(C_8H_{12})$ in the presence of H_2. It is thought that the content of the yellow solution obtained from the solution synthesis and the low catalytic activity observed in the solid samples is due to the formation of the $Ru(arene)(C_8H_{12})$ complex which is difficult to be reduced at low temperature and is washed away during purification step.

NMR studies with POSS and organometallic complexes evidenced that there is interaction between surface hydroxyl groups and metal precursors at elevated temperatures even in the absence of hydrogen. The acidic protons on the surface can be removed by the negative allyl ligands, leading to propylene or butene gas from $Re_2(C_3H_5)_4$ and $Ru(C_4H_8)_2(C_8H_{12})$ complexes respectively. While $Re_2(C_3H_5)_4$ interacts with the silanol groups on the POSS surface and is completely decomposable, part of the compound $Ru(C_4H_8)_2(C_8H_{12})$ remains intact when heated with POSS. This is presumably due to the fact that the dihydroxylation of the surface -OH groups are faster than the abstraction of proton in the presence of $Ru(C_4H_8)_2(C_8H_{12})$.

Initial catalytic tests of the prepared catalysts in selective hydrogenation of 1-acetylpiperidine to ethylpiperidine were performed under 40 bar H_2 at 150°C for 2 hours. The Re and Ru supported on porous materials (SBA-15, MCM-48,) showed at least 2-fold better catalytic activity compared to non-porous supports, *i.e.* TiO_2 and SiO_2. Among the porous structures, the highest catalytic activity was obtained by large pore size ReRu/SBA-15. After catalyst screening experiments, further catalytic reaction conditions optimisation has been conducted by investigating the effect of solvent, Ru: Re metal ratio and mass/heat transfer limitations. The results evidenced that solvent should be selected carefully based the polarity, thus solubility of amide substrates and corresponding amines formed during catalytic hydrogenation in order to obtain high yield and accurate analysis of reaction products. In addition, high speed stirring was found to be necessary to overcome the internal diffusion mass transfer within the pores of ReRu/SBA-15 catalysts. Increasing the amount of Ru in the catalysts enhanced the reaction kinetics due to faster H_2 activation and hydrogen transfer to the amide substrates; while the hydrogenation of other functional groups, such as arene moieties, in the amides were also enhanced. As a drawback, it has been observed that halides, esters and aromatic groups are not tolerated over ReRu/SBA-15 catalysts. The total catalytic test results were listed in Table 4.1.

The originality of this work lies on the development of few-atom-cluster alloys using organometallic complexes and porous support materials which led to high reaction kinetics for 1-acetylpiperidine hydrogenation. In this perspective, the first aim of the project has been achieved (i.e. highly dispersed few-atom clustered alloy formation). However, the developed catalysts were not found to be tolerant to functional groups and the reaction kinetics suffer from diffusion limitations when large molecules are used. Further mechanistic studies and improvement are necessary to achieve highly active and selective catalysis.

Nevertheless, these results are promising in terms of atom efficient catalysis and showed that amides can be hydrogenated at high reaction rates in the presence of few-atoms-alloy-clusters. Our work confirms the findings of other researchers which shows that alloy formation is the key for efficient amide hydrogenation under mild reaction conditions as individual atoms (Ru or Re) were not active. Future work should focus on the investigation of the active catalyst more extensively, with the aim of more conclusively attributing the activity to a particular source, i.e. the size and composition of Ru-Re bimetallic alloy clusters. DFT calculation might be helpful in this concern. In addition, in order to prevent Ru-Re bond and avoid the random distribution of metals, organometallic complexes consisting Ru-Re bond can be used as a precursor, such as CpReRu $(CO)_7$.

Table 0.1: The summary of catalytic hydrogenation of tertiary amides.

	Amide	Catalyst	Conditions	Product	Conversion (%)	Selectivity
1		ReRu/SBA-15	2 h		65.1	>99
2		ReRu/SBA-15	24 h		100	>99
3	APP	Re/SBA-15	2 h	EPP	4.8	>99
4		Ru/SBA-15	2 h		2.8	0
5		ReRu/MCM-48	2 h		64.0	98
6		ReRu/SiO$_2$	2 h		25.6	98
7		ReRu/SBA-15	2 h/ Octane	AMH	100	73.1
				MCHE		26.9
8		ReRu/SBA-15	24 h/ DME	EMB	100	47.3
				MCHE		52.6
9	MAA	Re$_3$Ru/SBA-15	2 h/ Octane	EMB	100	69
				MCHE		30
				EMB		1
10		ReRu$_3$/SBA-15	2 h/ Octane	EMB	100	41.6
				MCHE		58.4
11		ReRu$_3$/SBA-15	2 h/ DME	EMB	100	62.9
				MCHE		37.1
12	MP	ReRu/SBA-15	24h/ Octane	MP*	70.5	>95
13		ReRu/SBA-15	24h/ Octane	TMU	96.4	>99
	DCC			DEA		trace
14		ReRu$_3$/SBA-15	24h/ Octane	TMU	97.2	>99
				DEA		trace
15	MOA	ReRu/SBA-15	24h/ Octane	EPO	-	-
				MPO	-	-

MP: N-Methyl-2-Pyrrolidone, DCC: Dimethylcarboxyl Chloride, MOA: Methyl 2-(2-oxopyrrolidin-1-yl)acetate, MAA: N-Methylacetanilide, AMH:N-Acetyl-N-methylcyclohexanamine, MCHE: N-methyl,N-cyclohexane ethanamine, EMB: N-ethyl-N-methyl-Benzenamine, MP*:N-Methyl-2-Pyrrolidine, TMU: Tetramethylurea, DEA: Dimethylamine, EPO: 1-Ethylpyrrolidin-2-One, MPO: N-Methyl-2-Pyrrolidone, APP: 1-Acetylpiperidine, EPP:1-Ethylpiperidine

REFERENCES

[1]   Martínez, C., Corma, A., (2011), "Inorganic Molecular Sieves: Preparation, Modification and Industrial Application in Catalytic Processes", Coord. Chem. Rev., 255, 1558–1580.

[2]   Constable, D. J. C., Dunn, P. J., Hayler, J. D., Humphrey, G. R., Leazer, J. L., (2007), "Key Green Chemistry Research Areas: A Perspective from Pharmaceutical Manufacturers", Green Chem., 9, 411–420.

[3]   Hayes, K. S., (2001), "Industrial Processes for Manufacturing Amines", Appl. Catal. A Gen., 211 (1), 187–195.

[4]   McAlees, A. J., McCrindle, R., (1969), "Catalytic Hydrogenations of Cyclic Imides and Anhydrides", J. Chem. Soc. C Org., 1013–1014.

[5]   Smith, A. M., Whyman, R., (2014), "Review of Methods for The Catalytic Hydrogenation of Carboxamides", Chem. Rev., 114 (10), 5477–5510.

[6]   Werkmeister, S., Junge, K., Beller, M., (2014), "Catalytic Hydrogenation of Carboxylic Acid, Esters, Amides, and Nitriles with Homogeneous Catalysts", Am. Chem. Soc., 18 (2), 289–302.

[7]   Nowicki, A., Boulaire, V., Roucoux, A., (2007), "Nanoheterogeneous Catalytic Hydrogenation of Arenes: Evaluation of The Surfactant-Stabilized Aqueous Ruthenium(O) Colloidal Suspension", Adv. Synth. Catal., 349 (14–15), 2326–2330.

[8]   Sommerdijk, N. A. J. M., Friedrich, H., Zečević, J., Eggenhuisen, T. M., de Jong, K. P., (2013), "Controlling The Distribution of Supported Nanoparticles by Aqueous Synthesis", Chem. Mater., 25 (6), 890–896.

[9]   Zourob, M., Hawkes, J. J., Coakley, W. T., Brown, B. J. T., Fielden, P. R., (2015), "Dark-Field Microscopy Studies of Single Metal Nanoparticles: Understanding The Factors That Influence The Linewidth of The Localized Surface Plasmon Resonance", Anal. Chem., 15, 8787–8831.

[10]   Salata, O. V, (2004), "Applications of Nanoparticles in Biology and Medicine", J. Nanobiotechnology, 2 (1), 3.

[11]   Nitta, N., Wu, F., Lee, J. T., Yushin, G., (2015), "Li-ion Battery Materials: Present and Future", Mater. Today, 18 (5), 252–264.

[12]   Tee, B. C. K., Wang, C., Allen, R., Bao, Z., (2012), "An Electrically and Mechanically Self-Healing Composite with Pressure and Flexion-Sensitive Properties for Electronic Skin Applications", Nat. Nanotechnol., 7 (12), 825–832.

[13]   Aiken, J. D., Finke, R. G., (1999), "A Review of Modern Transition-Metal Nanoclusters: Their Synthesis, Characterization, and Applications in Catalysis", J. Mol. Catal. A Chem., 145, 1–44.

[14]   McCaffrey, R., Long, H., Jin, Y., Sanders, A., Park, W., (2014), "Template Synthesis of Gold Nanoparticles with An Organic Molecular Cage", J. Am.

Chem. Soc., 136 (5), 1782–1785.

[15]	Schmid, G., (1992), "Large Clusters and Colloids. Metals in The Embryonic State", Chem. Rev., 92 (8), 1709–1727.

[16]	Horikoshi, S., Serpone, N., (2013), "Microwaves in Nanoparticle Synthesis: Fundamentals and Applications", ISBN: 9783527331970, Wiley-VCH Verlag GmbH & Co.

[17]	Sakthivel, S., Krishnan, V. V., Pitchumani, B., (2008), "Influence of Suspension Stability on Wet Grinding for Production of Mineral Nanoparticles", Particuology, 6 (2), 120–124.

[18]	Link, S., El-Sayed, M. A., (1999), "Size and Temperature Dependence of The Plasmon Absorption of Colloidal Gold Nanoparticles", J. Phys. Chem. B, 103 (21), 4212–4217.

[19]	Guari, Y., Thieuleux, C., Mehdi, A., Reyé, C., Corriu, R. J. P., (2001), "Formation of Gold Nanoparticles within Functionalised Ordered Mesoporous Silica an Organometallic 'Chimie Douce' Approach", Chem. Commun., (15), 1374–1375.

[20]	Finney, E. E., Finke, R. G., (2008), "Nanocluster Nucleation and Growth Kinetic and Mechanistic Studies: A Review Emphasizing Transition-Metal Nanoclusters.", J. Colloid Interface Sci., 317 (2), 351–374.

[21]	Schmid, G. D., (2008), "General Features of Metal Nanoparticles Physics and Chemistry", ISBN: 9780444530578, Elsevier Science.

[22]	Hornstein, B. J., Finke, R. G., (2004), "Transition-Metal Nanocluster Kinetic and Mechanistic Studies Emphasizing Nanocluster Agglomeration: Demonstration of A Kinetic Method That Allows Monitoring of All Three Phases of Nanocluster Formation and Aging", Chem. Mater., 16 (20), 3972.

[23]	Leisner, T., Rosche, C. H., Wolf, S., Granzer, F., Wöste, L., (1996), "The Catalytic Role of Small Coinage-Metal Clusters in Photography", Surf. Rev. Lett., 3 (1), 1105–1108.

[24]	Faraday, M., (1857), "Experimental Relations of Gold (and Other Metals) to Light", Philos. Trans. R. Soc. London, 147, 145–181.

[25]	Cavicchioli, M., Varanda, L. C., Massabni, A. C., Melnikov, P., (2005), "Silver Nanoparticles Synthesized by Thermal Reduction of A Silver(I)–Aspartame Complex in Inert Atmosphere", Mater. Lett., 59 (28), 3585–3589.

[26]	Eustis, S., El-Sayed, M. A., (2006), "Molecular Mechanism of The Photochemical Generation of Gold Nanoparticles in Ethylene Glycol: Support for The Disproportionation Mechanism", J. Phys. Chem. B, 110 (29), 14014–14019.

[27]	Wiaderek, K. M., Cox, J. A., (2011), "Preparation and Electrocatalytic Application of Composites Containing Gold Nanoparticles Protected with Rhodium-Substituted Polyoxometalates", Electrochim. Acta, 56 (10), 3537–3542.

[28]	Ponce, A. A., Klabunde, K. J., (2005), "Chemical and Catalytic Activity of Copper Nanoparticles Prepared via Metal Vapor Synthesis", J. Mol. Catal. A Chem., 225, 1–6.

[29]   Ratheesh, V. K., Gopidas, K. R., (2011), "Palladium Nanoparticle-Cored G1-Dendrimer Stabilized by Carbon-Pd Bonds: Synthesis, Characterization and Use As Chemoselective, Room Temperature Hydrogenation Catalyst", Tetrahedron Lett., 52, 3102–3105.

[30]   Sperling, R. A., Parak, W. J., (2010), "Surface Modification, Functionalization and Bioconjugation of Colloidal Inorganic Nanoparticles", Philos. Trans. A. Math. Phys. Eng. Sci., 368 (1915), 1333–1383.

[31]   Roucoux, A., Schulz, J., Patin, H., (2002), "Reduced Transition Metal Colloids: A Novel Family of Reusable Catalysts?", Chem. Rev., 102 (10), 3757–3778.

[32]   Kinayyigit, S., Lara, P., Lecante, P., Philippot, K., Chaudret, B., (2014), "Probing The Surface of Platinum Nanoparticles with ^{13}CO By Solid-State NMR and IR Spectroscopies", Nanoscale, 6, 539–546.

[33]   Pan, C., Pelzer, K., Philippot, K., Chaudret, B., Dassenoy, F., (2001), "Ligand-Stabilized Ruthenium Nanoparticles: Synthesis, Organization, and Dynamics", J. Am. Chem. Soc., 123 (31), 7584–7593.

[34]   Muñoz-Navia, M., Dorantes-Dávila, J., Zitoun, D., Amiens, C., Jaouen, N., (2009), "Tailoring The Magnetic Anisotropy in CoRh Nanoalloys", Appl. Phys. Lett., 95 (23), 233107.

[35]   de Caro, D., Wally, H., Amines, C., Chaudret, B., (1994), "Synthesis and Spectroscopic Properties of A Novel Class of Copper Particles Stabilized by Triphenylphosphine", J. Chem. Soc. Chem. Commun., (16), 1891–1892.

[36]   Ayvalı, T., Lecante, P., Fazzini, P. F., Gillet, A., Philippot, K., (2014), "Facile Synthesis of Ultra-Small Rhenium Nanoparticles", Chem. Commun., 50 (74), 10809–10811.

[37]   Moulijn, J. A., (2019), "Catalysis : An Integrated Approach to Homogeneous, Heterogeneous and Industrial Catalysis", ISBN:9780444829634, Elsevier Science.

[38]   Snoeckx, R., Bogaerts, A., (2017), "Plasma Technology: A Novel Solution for CO_2 Conversion?", Chem. Soc. Rev., 46, 5805–5863.

[39]   Polshettiwar, V., Varma, R. S., (2010), "Green Chemistry by Nano-catalysis", Green Chem., 12 (5), 743–754.

[40]   Schlögl, R., Abd Hamid, S. B., (2004), "Nanocatalysis: Mature Science Revisited or Something Really New?", Angew. Chemie Int. Ed., 43 (13), 1628–1637.

[41]   Astruc, D., Lu, F., Aranzaes, J. R., (2005), "Nanoparticles as Recyclable Catalysts: The Frontier between Homogeneous and Heterogeneous Catalysis", Angew. Chemie Int. Ed., 44 (48), 7852–7872.

[42]   Narayanan, R., El-Sayed, M. A., (2004), "Effect of Nanocatalysis in Colloidal Solution on The Tetrahedral and Cubic Nanoparticle SHAPE: Electron-Transfer Reaction Catalyzed by Platinum Nanoparticles", J. Phys. Chem. B, 108 (18), 5726–5733.

[43]   Astruc, D., Lu, F., Aranzaes, J. R., (2005), "Nanoparticles as Recyclable Catalysts: The Frontier between Homogeneous and Heterogeneous Catalysis", Angew. Chemie Int. Ed., 44 (48), 7852–7872.

[44] LaMer, V.K., Dinegar, R.H., (1950), "Theory, Production and Mechanism of Formation of Monodispersed Hydrosols", J. Am. Chem. Soc., 72 (11), 4847–4854.

[45] Guo, D., Zhu, L., Huang, Z., Zhou, H., Ge, Y., (2013), "Anti-Leukemia Activity of PVP-Coated Silver Nanoparticles via Generation of Reactive Oxygen Species and Release of Silver Ions", Biomaterials, 34 (32), 7884–7894.

[46] Smolensky, E. D., Neary, M. C., Zhou, Y., Berquo, T. S., Pierre, V. C., (2011), "Fe_3O_4@organic@Au: Core–Shell Nanocomposites with High Saturation Magnetisation as Magnetoplasmonic MRI Contrast Agents", Chem. Commun., 47 (7), 2149–2151.

[47] Weir, A., Westerhoff, P., Fabricius, L., Hristovski, K., von Goetz, N., (2012), "Titanium Dioxide Nanoparticles in Food and Personal Care Products", Environ. Sci. Technol., 46 (4), 2242–2250.

[48] Walkey, C., Das, S., Seal, S., Erlichman, J., Heckman, K., (2015), "Catalytic Properties and Biomedical Applications of Cerium Oxide Nanoparticles", Environ. Sci. Nano, 2 (1), 33–53.

[49] Chung, J., Bieri, N. R., Ko, S., Grigoropoulos, C. P., Poulikakos, D., (2004), "In-Tandem Deposition and Sintering of Printed Gold Nanoparticle Inks Induced by Continuous Gaussian Laser Irradiation", Appl. Phys. A, 79 (4), 1259–1261.

[50] Chung, J., Ko, S., Bieri, N. R., Grigoropoulos, C. P., Poulikakos, D., (2004), "Conductor Microstructures by Laser Curing of Printed Gold Nanoparticle Ink", Appl. Phys. Lett., 84 (5), 801–803.

[51] Geboers, J., Van de Vyver, S., Carpentier, K., de Blochouse, K., Jacobs, P., (2010), "Efficient Catalytic Conversion of Concentrated Cellulose Feeds To Hexitols with Heteropoly Acids and Ru on Carbon", Chem. Commun., 46 (20), 3577–3579.

[52] Wang, A. Q., Chang, C. M., Mou, C. Y., (2005), "Evolution of Catalytic Activity of Au−Ag Bimetallic Nanoparticles on Mesoporous Support for CO Oxidation", J. Phys. Chem. B, 109 (40), 18860–18867.

[53] Burch, R., Paun, C., Cao, X. M., Crawford, P., Goodrich, P., (2011), "Catalytic Hydrogenation of Tertiary Amides at Low Temperatures and Pressures Using Bimetallic Pt/Re-Based Catalysts", J. Catal., 283 (1), 89–97.

[54] GINSBURG, D., (1967), "Types of Amines", ISBN:9781483185903, Pergamon.

[55] Stein, M., Breit, B., (2013), "Catalytic Hydrogenation of Amides to Amines under Mild Conditions", Angew. Chemie Int. Ed., 52 (8), 2231–2234.

[56] Stein, M., Robin, W., (2014), "Review of Methods for the Catalytic Hydrogenation of Carboxamides", American Chemical Society., 114 (10), 5477-5510.

[57] Newman, M. S., Fukunaga, T., (1960), "The Reduction of Amides to Amines via Nitriles by Lithium Aluminum Hydride1", J. Am. Chem. Soc., 82 (3), 693–696.

[58] Brown, H. C., Tsukamoto, A., (1961), "The Reaction of 1-Acylaziridines with

Lithium Aluminum Hydride A New Aldehyde Synthesis", J. Am. Chem. Soc., 83 (8), 2016–2017.

[59]   Baumgarten, H. E., Bower, F. A., (1957), "Reactions of Amines. II. Degradation via Tertiary Amine Oxides1", J. Am. Chem. Soc., 79 (12), 3145–3149.

[60]   Heinzman, S. W., Ganem, B., (1982), "Mechanism of Sodium Borohydride-Cobaltous Chloride Reductions", J. Am. Chem. Soc., 104 (24), 6801–6802.

[61]   Akabori, S., Takanohashi, Y., (1991), "Novel Borane–Selenium Complex: Highly Selective Reduction of Tertiary Amides and Nitriles to The Corresponding Amines with Sodium Borohydride–Dialkylselenium Dibromide", J. Chem. Soc. Perkin Trans. 1 (2), 479–482.

[62]   Ellzey, S. E., Mack, C. H., Connick, W. J., (1967), "Dehydration of Primary Amides with Sodium Borohydride", J. Org. Chem., 32 (3), 846–847.

[63]   Kuehne, M. E., Shannon, P. J., (1977), "Reduction of Amides and Lactams to Amines by Reactions with Phosphorus Oxychloride and Sodium Borohydride", J. Org. Chem., 42 (12), 2082–2087.

[64]   Kikugawa, Y., Ikegami, S., Yamada, S., (1969), "Chemistry of Diborane and Sodium Borohydride. VI. The Reaction of Amides with Sodium Borohydride", Chem. Pharm. Bull. (Tokyo)., 17 (1), 98–104.

[65]   Ren, J., Li, L. C., Liu, J. K., Zhu, H. J., Pittman, C. U., (2006), "Investigations of Different Chemoselectivities in Primary, Secondary and Tertiary Amide Reactions with Sodium Borohydride", European J. Org. Chem., 2006 (8), 1991–1999.

[66]   Zhu, H. J., Lu, K. T., Sun, G. R., He, J. B., Li, H. Q., (2003), "Reduction of Amides with $NaBH_4$ in Diglyme at 162°C", New J. Chem., 27 (2), 409–413.

[67]   Brown, H. C., Heim, P., (1964), "Diborane as A Mild Reducing Agent for The Conversion of Primary, Secondary, and Tertiary Amides into The Corresponding Amines", J. Am. Chem. Soc., 86 (17), 3566–3567.

[68]   Kornet, M. J., Thio, P. A., Tan, S. I., (1968), "Borane Reduction of Amido Esters", J. Org. Chem., 33 (9), 3637–3639.

[69]   Shono, T., Masuda, H., Murase, H., Shimomura, M., Kashimura, S., (1992), "Electroorganic Chemistry: Facile Electroreduction of Methyl Esters and N,N-Dimethylamides of Aliphatic Carboxylic Acids to Primary Alcohols", J. Org. Chem., 57 (4), 1061–1063.

[70]   Deprez, D., Margraff, R., Bizot, J., Pulicani, J. P., (1987), "Reduction electrochimique de la Fonction Amide d'un Compose Antitumoral, l'Echinosporine", Tetrahedron Lett., 28 (40), 4679–4680.

[71]   Quadback-Seeger H. J., Tonne, P., (1975), German Patent DE 2328757, 125055.

[72]   Smith, A. M., Whyman, R., (2014), "Review of Methods for The Catalytic Hydrogenation of Carboxamides", Chem. Rev., 114 (10), 5477–5510.

[73]   Anon., (1938), German Patent DE 667627.

[74]   Lazier, W. A., (1940), "Process for Hydrogenating Amides and Imides to

Amines",U.S. Patent 2187745, 3764.

[75] Guyer, A., Bieler, A., Gerliczy, G., (1955), "Über die Katalytische Reduktion Aliphatischer Carbonsäureamide", Helv. Chim. Acta, 38 (6), 1649–1654.

[76] Broadbent, H. S., Campbell, G. C., Bartley, W. J., Johnson, J. H., (1959), "Rhenium and Its Compounds as Hydrogenation Catalysts. III. Rhenium Heptoxide1,2,3", J. Org. Chem., 24 (12), 1847–1854.

[77] Anon., (1968), French Patent FR 1532063, 49228k.

[78] Beamson, G., Papworth, A. J., Philipps, C., Smith, A. M., Whyman, R., (2011), "Selective Hydrogenation of Amides Using Bimetallic Ru/Re and Rh/Re Catalysts", J. Catal., 278 (2), 228–238.

[79] Beamson, G., Papworth, A. J., Philipps, C., Smith, A. M., Whyman, R., (2010), "Selective Hydrogenation of Amides Using Rh/Mo Catalysts", J. Catal., 269 (1), 93–102.

[80] Beamson, G., Papworth, A. J., Philipps, C., Smith, A. M., Whyman, R., (2010), "Selective Hydrogenation of Amides Using Ruthenium/ Molybdenum Catalysts", Adv. Synth. Catal., 352 (5), 869–883.

[81] Stein, M., Breit, B., (2013), "Catalytic Hydrogenation of Amides to Amines under Mild Conditions", Angewandte, 52(8),2231–2234.

[82] Smith, A. A., Dani, P., Higginson, P. D., Pettman, A.J., (2005), WO Patent 2005066112, 133270.

[83] Burch, R., Paun, C., Cao, X., Crawford, P., Goodrich, P., (2011), "Catalytic Hydrogenation of Tertiary Amides at Low Temperatures and Pressures Using Bimetallic Pt / Re-Based Catalysts", Journal of Catalysis, 283 (1), 89–97.

[84] Balaraman, E., Gnanaprakasam, B., Shimon, L. J. W., Milstein, D., (2010), "Direct Hydrogenation of Amides to Alcohols and Amines under Mild Conditions.", J. Am. Chem. Soc., 132 (47), 16756–16758
.

[85] Ito, M., Ootsuka, T., Watari, R., Shiibashi, A., Himizu, A., (2011), "Catalytic Hydrogenation of Carboxamides and Esters by Well-Defined Cp*Ru Complexes Bearing A Protic Amine Ligand", J. Am. Chem. Soc., 133 (12), 4240–4242.

[86] John, J. M., Bergens, S. H., (2011), "A Highly Active Catalyst for The Hydrogenation of Amides to Alcohols and Amines", Angew. Chemie Int. Ed., 50 (44), 10377–10380.

[87] Miura, T., Naruto, M., Toda, K., Shimomura, T., Saito, S., (2017), "Multifaceted Catalytic Hydrogenation of Amides via Diverse Activation of A Sterically Confined Bipyridine–Ruthenium Framework", Sci. Rep., 7 (1), 1586.

[88] Magro, A. A. N., Eastham, G. R., Cole-Hamilton, D. J., (2007), "The Synthesis of Amines by The Homogeneous Hydrogenation of Secondary and Primary Amides", Chem. Commun., (30), 3154–3156.

[89] vom Stein, T., Meuresch, M., Limper, D., Schmitz, M., Hölscher, M., (2014), "Highly Versatile Catalytic Hydrogenation of Carboxylic and Carbonic Acid Derivatives Using A Ru-Triphos Complex: Molecular Control Over Selectivity and Substrate Scope", J. Am. Chem. Soc., 136 (38), 13217–13225.

[90]   Coleman, G. H., Maxwell, R. D., (1934), "The Reaction of Potassium Amide in Liquid Ammonia with Chloroethenes", J. Am. Chem. Soc., 56 (1), 132–134.

[91]   Broadbent, H. S., Campbell, G. C., Bartley, W. J., Johnson, J. H., (1959), "Rhenium and Its Compounds as Hydrogenation Catalysts. III. Rhenium Heptoxide1,2,3", J. Org. Chem., 24 (12), 1847–1854.

[92]   Richard, M. K., (1984), "Catalytic Hydrogenation of N,N-Disubstituted Amides to Amines", US4448998A.

[93]   Ian D., Werner A., (1990), "Process for The Production of Amines", US4912260.

[94]   Beamson, G., Papworth, A. J., Philipps, C., Smith, A. M., Whyman, R., (2011), "Selective Hydrogenation of Amides Using Bimetallic Ru / Re and Rh / Re Catalysts", J. Catal., 278 (2), 228–238.

[95]   Hirosawa, C., Wakasa, N., Fuchikami, T., (1996), "Hydrogenation of Amides by The Use of Bimetallic Catalysts Consisting of Group 8 to 10, and Group 6 or 7 Metals", Tetrahedron Lett., 37 (37), 6749–6752.

[96]   John, J. M., Loorthuraja, R., Antoniuk, E., Bergens, S. H., (2015), "Catalytic Hydrogenation of Functionalized Amides under Basic and Neutral Conditions", Catal. Sci. Technol., 5 (2), 1181–1186.

[97]   Burch R., Paun, C., Cao, X. M., Crawford, P., Goodrich, P., Hardacre, C., Hu, P., McLaughlin, L., Sá, J., Thompson, J. M., (2011), "Catalytic Hydrogenation of Tertiary Amides at Low Temperatures and Pressures Using Bimetallic Pt/Re-Based Catalysts", J. Catal., 283 (1), 89-97.

[98]   Mitsudome, T., Miyagawa, K., Maeno, Z., Mizugaki, T., Jitsukawa, K., (2017), "Mild Hydrogenation of Amides to Amines over A Platinum-Vanadium Bimetallic Catalyst", Angew. Chemie - Int. Ed., 56 (32), 9381–9385.

[99]   vom Stein, T., Meuresch, M., Limper, D., Schmitz, M., Hölscher, M., (2014), "Highly Versatile Catalytic Hydrogenation of Carboxylic and Carbonic Acid Derivatives using A Ru-Triphos Complex: Molecular Control over Selectivity and Substrate Scope", J. Am. Chem. Soc., 136 (38), 13217–13225.

[100]   Ali, M., Md Motiar, R., Sarkar, M., Abd Hamid, S. B., (2014), "Heterogeneous Metal Catalysts for Oxidation Reactions", Journal of Nanomaterials, 2014, 23.

[101]   Ayvali, T.,(2015)," Rhenium Based Mono and Bi-Metallic Nanoparticles : Synthesis, Characterization and Application in Catalysis", PhD Thesis, University of Toulouse.

[102]   Marbella, L. E., Millstone, J. E., (2015), "NMR Techniques for Noble Metal Nanoparticles", Chem. Mater., 27 (8), 2721–2739.

[103]   Beamson, G., Papworth, A. J., Philipps, C., Smith, A. M., Whyman, R., (2011), "Selective Hydrogenation of Amides Using Bimetallic Ru/Re and Rh/Re Catalysts", J. Catal., 278, 228–238.

[104]   Ayvalı, T., Fazzini, P. F., Lecante, P., Mayorale, A., Philippot, K., (2017), "Control of Reactivity Through Chemical Order in Very Small RuRe Nanoparticles", Dalt. Trans., 46, 15070–15079.

[105]   Lara, P., Ayvalı, T., Casanove, M. J., Lecante, P., Mayoral, A., (2013), "On the

Influence of diphosphine Ligands on The Chemical Order in Small RuPt Nanoparticles: Combined Structural and Surface Reactivity studies", Dalt. Trans., 42, 372–382.

[106] Toyao, T., Siddiki, S. M. A. H., Morita, Y., Kamachi, T., Touchy, A. S., (2017), "Rhenium-Loaded TiO$_2$: A Highly Versatile and Chemoselective Catalyst for The Hydrogenation of Carboxylic Acid Derivatives and The N-Methylation of Amines Using H$_2$ and CO$_2$", Chem. - A Eur. J., 23 (59), 14848–14859.

[107] Pertici, P., Vitulli, G., Lazzaroni, R., Salvadori, P., Barili, P. L., (1982), "A Simple Preparation for (η 6 -arene)(η 4 -cyclo-octa-1,5-diene)Ruthenium-(0) Complexes and Their Conversion into The Corresponding Arene–Dichlororuthenium(II) complexes", J. Chem. Soc., Dalt. Trans., 5 (6), 1019–1022.

[108] Schneider, A., Popovska, N., Holzmann, F., Gerhard, H., Topf, C., (2005), "[(1,5-Cyclooctadiene)(toluene)Ruthenium(0)]: A Novel Precursor for The MOCVD of Thin Ruthenium Films", Chem. Vap. Depos., 11 (2), 99–105.

[109] Naskar, M. K., Eswaramoorthy, M., (2008), "Significant Improvement in The Pore Properties of SBA-15 Brought About by Carboxylic Acids and Hydrothermal Treatment", J. Chem. Sci., 120 (1), 181–186.

[110] Quadrelli, E. A., Basset, J. M., (2010), "On Silsesquioxanes' Accuracy as Molecular Models for Silica-Grafted Complexes in Heterogeneous Catalysis", Coord. Chem. Rev., 254 (5), 707–728.

[111] Cohen Sagiv, M., Eliaz, N., Gileadi, E., (2013), "Incorporation of Iridium into Electrodeposited Rhenium–Nickel Alloys", Electrochem. Acta, 88, 240–250.

[112] Morgan, D. J., (2015), "Resolving Ruthenium: XPS Studies of Common Ruthenium Materials", Surf. Interface Anal., 47 (11), 1072–1079.

BIOGRAPHY

Ahmet Musap Mert is a Master of Science Student at Institute of Nanotechnology, Gebze Technical University. He was born on 02.05.1991 in Istanbul. He graduated from Istanbul Technical University Food Engineering Department in 2015. He worked on production of nanofiber and applications in his undergraduate thesis. He started to work as Research Assistant on Nanocatalyst and Clean Energy Application Laboratory in Gebze Technical University, Institute of Nanotechnology.

APPENDICES

Appendix A: The General Properties of Support Materials

The surface interactions play a vital role on the catalyst's stability, selectivity and activity. Also, the particle size, shape and morphology are significant parameters because these properties effect to the accessible active surface area of catalyst. Despite smaller particle size gives high surface area, the smaller particle size should cause undesired effects such as surface penetration by foreign atoms, agglomeration etc. Small particles are generally unstable, so support materials are a vehicle to increase stability of them [101–103]. The supports materials serve very important features functions;

- The supports have large surface area and the active components spread over the surface area, so the possibility of contact between the active components and reactants increase. Because of this advantage, the active components' amount can be decreased according to economical reason. The active components such as Platinum, Rhenium, Ruthenium, Palladium etc. are so expensive materials that the main purpose of studies reduce to costs.

- The supports prevent to sintering of active component on the surface, the active components are adjusted as the micro-crystalline particles on the surface by the support materials.

- The supports increase the activity and selectivity of catalysts.

- The porous supports should control the transport of reactant and the products, so overall conversion rate is affected by this function.

- The main function of support materials as fixation of the active components, formation of high dispersed particles, stabilization and enlargement of the specific surface area.

In addition, any support materials must be having some physical and chemical properties as inertness to undesired reaction, resistance to hardness and compressive strength, stability under reaction conditions, high surface area, porosity and small pore sizes and low cost. The Silica, Alumina, Titania, Carbon complexes, Zeolite can be illustrated as the examples of catalyst support materials. The catalyst supports are

divided into two main groups as non-porous (TiO$_2$, SiO$_2$ Al$_2$O$_3$) and porous (SBA-15, MCM-48, Al-MCM-48, Ti-SBA-15 etc.) [102,104,105]. The widely used supports materials and their properties are listed in Table A.1.

Table A.1: The summary of support materials in catalytic reactions.

Supports	Features	Advantages	Disadvantages
Alumina	(1) Hardness (2) High melting point and high compression strength (3) Resistant to abrasion and chemical attack (4) High thermal conductivity	(1) Thermally stable (2) Randomly ordered (3) High surface area and pore volume (4) Well-ordered pore (5) Narrow pore size	(1) Difficult to control the hydrolysis rate of aluminum precursors
Silica	(1) Tendency to form large networks (2) Found in nature and living organisms (3) Hardness	(1) High efficiency (2) High selectivity (3) Highly stable (4) Mechanical strength	(1) Low compatibility (2) Formation of aggregates/agglomerates
Zeolite	(1) Microporous (2) Inertness (3) Excellent electron conductivity	(1) Highly effective (2) Less or no corrosion (3) No waste or disposal problems (4) High thermo stability (5) Easy set-up of continuous processes (6) Great adaptability to practically all types of catalysis	(1) Irreversible adsorption or steric blockage of heavy secondary products (2) Impossibility of using microporosity (3) Difficult to exploit the shape selectivity
Carbon	(1) Nonmetallic (2) Tetravalent (3) Porous structure	(1) High mechanical strength (2) Large surface area (3) Excellent electron conductivity (4) Good elasticity (5) Thermal stability (6) Inertness	(1) High temperature physical activation (2) Expensive (3) Emission of greenhouse gasses during pyrolysis

In this study, SiO$_2$ and silica based mesoporous support materials (SBA-15, Ti-SBA-15, MCM-48 and Al-MCM-48) will be used with ReRu bimetallic system in the hydrogenation of amide to amine, so these support materials will be explained detailly in below.

Silicone di-oxide (SiO$_2$) is widely used as support material for heterogeneous catalyst because it has vital features such as nontoxicity, long-term photo stability and

high effectiveness. Also, it shows good mechanical resistance and stability in acidic and oxidative environments [106]. SiO_2 can be found in many atomic structures: rutile, anatase, brookite. The anatase phase is used more commonly as a support material and is typical of this phase surface area is 80 m^2 / g. It has a low surface area compared to alumina and silica. The surface area decreases to around 550°C and passes to the rutile phase. This is the low temperature for the use of titanium dioxide as a backing material and that they are suitable for reactions such as selective catalytic reduction [107].

Mesoporous silicas (SBA-15, MCM-48 etc.) are inorganic materials that they are synthesized in the presence of surfactants as templates for the polycondensation of silica species come from different sources' silica as sodium silicate, alkoxides etc. The source of silica, type of surfactant, pH, reaction mixture composition, temperature and duration of reaction determine to porous structure morphology as diameter, volume and wall thickness. Many different ionic and non-ionic surfactants are widely used for synthesising of MCM-x (Mobile cubic Crystalline Material) type materials. Different morphological and porous characteristic MCM-x materials were synthesised as MCM-41, MCM-48 and MCM-50. Also, MCM type materials can be doped with metal ion such as Ti, Al etc. for gaining different properties. The pore size and wall thickness do not get over beyond 4 nm and 2 nm, respectively. In comparison with MCM type material, SBA (Santa Barbara University) type materials are synthesised by using cationic surfactants in acidic medium, but porous characteristics are same as MCM-x type materials. SBA-15 and SBA-16 materials have larger pore sizes and thicker walls. The pore size of these materials can be deteriorated by adjusting reaction time, temperature, calcination conditions etc. [102]. The structure of materials is shown in Figure A.1.
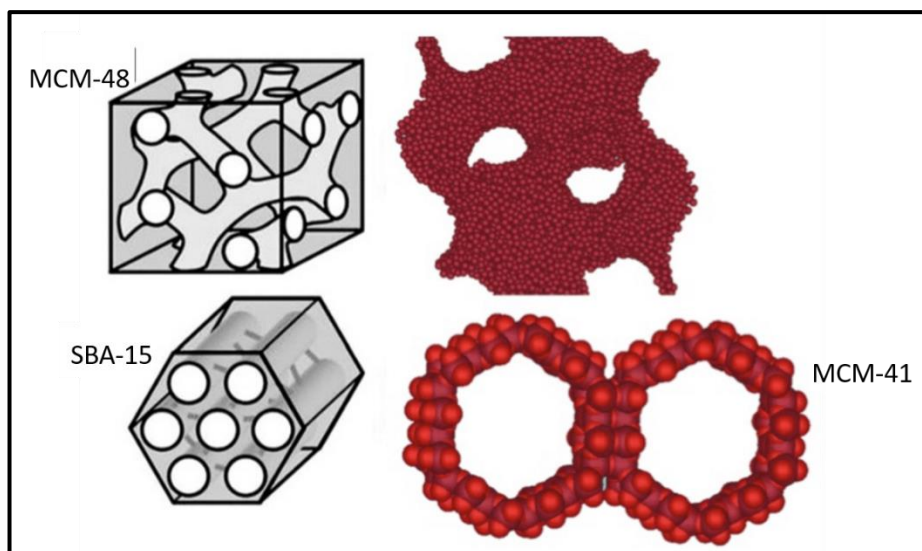
Figure A.1: The structure of mesoporous silica materials.

The SBA-15 and MCM-48 materials were purchased from ACS Materials in this study and the physical and chemical properties of materials are shown in Figure A.2 and Table A.2.

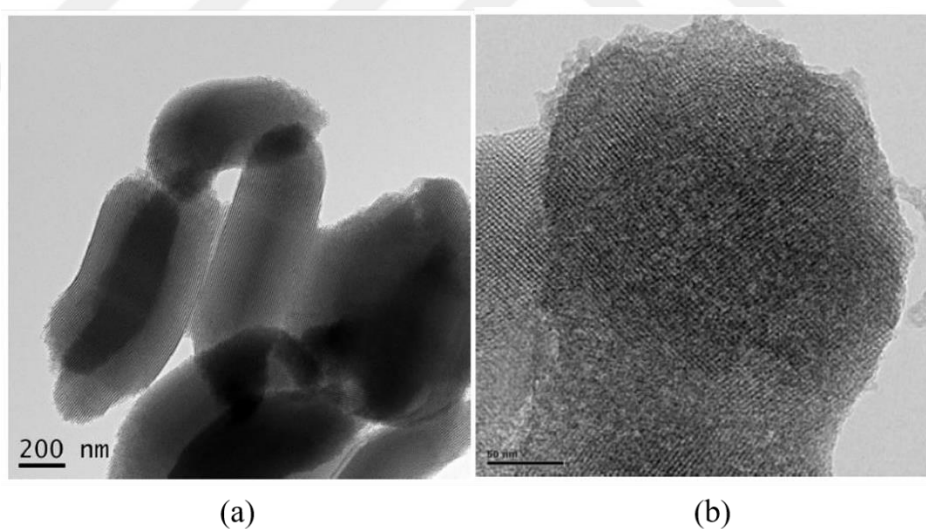(a)   (b)

Figure A.2: The physical and chemical properties of SBA-15 (a) and MCM-48 (b). (Adapted from ACS Materials).

Table A.2: Mesoporous support materials proposed to be used as hosts for ReRu bimetallic NPs and their physical properties.

Mesoporous Structures	Nature	Pore size (Å)	BET Surface Area (m²/g)
SBA-15	Silica	40	605
Ti-SBA-15 (7% Ti)	Titanosilicate	40	525
MCM-48	Silica	25	1485
Al-MCM-48 (4% Al)	Aluminosilicate	35	930
SiO₂	Silicon dioxide	-	376

Appendix B: General properties of Rhenium

Rhenium has been discovered by Ida Tacke-Noddack, Walter Noddack and Otto carl Berg in 1925. It is a transition element in third-row, group VII element. It is extracted from molybdenum and copper ores as a by-product. Atomic number is 75 and average concentration is 0,027 ppm. There are two natural isotopes as ^{185}Re (37,4%) and ^{187}Re (62,6%). Rhenium is the third element in the periodic table that has highest melting point (3186°C). The crystal structure of rhenium is hexagonal close-packed and lattice parameters a=276,1 pm and c=445,6 pm. Resisting to corrosion but slowly tarnishes in moist air.

The high melting point, mechanical strength and chemical resistance against poisoning are important features of rhenium elements, so it is attractive for jet engines as engine turbine, rocket engine parts etc., power devices and electronics. Rhenium is also widely preferred as catalysis. Pt-Re alloy is used for petroleum reforming reaction at 500°C and 15 atm. Moreover, Re-based catalysts are used for catalytic hydrogenation, oxidation or coupling reactions. Especially, it is used for cancer treatment as radiotherapy or anticancer agent.

Rhenium has a large number of easily accessible oxidation states between -3 to +7 under mild redox conditions, so experimental conditions and yield of products must be controlled to repeatable results. Also, rhenium has high bond strengths with the ligands, which make available to high coordination with molecular complexes. They provide unusual and unique reaction pathway for rhenium complexes such as halides, oxides, alkyls, carbonyls, hydrides etc.